PH-RESPONSIVE AMPHIPHILIC MACROMOLECULES FOR ANTICANCER DRUG AND SIRNA DELIVERY

by

LI GU

A dissertation submitted to the

Graduate School-New Brunswick

Rutgers, The State University of New Jersey

In partial fulfillment of the requirements

For the degree of

Doctor of Philosophy

Graduate Program in Chemistry

Written under the direction of

Professor Kathryn E. Uhrich

And approved by

_____

_____

_____

_____

New Brunswick, New Jersey

JANUARY 2014

ABSTRACT OF THE DISSERTATION

pH-Responsive Amphiphilic Macromolecules

for Anticancer Drug and siRNA Delivery

By LI GU

Dissertation Director:

Kathryn E. Uhrich

Amphiphilic macromolecules (AMs), composed of a macromolecular hydrophobic segment and a hydrophilic poly(ethylene glycol) (PEG) are used as drug delivery systems and therapeutics. In this dissertation, AMs maintained physicochemical and biological properties after commercial sterilization treatment indicating AMs are suitable for commercialization. Furthermore, AMs are modified for anticancer drug and siRNA delivery.

In this dissertation, pH-sensitive AMs were successfully synthesized to solve the dilemma between stability during circulation and quick drug release at target site. Critical

micelle concentrations of the pH-sensitive AMs indicated stability against dilution which occurs during blood circulation. Doxorubicin (DOX) was chosen as the anticancer drug to investigate the pH-dependent drug release profile. Enhanced DOX release at pH 5 was compared to pH 7.4 due to the cleavage of hydrazone in the AM backbone. Further cytotoxicity studies showed that pH-senstive AMs decreased cell viability compared to free DOX and controll micelles. Therefore, the pH-sensitive AMs can achieve both stability in physiological condition and quick drug release at target site.

The delivery of short interfering ribonucleic acid (siRNA), a potent gene knock-down therapeutic, is a main issue in biomedical field. In this dissertation, novel cationic amphiphilic macromolecule (CAM)-lipid complexes were developed with comparable transfection efficiency to Lipofectamin, a gold standard siRNA delivery vehicle *in vitro*. Dynamic light scattering indicated that CAM-lipid complexes possess the pH-responsive features: stable at pH 7.4 (physiological pH) and instable at pH 5 (endosomal pH). Intracellular trafficking demonstrated the endosomal escape of siRNA possibly because of the pH-responsive feature. Furthermore, this dissertation is the first example of using isothermal titration calorimetry to study siRNA release from polymer-liposome systems. Overall, CAM-lipid complex was developed as an efficient siRNA carrier *in vitro* and mechanistic insights in delivery process provided.

ACKNOWLEDGEMENTS

I would like thank all people who have contributed, guided, and supported the work described in the dissertation.

With special thanks to:

First and also foremost, I would like to thank my advisor, Professor Kathryn E. Uhrich. She has been supportive during my PhD career in every aspect. Her guidance, inspiration, and patience have grown me into a better scientist. More importantly, she has provided me the independence to delve into my own research interests. Next, I would also thank my committee members: Professor Ralf Warmuth, Professor Deirdre O'Carroll, Professor Lawrence Romsted, and Professor Charles Roth. Their scientific input and guidance has been much help to accomplish this dissertation.

I would also like to thank my collaborators: Professor Probhas Moghe, Professor Charles Roth, Leora Nusblat, and Professor Evan Mintzer. Their efforts and help have laid the ground of much work done in this dissertation.

I would like to thank current and former members of Uhrich and Moghe group: Allison Faig, Nick Stebbins, Weiling Yu, Yingyue Zhang, Jonathan Faig, Jennifer Chan, Rose Soskind, Dr. Michelle Morano, Dr. Roselin Rosario-Melendez, Dr. Sabrina Snyder, Dr. Alex Harmon, Dr. Sarah Sparks, Dr. Sarah Hehir, Dr. Dawanne Poree, Dr. Dalia Abdelhamid, Dr. Roberto Delgado-Rivera, Dr. Bryan Langowski, Dave Orban, Isita Amine, Dr. Adam York, Dr. Latrisha Peterson, Dr. Daniel Lewis, Adriana Martin, Dr. Nicole Ploudre, and other current and past undergraduate researchers. The inspirational and intellectual contributions to my work are much appreciated.

I also want to thank my friends: Da Xu, Dr. Gaojie Hu, Dr. Fuguo Jiang, Yongliang Zhang, and others. Their help during graduate school has made my life a lot easier and fun.

Finally, I would like to thank my family for providing me the encouragement and motivation to work through my entire PhD career. They have worked hard to provide me with the best education of their ability. They also kept me positive and focused over many years. My in-laws have also been extremely supportive and providing me encouragement. My wife, Shuchi Zhang, has been on my side since we were married. All the love, care, help, patience, and faith she has given to me is extremely important. My one-and-a-half year daughter, Lusia Gu, has been a constant source of motivation since she was born on my birthday. I could not have accomplished my dissertation work without their support.

TABLE OF CONTENTS

LIST OF TABLES

LIST OF FIGURES

ABBREVIATIONS

AM	Amphiphilic macromolecule	NHS	N-hydroxysuccinimide
CAM	Cationic amphiphilic macromolecule	NMR	Nuclear magnetic resonance
CMC	Critical micelle concentration	N/P	Nitrogen to phosphate ratio
CO_2	Carbon dioxide	oxLDL	Oxidized low-density lipoprotein
DCC	Dicyclocarbodiimide	PBS	Phosphate buffered saline
DCM	Dichloromethane	PDI	Polydispersity index
DMF	Dimethyl formamide	PEG	Poly(ethylene glycol)
DMSO	Dimethylsulfoxide	PEO	Poly(ethylene oxide)
DMEM	Dulbecco's modified eagle's medium	PEI	Polyethyleneimine
DLS	Dynamic light scattering	PLGA	Poly(lactide-*co*-glycolide)
DOPE	1,2-Dioleoyl-sn-glycero-3-phosphoethanolamine	PCL	Poly(caprolactone)
DOTAP	1,2-Diolecyl-3-trimethylammonium-propane	PPO	Poly(propylene oxide)
DSC	Differential scanning calorimetry	PVA	Poly(vinyl alcohol)
EPR	Enhanced permeation retention	PVP	Poly(N-vinyl-2-pyrrolidone)
FBS	Fetal bovine serum	RNAi	RNA interference
FTIR	Fourier transform infrared spectroscopy	siRNA	Short interfering ribonucleic acid
FITC	Fluorescein isothiocyanate	SRA	Scavenger receptor A
GPC	Gel permeation chromatography	THF	Tetrahydrofuran
HEPES	4-(2-hydroxyethyl)-1-piperazineethanesulfonic acid	TEM	Transmission electron microscopy
HPLC	High performance liquid chromatography	UV/Vis	Ultraviolet/visible
HUVEC	Human umbilical vein endothelial cell	DOX	Doxorubicin
ITC	Isothermal titration calorimetry	MPS	Mononuclear phagocytic system
LDL	Low-density lipoprotein	MALDI-TOF	Matrix assisted laser desorption/ionization-time of flight

1 Overview

1.1 Overall introduction to drug delivery

A drug is a medicinal substance administered to mammals to treat disease. Multiple kinds of drugs, including natural products, synthetic medicines, nucleic acids, proteins, and peptides, have been developed to combat various diseases [1, 2]. Administering drugs to the human body, however, is complicated due to the many barriers that impede drugs from reaching their desired target site *in vivo,* thus reducing drug efficacy [3-7]. As an example, anticancer drugs with high bioactivity *in vitro* often exhibit extremely low water-solubility which leads to overall poor absorption and reduced bioavailability [8]. As another example, macromolecule drugs such as nucleic acid are easily degraded by the mononuclear phagocyte systems (MPS), a group of organs responsible for clearing foreign macromolecules from the human body [9].

To improve drug efficacy, drug delivery systems are developed to overcome physiological hurdles. Drug delivery systems can be designed to: enhance drug solubility, maintain drug stability while circulating in the body, minimize drug side effects, enhance drug availability in target tissues, and control drug release rate once in the pathological zone [6, 10, 11]. The aforementioned examples associated with poor drug water solubility and MPS-induced drug degradation, for instance, can be circumvented through the use of drug delivery systems. Increased drug solubility can be achieved by developing reservoir to solubilize insoluble drugs within the carrier system. Using a protective outer-layer in this carrier system can also prevent premature drug degradation leading to prolonged circulation times. However, even if the drug's solubility and stability issues are solved,

safety of the drug is still a considerable issue. Drugs' adverse effects are usually associated with off-site toxicity and can be minimized by encapsulating the drug within the carrier and ensuring that the drug will only accumulate within the pathological zone. In cancer treatment, this accumulation can be obtained through passive targeting pathways, often relying on the enhanced permeability and retention (EPR) effect, in which tumor tissues' leaky vasculature and lack of effective lymphatic drainage enable carrier systems of certain sizes (typically 10 – 30 nm) to preferentially accumulate in tumor tissue [12-17]. Another means to obtain enhanced drug accumulation in the pathological zone involves conjugating targeting ligands to the drug carrier, thus, guiding therapeutics to the disease site based on the specific interactions between targeting ligands and receptors on pathological cells. For example, folate is widely used to actively target various cancer cells with overexpressed folate receptors [18].

While drug delivery systems can improve upon drug administration and enhance drug efficacy, current delivery systems face a dilemma between maintaining stability while circulating and then effectively releasing the drug once in the pathological zone. One strategy to solve this dilemma is using stimuli-responsive delivery systems [19, 20]. Numerous stimuli, including temperature [21-23], enzymes [24, 25], magnetic field [26, 27], reductive environment [28, 29], and pH [30-34], have been investigated as triggers to promote targeted drug release. pH is an especially important biological stimulus in the human body; as one example, tumor tissues exhibit acidic pH due to lactic acid production. As another example, intracellular compartments, such as endosomes and lysosomes, are generally acidic with pH varies ranging from 4 to 6. Through

incorporating pH-responsive features into drug delivery systems, the system can be triggered to achieve drug release in pH-specific conditions.

1.2 Drug delivery systems

1.2.1 Polymeric micelles for drug delivery

Polymeric micelles are colloidal aggregates that are self-assembled from amphiphilic polymers in aqueous media. The amphiphilic polymers are typically composed of hydrophobic and hydrophilic polymers tethered together, and when their concentration reaches a critical micelle concentration (CMC), they will self-assemble into micelles having a hydrophobic core and hydrophilic shell or corona (Figure 1.1) [35]. The polymers' self-assembly behavior is based on a hydrophobic effect in which the aggregation of hydrophobic segments will increase the system's disorder by displacing water molecules that were previously organized about the hydrophobic domain. This water displacement results in an entropy increase and, thus, yields a thermodynamically favorable assembly [36]. A variety of micelle morphologies, including spherical micelles, cylindrical micelles, and vesicles with curved bilayers, can be obtained depending on the amphiphilic polymer's molecular geometry and packaging behavior [36]. For medical applications, hydrophobic polymers, including poly(D,L-lactide-*co*-glycolide) (PLGA), poly(propylene oxide) (PPO), poly(L-lysine), poly(aspartic acid), and poly(caprolactone) (PCL), make up the hydrophobic component of the amphiphilic polymer [35]. For the hydrophilic portion, poly(ethylene glycol) (PEG) is often used as it is a common component in many FDA-pproved pharmaceutical formations [37]. Using PEG as the hydrophilic shell has many advantages including low cytotoxicity, low cost, extremely high water-solubility, and functionalization ease [37]. Furthermore, much research has

demonstrated that PEG can provide steric protection against MPS recognition, leading to enhanced micelle stability and prolonged blood circulation [38]. Aside from PEG, alternative hydrophilic polymers include poly(N-vinyl-2-pyrrolidone) (PVP), poly(vinyl alcohol) (PVA), and poly(vinyl alcohol-co-vinyloleate) [35].

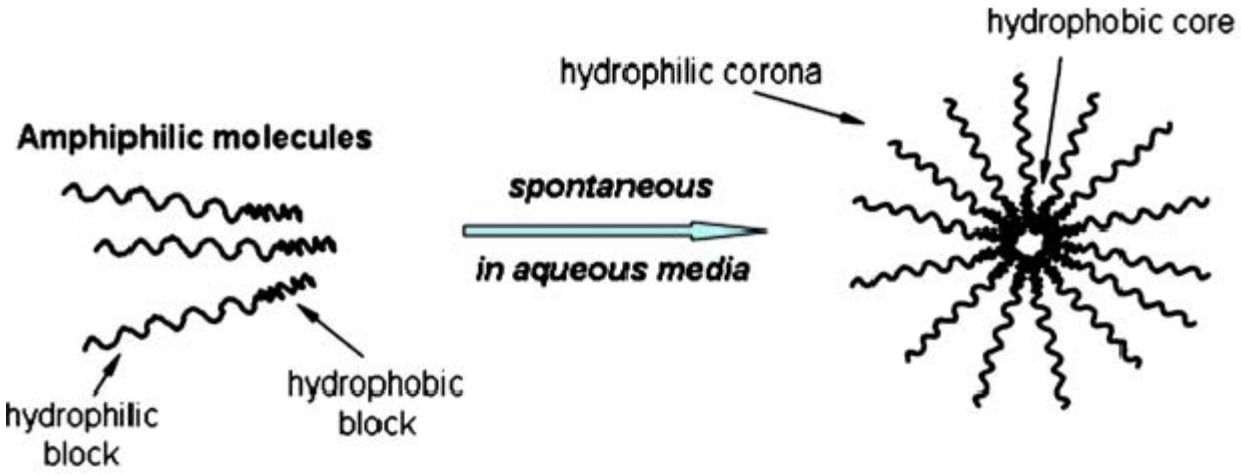

Figure 1.1 Polymeric micelle formation through self-assembly of amphiphilic polymers in aqueous media [35]

A critical characteristic of many drug delivery systems is the ability to solubilize water-insoluble drugs in an aqueous media such as the human body. Polymeric micelles possess this ability as they contain a hydrophobic core which can serve as the reservoir for hydrophobic drugs (Figure 1.2) [39]. Drug loading into polymeric micelles can be carried out by various methods such as oil-in-water emulsions, evaporation, and dialysis in water [40-42]. The amount of drug loaded in polymeric micelles is typically influenced by the size of the drug and the length of the hydrophobic and hydrophilic polymer blocks, both of which can be tuned to obtain optimal drug loading [43].

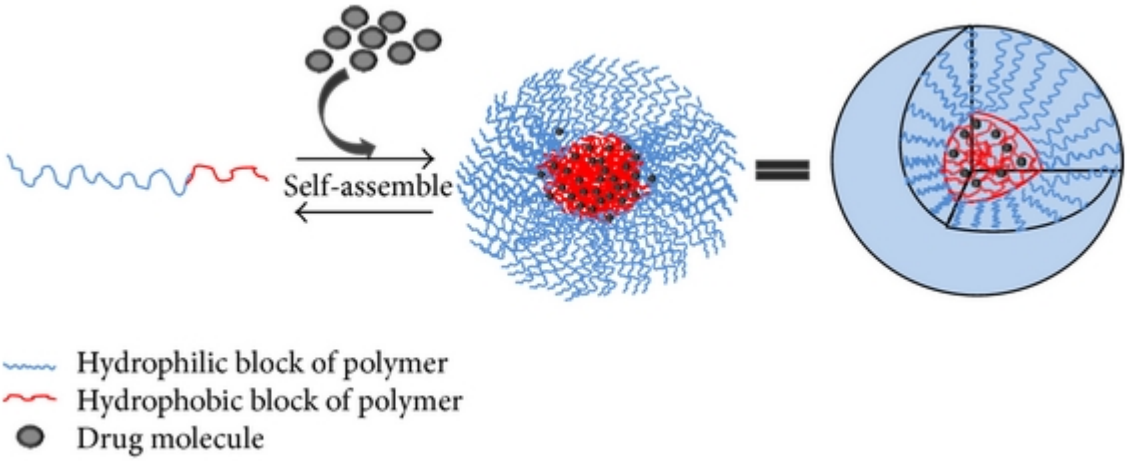

Figure 1.2 Formation and drug loading of polymeric micelles by self-assembly of amphiphilic polymers in aqueous solution [39]

Another characteristic of polymeric micelles is their nanoscale size which allows for accumulation in tumor tissues. The nanoscale size not only contributes to this enhanced accumulation in tumor tissue but can also provide an optimal size range (10 – 200 nm) for intracellular uptake [44]. Micelles size less than 10 nm are rapidly cleared via kidney filtration [45-47], thus, by altering the length of the hydrophobic and hydrophilic blocks, micelle sizes can be tuned to obtain optimal sizes for drug delivery applications. Furthermore, through modifying the hydrophobic and hydrophilic blocks, CMCs can also be tuned. Research suggests that low CMCs ($<10^{-8}$ M) can lead to higher micelle stability against dilution once administered in the human body [3, 6], thus amphiphilic polymers are often modified to achieve this stability.

1.2.2 Liposomes for drug delivery

Similar to micelles, liposomes are comprise of hydrophobic and hydrophilic zones and are spherical. Unlike micelles, liposomes are organized into bilayers of layer structure. Typically, the amphiphilic moieties are lipids, which consist of hydrophobic alkyl chain and hydrophilic head group, and are biocompatible. Based on their structural properties, liposomes can be classified into different types, including multilamellar large vesicles (MLVs), small unilamellar vesicles (SUVs), and large unilamellar vesicles (LUVs). Using unilamellar vesicles as an example, the liposome has a continuous interior hydrophilic phase which can solubilize hydrophilic molecules and a hydrophobic bilayer which can solubilize hydrophobic drugs (Figure 1.3) [48]. Hydrophilic molecules encapsulated within liposomes typically include therapeutic and/or diagnostic agents that are not able to pass through the cell membrane [48]. Liposomes' hydrophobic bilayer, similar to polymeric micelles core, can solubilize water-insoluble drugs to improve their absorption and bioavailability.

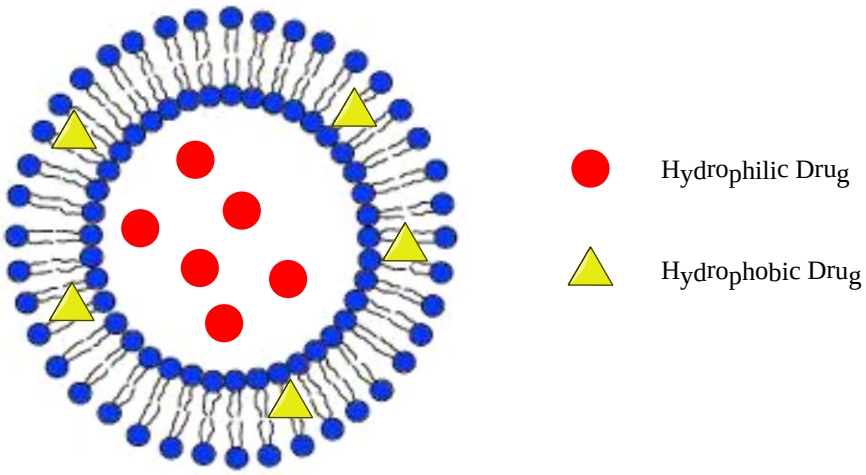

Figure 1.3 Liposomes with hydrophilic drugs loaded in interior phase and hydrophobic drugs loaded in hydrophobic bilayer

Due to their lipophilic bilayer, liposomes have the unique ability of fusing with lipid cell membranes [49, 50]. This fusion can influence endocytosis via lipid rafts, which are microdomain-containing glycosphingolipids and protein receptors on cell membrane, and lead to an enhanced intracellular uptake of liposomes [51-53]. Liposomes can also be obtained in the 100 – 200 nm size range via membrane extrusion, and are thus an optimal size for drug delivery applications. Similar to polymeric micelles, liposomes' size allows them to carry chemotherapeutics to tumor tissue based on the EPR effect. Active targeting can also be achieved by surface-functionalizing liposomes with targeting ligands. One main drawback of liposomes, however, is their instability under physiological condition due to their aggregation and adsorption induced by serum proteins in the blood stream [54, 55]. To address the instability, various strategies have been introduced including formulating liposomes with PEGylated lipids and/or cholesterol. Given their ease of functionalization and formulation, liposomes with targeting groups on the surface, stabilizing reagents, stimuli-responsive features, diagnostic reagents, and therapeutics can be obtained to produce multifunctional drug carriers and tackle a variety of drug delivery issues [56-59].

1.2.3 Amphiphilic macromolecules as drug delivery systems

Amphiphilic macromolecules (AMs), composed of a macromolecular hydrophobic segment and hydrophilic tail, can self-assemble in aqueous media [60]. The polymeric micelles formed from AMs have nanoscale size (15-20 nm), low CMC value (10^{-7}M), and cytocompatibility [61, 62].

Stemming from previous work using AMs as anticancer drug delivery system [62, 63], pH-responsive AMs are synthesized. Physicochemical characterizations such as 1H NMR and DLS were used to elucidate the cleavage of acid-labile hydrazone in AMs. Drug release studies indicated that acidic pH conditions enhanced drug release rate compared to neutral pH. Furthermore, the pH-sensitive AMs are used to deliver doxorubicin, a model chemotherapeutic against cancer cell. The doxorubicin-loaded, pH-sensitive micelles show higher efficiencies than free doxorubicin and control micelles in killing cancer cells.

Building upon previous work in developing cationic AMs as nucleic acid delivery vehicles, AM-lipid complexes are developed to serve as short interfering ribonucleic acid (siRNA) delivery systems. In the project, cationic AMs are incorporated within cationic liposomes. Thermodynamic measurements illustrated favorable complexation between cationic AMs and lipid. Physicochemical characterizations reveal that the AM-lipid complexes are suitable for siRNA delivery due to the cationic and lipid feature. *In vitro* assays demonstrated that certain complexes have comparable efficiencies to Lipofectamine, a gold standard for gene delivery. In-depth mechanistic studies exhibit the pH-responsive feature of same AM-lipid complexes lead to the endosomal escape, a critical step in siRNA delivery. This project demonstrates that AM-lipid complexes can be an efficient delivery vehicles for siRNA.

1.3 Sterilization

Sterilization is the process to eliminate any microbial species such as fungi, bacteria, and viruses [64]. It is a mandatory step in drug or medical device commercialization [64]. Typical sterilization methods include heat sterilization, chemical sterilization, radiation sterilization, and filtration sterilization [65-67]. As AMs are promising for biomedical applications, their ability to withstand sterilization process is evaluated in this dissertation. Electron-beam and gamma radiation methods are chosen as both of them do not involve heat or chemicals and are more convenient [68]. Physicochemical and biological properties of AMs are examined after sterilization and compared to untreated AMs.

1.4 References

[1] L.J. Gershell, J.H. Atkins. A Brief History of Novel Drug Discovery Technologies. *Nat Rev Drug Discov* **2003** *2* 321-327.
[2] P. Cozzi. The Discovery of a New Potential Anticancer Drug: A Case History. *Farmaco* **2003** *58* 213-220.
[3] C. Demetzos, N. Pippa. Advanced Drug Delivery Nanosystems (Addnss): A Mini-Review. *Drug Deliv* **2013** doi:10.3109/10717544.2013.844745.
[4] M. Bhavna, S. Ali, J. Baboota, Patents on Nanoparticulate Drug Delivery Systems--a Review. *Recent Pat Drug Deliv Formul* **2008** *2* 83-89.
[5] V. Jogani, K. Jinturkar, T. Vyas, A. Misra. Recent Patents Review on Intranasal Administration for Cns Drug Delivery. *Recent Pat Drug Deliv Formul* **2008** *2* 25-40.
[6] M.S. Arayne, N. Sultana. Review: Nanoparticles in Drug Delivery for the Treatment of Cancer. *Pak J Pharm Sci* **2006** *19* 258-268.
[7] K. Braun, R. Pipkorn, W. Waldeck. Development and Characterization of Drug Delivery Systems for Targeting Mammalian Cells and Tissues: A Review. *Curr Med Chem* **2005** *12* 1841-1858.
[8] A. Bartal, Z. Matrai, A. Szucs, G. Belinszkaja, Z. Langmar, A. Rosta. Novel Oral Anticancer Drugs: A Review of Adverse Drug Reactions, Interactions and Patient Adherence. *Orv Hetil* **2012** *153* 66-78.
[9] I. Carr, J. Wright. The Reticuloendothelial and Mononuclear Phagocyte Systems and the Macrophage. *Can Med Assoc J* **1978** *118* 882, 884-885.
[10] D. Maurice. Review: Practical Issues in Intravitreal Drug Delivery. *J Ocul Pharmacol Ther* **2001** *17* 393-401.
[11] M. Szycher. Controlled Drug Delivery: A Critical Review. *J Biomater Appl* **1986** *1* 171-182.

[12] H. Maeda, J. Wu, T. Sawa, Y. Matsumura, K. Hori. Tumor Vascular Permeability and the Epr Effect in Macromolecular Therapeutics: A Review. *J Control Release* **2000** *65* 271-284.
[13] H. Maeda. Vascular Permeability in Cancer and Infection as Related to Macromolecular Drug Delivery, with Emphasis on the Epr Effect for Tumor-Selective Drug Targeting. *Proc Jpn Acad Ser B Phys Biol Sci* **2012** *88* 53-71.
[14] H. Maeda, G.Y. Bharate, J. Daruwalla. Polymeric Drugs for Efficient Tumor-Targeted Drug Delivery Based on Epr-Effect. *Eur J Pharm Biopharm* **2009** *71* 409-419.
[15] S. Modi, J. Prakash Jain, A.J. Domb, N. Kumar. Exploiting Epr in Polymer Drug Conjugate Delivery for Tumor Targeting. *Curr Pharm Des* **2006** *12* 4785-4796.
[16] T. Tanaka, S. Shiramoto, M. Miyashita, Y. Fujishima, Y. Kaneo. Tumor Targeting Based on the Effect of Enhanced Permeability and Retention (Epr) and the Mechanism of Receptor-Mediated Endocytosis (Rme). *Int J Pharm* **2004** *277* 39-61.
[17] V. Torchilin. Tumor Delivery of Macromolecular Drugs Based on the Epr Effect. *Adv Drug Deliv Rev* **2011** *63* 131-135.
[18] X.N. Gao, S.Q. Tang. Folate Receptor and Its Application in the Selective Receptor-Mediated Targeting Therapy of Tumor Cells--Review. *Zhongguo Shi Yan Xue Ye Xue Za Zhi* **2005** *13* 911-914.
[19] S.R. MacEwan, D.J. Callahan, A. Chilkoti. Stimulus-Responsive Macromolecules and Nanoparticles for Cancer Drug Delivery. *Nanomedicine (Lond)* **2010** *5* 793-806.
[20] K.S. Soppimath, T.M. Aminabhavi, A.M. Dave, S.G. Kumbar, W.E. Rudzinski. Stimulus-Responsive "Smart" Hydrogels as Novel Drug Delivery Systems. *Drug Dev Ind Pharm* **2002** *28* 957-974.
[21] A.C. Lima, W. Song, B. Blanco-Fernandez, C. Alvarez-Lorenzo, J.F. Mano. Synthesis of Temperature-Responsive Dextran-Ma/Pnipaam Particles for Controlled Drug Delivery Using Superhydrophobic Surfaces. *Pharm Res* **2011** *28* 1294-1305.
[22] W.D. Ma, H. Xu, S.F. Nie, W.S. Pan. Temperature-Responsive, Pluronic-G-Poly(Acrylic Acid) Copolymers in Situ Gels for Ophthalmic Drug Delivery: Rheology, in Vitro Drug Release, and in Vivo Resident Property. *Drug Dev Ind Pharm* **2008** *34* 258-266.
[23] S. Chen, Y. Li, C. Guo, J. Wang, J. Ma, X. Liang, L.R. Yang, H.Z. Liu. Temperature-Responsive Magnetite/Peo-Ppo-Peo Block Copolymer Nanoparticles for Controlled Drug Targeting Delivery. *Langmuir* **2007** *23* 12669-12676.
[24] Y. Yang, J. Aw, K. Chen, F. Liu, P. Padmanabhan, Y. Hou, Z. Cheng, B. Xing. Enzyme-Responsive Multifunctional Magnetic Nanoparticles for Tumor Intracellular Drug Delivery and Imaging. *Chem Asian J* **2011** *6* 1381-1389.
[25] M.R. Lee, K.H. Baek, H.J. Jin, Y.G. Jung, I. Shin. Targeted Enzyme-Responsive Drug Carriers: Studies on the Delivery of a Combination of Drugs. *Angew Chem Int Ed Engl* **2004** *43* 1675-1678.
[26] L.A. Tziveleka, P. Bilalis, A. Chatzipavlidis, N. Boukos, G. Kordas. Development of Multiple Stimuli Responsive Magnetic Polymer Nanocontainers as Efficient Drug Delivery Systems. *Macromol Biosci* **2013 DOI: 10.1002/mabi.201300212**.
[27] S.L. McGill, C.L. Cuylear, N.L. Adolphi, M. Osinski, H.D. Smyth. Magnetically Responsive Nanoparticles for Drug Delivery Applications Using Low Magnetic Field Strengths. *IEEE Trans Nanobioscience* **2009** *8* 33-42.

[28] H. Wen, C. Dong, H. Dong, A. Shen, W. Xia, X. Cai, Y. Song, X. Li, Y. Li, D. Shi. Engineered Redox-Responsive Peg Detachment Mechanism in Pegylated Nano-Graphene Oxide for Intracellular Drug Delivery. *Small* **2012** *8* 760-769.
[29] J. Liu, Y. Pang, W. Huang, Z. Zhu, X. Zhu, Y. Zhou, D. Yan. Redox-Responsive Polyphosphate Nanosized Assemblies: A Smart Drug Delivery Platform for Cancer Therapy. *Biomacromolecules* **2011** *12* 2407-2415.
[30] H. Wang, L. Yang, G.L. Rempel. Preparation of Ph-Responsive Polymer Core-Shell Nanospheres for Delivery of Hydrophobic Antineoplastic Drug Ellipticine. *Macromol Biosci* **2013** doi: 10.1002/mabi.201300333.
[31] S. Thamphiwatana, V. Fu, J. Zhu, D. Lu, W. Gao, L. Zhang. Nanoparticle-Stabilized Liposomes for Ph-Responsive Gastric Drug Delivery. *Langmuir* **2013** *29* 12228-12233.
[32] Q. Duan, Y. Cao, Y. Li, X. Hu, T. Xiao, C. Lin, Y. Pan, L. Wang. Ph-Responsive Supramolecular Vesicles Based on Water-Soluble Pillar[6]Arene and Ferrocene Derivative for Drug Delivery. *J Am Chem Soc* **2013** *135* 10542-10549.
[33] R. Vivek, V. Nipun Babu, R. Thangam, K.S. Subramanian, S. Kannan. Ph-Responsive Drug Delivery of Chitosan Nanoparticles as Tamoxifen Carriers for Effective Anti-Tumor Activity in Breast Cancer Cells. *Colloids Surf B Biointerfaces* **2013** *111C* 117-123.
[34] Y. Dai, C. Zhang, Z. Cheng, P. Ma, C. Li, X. Kang, D. Yang, J. Lin. Ph-Responsive Drug Delivery System Based on Luminescent Caf(2):Ce(3+)/Tb(3+)-Poly(Acrylic Acid) Hybrid Microspheres. *Biomaterials* **2012** *33* 2583-2592.
[35] V.P. Torchilin. Micellar Nanocarriers: Pharmaceutical Perspectives. *Pharm Res* **2007** *24* 1-16.
[36] J. Isarelachivili, Intermolecular and Suface Forces, Second Edition, Harcourt Brace & Company, New York, 1998.
[37] R.B. Greenwald, C.D. Conover, Y.H. Choe. Poly(Ethylene Glycol) Conjugated Drugs and Prodrugs: A Comprehensive Review. *Crit Rev Ther Drug Carrier Syst* **2000** *17* 101-161.
[38] A. Tsuchiya, Y. Naritomi, S. Kushio, J.H. Kang, M. Murata, M. Hashizume, T. Mori, T. Niidome, Y. Katayama. Improvement in the Colloidal Stability of Protein Kinase-Responsive Polyplexes by Peg Modification. *J Biomed Mater Res A* **2012** *100* 1136-1141.
[39] W. Xu, P. Ling, T. Zhang. Polymeric Micelles, a Promising Drug Delivery System to Enhance Bioavailability of Poorly Water-Soluble Drugs. *J Drug Deliv* **2013** *2013* 340315.
[40] M.F. Francis, M. Piredda, F.M. Winnik. Solubilization of Poorly Water Soluble Drugs in Micelles of Hydrophobically Modified Hydroxypropylcellulose Copolymers. *J Control Release* **2003** *93* 59-68.
[41] A. Lavasanifar, J. Samuel, G.S. Kwon. The Effect of Fatty Acid Substitution on the in Vitro Release of Amphotericin B from Micelles Composed of Poly(Ethylene Oxide)-Block-Poly(N-Hexyl Stearate-L-Aspartamide). *J Control Release* **2002** *79* 165-172.
[42] A. Lavasanifar, J. Samuel, G.S. Kwon. Micelles Self-Assembled from Poly(Ethylene Oxide)-Block-Poly(N-Hexyl Stearate L-Aspartamide) by a Solvent Evaporation Method: Effect on the Solubilization and Haemolytic Activity of Amphotericin B. *J Control Release* **2001** *77* 155-160.
[43] A. Lavasanifar, J. Samuel, G.S. Kwon. Poly(Ethylene Oxide)-Block-Poly(L-Amino Acid) Micelles for Drug Delivery. *Adv Drug Deliv Rev* **2002** *54* 169-190.

[44] Y.S. Nam, H.S. Kang, J.Y. Park, T.G. Park, S.H. Han, I.S. Chang. New Micelle-Like Polymer Aggregates Made from Pei-Plga Diblock Copolymers: Micellar Characteristics and Cellular Uptake. *Biomaterials* **2003** *24* 2053-2059.
[45] I.M. Pecly, N.M. Melo-Filho, P.A. Mourao. Effects of Molecular Size and Chemical Structure on Renal and Hepatic Removal of Exogenously Administered Chondroitin Sulfate in Rats. *Biochim Biophys Acta* **2006** *1760* 865-876.
[46] X.Y. Xu, J.P. Zhou, L. Li, Y. Zhang, M.R. Huo, X. Wang, L. Lu. Preparation of Doxorubicin-Loaded Chitosan Polymeric Micelle and Study on Its Tissue Biodistribution in Mice. *Yao Xue Xue Bao* **2008** *43* 743-748.
[47] Z.G. Gao, D.H. Lee, D.I. Kim, Y.H. Bae. Doxorubicin Loaded Ph-Sensitive Micelle Targeting Acidic Extracellular Ph of Human Ovarian A2780 Tumor in Mice. *J Drug Target* **2005** *13* 391-397.
[48] V.P. Torchilin. Recent Advances with Liposomes as Pharmaceutical Carriers. *Nat Rev Drug Discov* **2005** *4* 145-160.
[49] B.R. Lentz, V. Malinin, M.E. Haque, K. Evans. Protein Machines and Lipid Assemblies: Current Views of Cell Membrane Fusion. *Curr Opin Struct Biol* **2000** *10* 607-615.
[50] B. Morein, D. Barz, U. Koszinowski, V. Schirrmacher. Integration of a Virus Membrane Protein into the Lipid Bilayer of Target Cells as a Prerequisite for Immune Cytolysis. Specific Cytolysis after Virosome-Target Cell Fusion. *J Exp Med* **1979** *150* 1383-1398.
[51] P.J. Lin, Y.Y. Tam, I. Hafez, A. Sandhu, S. Chen, M.A. Ciufolini, I.R. Nabi, P.R. Cullis. Influence of Cationic Lipid Composition on Uptake and Intracellular Processing of Lipid Nanoparticle Formulations of Sirna. *Nanomedicine* **2013** *9* 233-246.
[52] S. Martins, S. Costa-Lima, T. Carneiro, A. Cordeiro-da-Silva, E.B. Souto, D.C. Ferreira. Solid Lipid Nanoparticles as Intracellular Drug Transporters: An Investigation of the Uptake Mechanism and Pathway. *Int J Pharm* **2012** *430* 216-227.
[53] V. Escriou, C. Ciolina, F. Lacroix, G. Byk, D. Scherman, P. Wils. Cationic Lipid-Mediated Gene Transfer: Effect of Serum on Cellular Uptake and Intracellular Fate of Lipopolyamine/DNA Complexes. *Biochim Biophys Acta* **1998** *1368* 276-288.
[54] D. Pozzi, G. Caracciolo, C. Marchini, M. Montani, A. Amici, L. Callipo, A.L. Capriotti, C. Cavaliere, A. Lagana. Surface Adsorption of Protein Corona Controls the Cell Uptake Mechanism in Efficient Cationic Liposome/DNA Complexes in Serum. *J Control Release* **2010** *148* e94-95.
[55] P. Opanasopit, K. Hyoudou, M. Nishikawa, F. Yamashita, M. Hashida. Serum Mannan Binding Protein Inhibits Mannosylated Liposome-Mediated Transfection to Macrophages. *Biochim Biophys Acta* **2002** *1570* 203-209.
[56] B. Xiang, D.W. Dong, N.Q. Shi, W. Gao, Z.Z. Yang, Y. Cui, D.Y. Cao, X.R. Qi. Psa-Responsive and Psma-Mediated Multifunctional Liposomes for Targeted Therapy of Prostate Cancer. *Biomaterials* **2013** *34* 6976-6991.
[57] M. Silindir, S. Erdogan, A.Y. Ozer, A.L. Dogan, M. Tuncel, O. Ugur, V.P. Torchilin. Nanosized Multifunctional Liposomes for Tumor Diagnosis and Molecular Imaging by Spect/Ct. *J Liposome Res* **2013** *23* 20-27.
[58] A.A. Kale, V.P. Torchilin. Environment-Responsive Multifunctional Liposomes. *Methods Mol Biol* **2010** *605* 213-242.

[59] X.F. Liang, H.J. Wang, H. Luo, H. Tian, B.B. Zhang, L.J. Hao, J.I. Teng, J. Chang. Characterization of Novel Multifunctional Cationic Polymeric Liposomes Formed from Octadecyl Quaternized Carboxymethyl Chitosan/Cholesterol and Drug Encapsulation. *Langmuir* **2008** *24* 7147-7153.
[60] L.Y. Tian, L.; Zhou, N.; Tat, H.; Uhrich, K. E. Amphiphilic Scorpion-Like Macromolecules: Design, Synthesis, and Characterization. *Macromolecules* **2004** *37* 5-11.
[61] J. Djordjevic, M. Barch, K.E. Uhrich. Polymeric Micelles Based on Amphiphilic Scorpion-Like Macromolecules: Novel Carriers for Water-Insoluble Drugs. *Pharm Res* **2005** *22* 24-32.
[62] J.D.R. Djordjevic, L.; Wang, J.; Uhrich, K.E. Amphiphilic Scorpion-Like Macromolecules as Micellar Nanocarriers. *Journal of Bioactive and Compatible Polymers* **2008** *23* 20-28.
[63] L.S. del Rosario, B. Demirdirek, A. Harmon, D. Orban, K.E. Uhrich. Micellar Nanocarriers Assembled from Doxorubicin-Conjugated Amphiphilic Macromolecules (Dox-Am). *Macromol Biosci* **2010** *10* 415-423.
[64] D.J. Dempsey, R.R. Thirucote. Sterilization of Medical Devices: A Review. *J Biomater Appl* **1989** *3* 454-523.
[65] J.P. Collier, L.C. Sutula, B.H. Currier, J.H. Currier, R.E. Wooding, I.R. Williams, K.B. Farber, M.B. Mayor. Overview of Polyethylene as a Bearing Material: Comparison of Sterilization Methods. *Clin Orthop Relat Res* **1996** 76-86.
[66] E. Hoxey. An Overview of the Revised Radiation Sterilization Standards. *Biomed Instrum Technol* **2006** *40* 85-87.
[67] L.S. Suarez, J.C. Richmond. Overview of Procurement, Processing, and Sterilization of Soft Tissue Allografts for Sports Medicine. *Sports Med Arthrosc* **2007** *15* 106-113.
[68] G. Sadler, W. Chappas, D.E. Pierce. Evaluation of E-Beam, Gamma- and X-Ray Treatment on the Chemistry and Safety of Polymers Used with Pre-Packaged Irradiated Foods: A Review. *Food Addit Contam* **2001** *18* 475-501.

2 pH-Responsive Amphiphilic Macromolecules for Anticancer Drug Delivery

2.1 Introduction

Cancer is one of the leading death causes in the world. Three main strategies to treat cancers are surgical resection, external radiotherapy, and chemotherapy. Although surgery is a curative treatment, many patients are not suitable for surgery because of the size and location of the tumor and/or it has metastasized [1]. External radiotherapy is an effective treatment, yet, it can cause a variety of side effects such as damage to other radiosensitive healthy organs, fatigue, skin irritation, fibrosis, epilation, and others [1]. Chemotherapy is a treatment strategy that can be applied alone or with surgery. Although numerous efforts have been spent to increase the specificity of chemotherapeutic drugs, the off-site toxicity is still a major side effect as many chemotherapeutics have low molecular weights that lead to rapid clearance by liver and/or kidneys [2]. Furthermore, effective chemotherapeutics are often extremely water-insoluble with logP values up to 7 [3].

One example of a chemotherapeutic widely used in treatments is doxorubicin (DOX). DOX is an anticancer drug based on the natural product daunomycin [4, 5] and has been used to treat breast, ovary, lung, and other cancers [6-8]. It works by intercalating DNA in the nucleus, which could impose life-threatening effects due to heart damage. Thus, successful delivery of DOX without off-site toxicity is of extreme importance when using DOX as the cancer treatment. Furthermore, using polymeric carriers can enhance the endocytosis, initiate the endosomal escape, prevent the endosome and lysosome exocytosis, and release the drug into nucleus (Figure 2.1) [9].

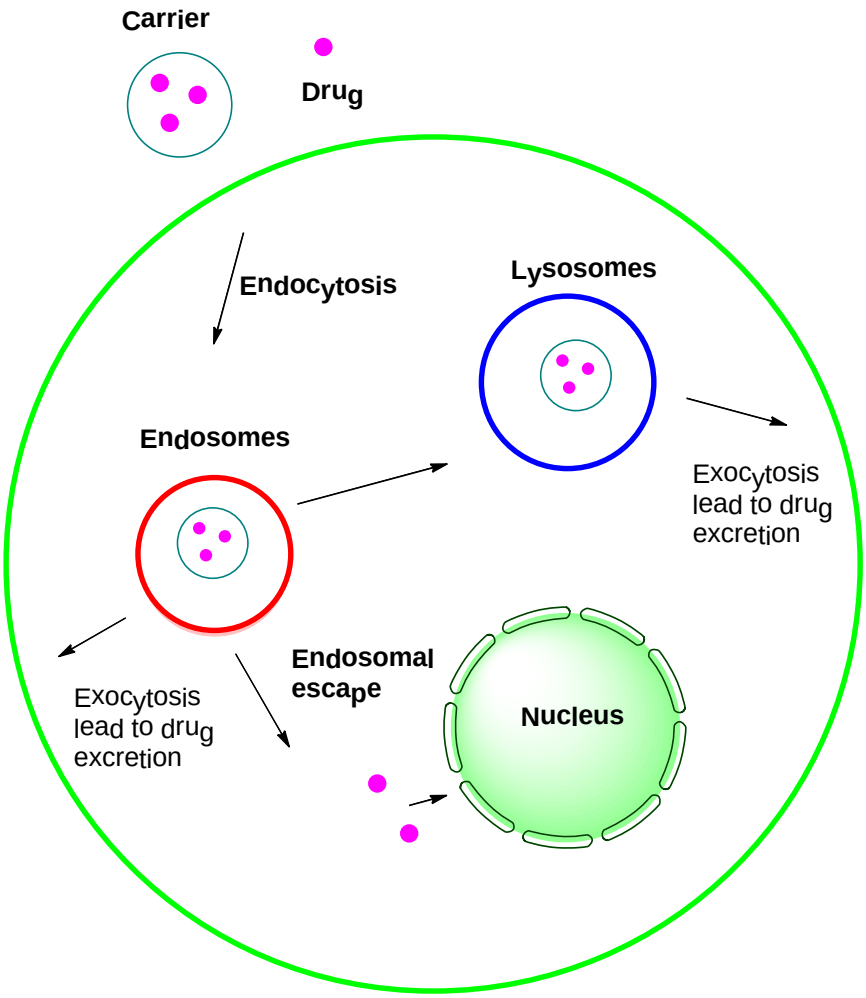

Figure 2.1 Potential intracellular pathways of anticancer drugs [9]

Among many polymer-based carriers, polymeric micelles are an important class of nanoscale carrier for cancer therapy [10]. Currently, five micellar formulations for cancer therapy are in clinical trials and one micellar formulation of paclitaxel (Genexol-PM) has been already FDA-approved for breast cancer (Table 2.1) [11]. Pluoronic L61 and P127 is the trade name of poly(ethylene oxide)-*b*-poly(propylene oxide) (PEO-PPO).

Table 2.1 Polymeric micelles for cancer therapy in clinical trials [11]

Trade Name	**Polymer**	**Drug**	**Micelle size (nm)**	**Target organ**	**Clinical stage**
NK012	PEG-PGlu(SN-38)	SN-38	20	Breast cancer	II
NK105	PEG-P(aspartate)	Paclitaxel	85	Advanced stomach cancer	II
SP1049C	Pluronic L61 and F127	Doxorubicin	25	Adenocarinoma of oesophagus	III
NC-6004	PEG-PGlu(cisplatin)	Cisplatin	30	Solid tumor	I/II
Genexol-PM	PEG-P(D,L-lactide)	Paclitaxel	20-50	Breast cancer	IV

Amphiphilic macromolecules (AMs) are amphiphiles composed of a hydrophobic segment and a hydrophilic tail. Like traditional amphiphilic polymers, AMs can self-assemble into micelles in aqueous media. In contrast to linear polymers such as Pluronic, AMs are biodegradable; they have an alkylated sugar, branched backbone as the hydrophobic component (Figure 2.2) [12].

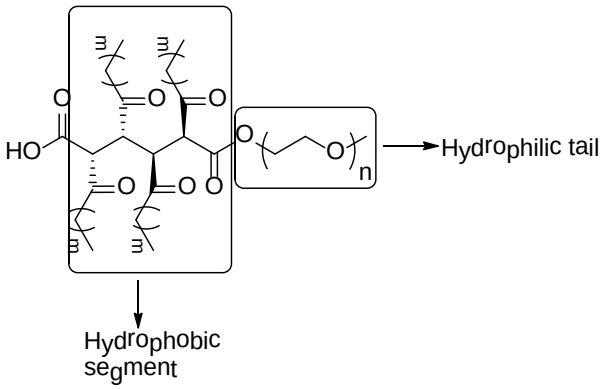

Figure 2.2 Chemical structure of AMs based upon alkylated mucic acid (MA) as hydrophobic segment and PEG as hydrophilic tail [12]

The original series of AMs are referred to as MxPy, in which M denotes mucic acid, x denotes each alkyl chain's total number of carbon atoms, P denotes PEG, and y refers to the PEG molecular weight in kilodaltons. Previous studies have shown that when keeping the PEG molecular weight constant, increasing the hydrophobic alkyl chain length decreases the CMC

value [13, 14]. Branching and length of the alkyl chains were demonstrated to be the key factors influencing AMs' CMC values, with M12P5 showing the lowest CMC value (1.25×10^{-7} M) among the original AMs (Table 2.2) [12].

Table 2.2 Molecular weights, melting temperatures, and CMCs of mucic acid-based AMs [12]

Sample	Mw (Da)	Tm (^{o}C)	CMC (M)
M6P2	2400	45.5	4.45×10^{-5}
M8P2	2500	46.9	4.76×10^{-6}
M10P2	2600	45.2	2.60×10^{-6}
M12P2	2800	45.4	1.27×10^{-6}
M6P5	5300	59.3	8.64×10^{-5}
M8P5	5400	57.1	7.87×10^{-6}
M10P5	5500	57.8	1.20×10^{-6}
M12P5	5900	56.4	1.25×10^{-7}

To investigate their utilities as chemotherapeutic delivery systems, the cellular internalization of AM was investigated in human umbilical vein endothelial cells (HUVECs) using a fluorescently labeled AM, fluorescein isothiocyanate (FITC)-conjugated M12P5. The FITC-M12P5 micelles were observed to internalize within the cytoplasm, endosomes, lysosomes, and nucleus within 60 mins [15]. Further studies using DOX and camptothecin (CPT) as anticancer drugs were carried out to evaluate the potential of using M12P5 as the nanocarrier. The weight loadings of CPT and DOX are 0.5% and 12%, respectively, which may be due to the different molecular sizes and hydrophobicities of the drugs. Although the CPT weight loading was rather low (0.5%), it was

still comparable to commercially available polymers such as Pluronic P85 (0.7%) and Cremophor EL (0.6%). Sizes of the drug-loaded micelles, ranging from 16 to 25 nm, demonstrated that these systems remained an appropriate size for drug delivery applications [16]. Release studies demonstrated that drug release from M12P5 micelles was sustained for more than 2 days for both drugs. However, when evaluating the potency of the drug-loaded micelles against cancer cells, no improved efficiencies compared to free chemotherapeutics were observed [17]. As the solubilization of chemotherapeutic in AMs was based on the hydrophobic interaction between the drug and the hydrophobic core of the micelles, the release of drug is mainly caused by the drug diffusion out of the micellar core. However, due to the favorable interaction between the hydrophobic core and the drug, the release rate can be slowed and impeded the anticancer efficiency. Drug release can be enhanced by applying an external trigger to the micelles.

Among the stimulus discussed in Chapter 1, pH is an important biological stimulus in the human body. For example, tumor tissue is acidic, caused by the accelerated rate of aerobic and anaerobic glycosis in cancer cells [18]. Due to the impaired vasculature and lymphatic drainage, the excretion and diffusion of lactate and other metabolic, acidic products are slowed, leading to acid accumulation within tumor tissue [19].

By incorporating pH-responsive features into drug delivery systems, a transition can be triggered to achieve quick release of the payload once the delivery vehicles are at the acidic, target sites. One strategy to establish rapid drug release is by protonation of pH-responsive blocks that form the hydrophobic core of polymeric micelle. In this approach, micelles are destabilized via two pathways: i) micelle dissociation caused by repulsion between charged groups between unimers and ii) rapid dissolution of the hydrophobic core following protonation. For example, poly(L-

histidine) is widely used as a pH-responsive polymer as it bears imidazole rings (pKa 6.5) and can be protonated in acidic media (pH <6.5) [20, 21]. Another strategy to obtain pH-triggered release is by incorporating acid labile bonds to dramatically change the polymer size in acidic media. A variety of acid labile bonds, including orthoester, hydrazone, acetal, vinyl ether, and *cis*-acotinyl bonds have been incorporated into the backbone or side chains of the polymers [22-29]. Once the polymeric micelles bearing acid labile bonds enter the acidic environment, the self-assembled micelles are disrupted following the cleavage of the acid labile bonds and the encapsulated drugs released.

In this work, pH-responsive AMs were synthesized using hydrazone bonds to link the hydrophobic segment and hydrophilic tail. Under acidic conditions, AM micelles are disrupted and the drug released. Effectiveness against cancer cells using DOX-loaded micelles are examined the ability of AMs to deliver anticancer drugs.

2.2 Results and discussion

2.2.1 Synthesis and physicochemical characterization of pH-sensitive AMs

The goal is to construct pH-sensitive AMs composed of an alkylated mucic acid backbone and a hydrophilic PEG tail with an acid-sensitive hydrazone linkage. The first step is to obtain the hydrophobic and hydrophilic segments with hydrazide and aldehyde groups, respectively, to yield the hydrazone linkage. Hydroxy-terminated PEG was subjected to Dess-Martin oxidation to give **PEG-CHO** (**1**, Figure 2.3). The oxidation was confirmed by appearance of aldehyde hydrogen in ^{1}HNMR spectra (9.60 ppm). To obtain the hydrazide group on the hydrophobic core, **2** (Figure 2.3) was activated with N-hydroxysuccinimide (NHS) via dicyclohexanecarbodiimide (DCC) coupling to prepare activated **3** (Figure 2.3). The hydrazide-functionalized precursor **4**

(Figure 2.3) was prepared by subjecting **3** (Figure 2.3) to anhydrous hydrazine. ^{1}H NMR and mass spectroscopies confirmed the chemical structure and molecular mass of hydrazide functionalized precursor (**4**, Figure 2.3). Using 0.1% trifluoroacetic acid (TFA) as a catalyst and activated molecular sieves as water adsorbents, compound **1** (Figure 2.3) was then conjugated to the precursor **4** (Figure 2.3) via the hydrazone linkage. By varying the stoichiometry, two pH-sensitive AMs with PEG chains were obtained: **AM-1** (**5**) has one PEG chain whereas **AM-2** (**6**)has two (Figure 2.3).

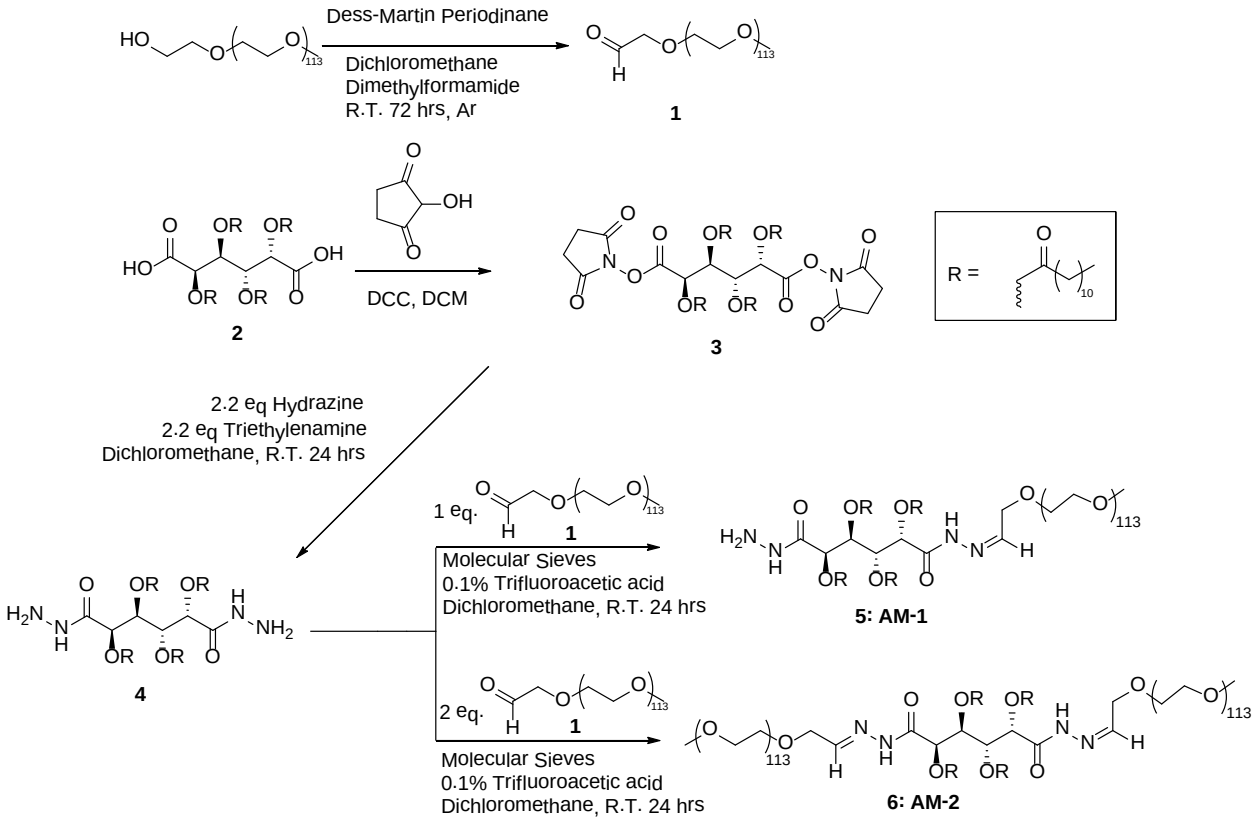

Figure 2.3 Synthetic scheme of pH-sensitive AMs

^{1}H NMR spectroscopies show the presence of the PEG methylene carbons (-OCH_2CH_2-, 3.60 ppm) in the pH-sensitive AMs. To exclude the possibility of a physical mixture of **1** and **4**,

MALDI-TOF spectroscopy was used to determine molecular weights. The molecular weights of **AM-1** (**5**) and **AM-2** (**6**) were found to be 6101 Da and 11,425 Da, respectively (Figure 2.4). Both of the MALDI-TOF and NMR results confirmed the successful coupling of PEG to the hydrophobic precursor.

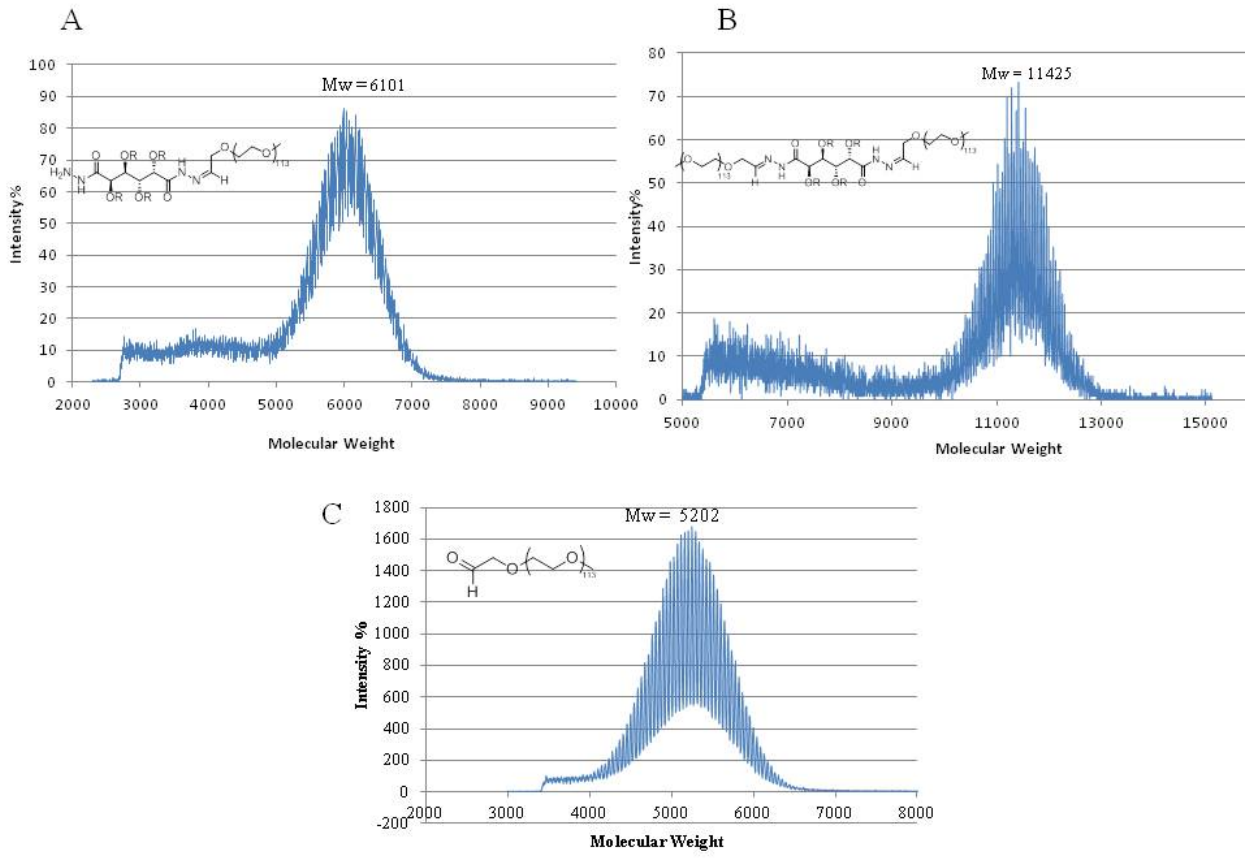

Figure 2.4 MALDI-TOF spectrum: (A) **AM-1**; (B) **AM-2**; (C) **PEG-CHO**

To study the self-assembly behavior of the AMs in aqueous media, a fluorescent assay using pyrene was used to determine the CMC values and indirectly assess micelle stability upon dilution. By partitioning into the hydrophobic core of the micelle, pyrene undergoes a shift from 332 nm to 334.5 nm in the excitation spectrum due to the polarity change of its microenvironment [12]. The fluorescent spectrum of pyrene was measured at a series of AM

concentrations (10^{-3} to 10^{-10} M). The fluorescent intensity ratios of 334.5 nm to 332 nm were calculated and plotted against the logarithm of AM concentrations (Figure 2.5). The CMC value was defined as the onset of micellization (Figure 2.5). The CMC values of **AM-1** and **AM-2** were 8.9 x 10^{-8}M and 4.4 x 10^{-6}M, respectively. **AM-2** likely had a higher CMC value than **AM-1** due its relatively higher hydrophilicity and lower solution stability. However, the CMCs of both AMs are extremely low compared to block copolymer micelles, which are typically in the range of 10^{-3}M to 10^{-5}M [10, 16]. These results indicate that these AMs could maintain micelle integrity upon dilution in physiological conditions, providing a stable carrier for hydrophobic drugs.

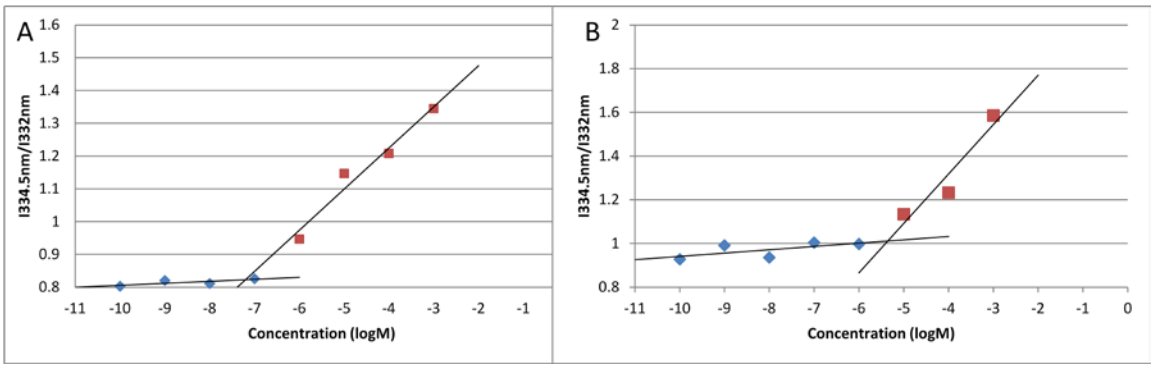

Figure 2.5 CMC values of AMs determined by fluorescent intensity ratios of pyrene excitation bands (I334.4 nm/I332 nm) as a function of concentration: (A) **AM-1** is 8.9 x 10^{-8}M and (B) **AM-2** is 4.4 x 10^{-6}M

2.2.2 Cleavage of hydrazone bond of AMs in acidic condition

As the pH-sensitive AMs are designed for enhanced release in acidic conditions, stability of AMs at lower pH values was investigated. Given that intracellular and tumor pH values range

from 4 to 6 [30], we chose pH 5 as the representative acidic condition. NMR spectroscopy was used to monitor hydrazone cleavage and appearance of AM degradation products. In the following discussion, **AM-2** will be chosen as an example. Before subjecting **AM-2** to acidic condition, **AM-2** was dissolved in $CDCl_3$ and the ^1H NMR spectra recorded (Figure 2.6A). Phosphate buffered saline at pH 5 was added to the **AM-2** solution. After incubation in the acidic media for 48 hrs, ^1H NMR spectra was recorded again (figure 2.6B). The distinctive aldehyde hydrogen peak appeared at 9.60 ppm while the methylene hydrogen of PEG appeared at 4.20 ppm. Using diethyl ether to isolate **1**, ^1H NMR and MS indicated that the other chemical structure in the media was identical to compound **4** (Figure 2.6B). Literature precedence also shows that hydrazone degrades to aldehyde and hydrazide under acidic condition [31-35]. A detailed kinetic study of hydrazone hydrolysis is suggested by monitoring the media with ^1H NMR at hourly time intervals.

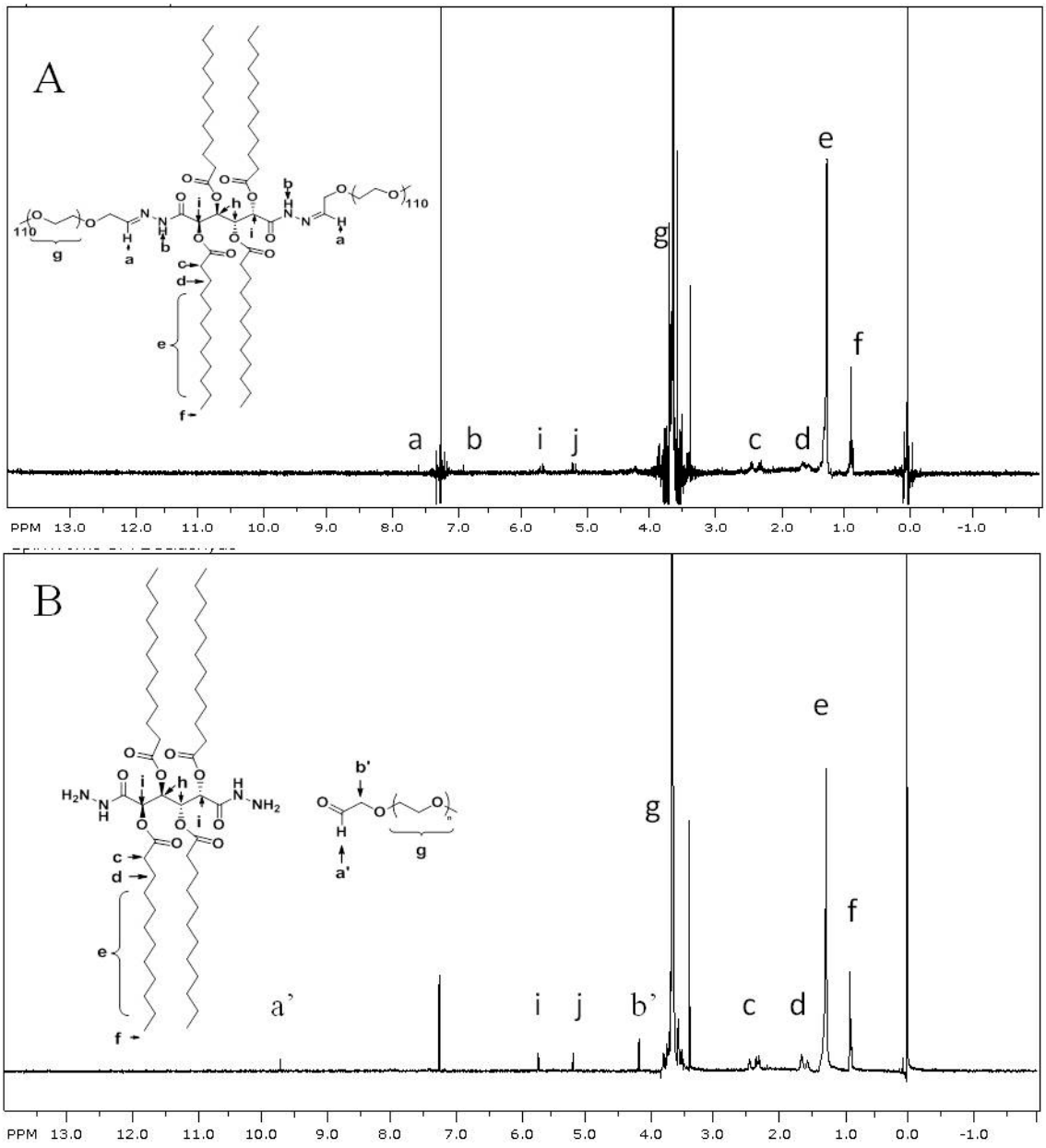

Figure 2.6 1H NMR spectra of **AM-2**: A) Neutral pH conditions and B) after 48 hrs incubation in pH 5 media

The hydrodynamic diameters of the AMs were also monitored using DLS at both pH values of 7.4 and pH 5. At pH 7.4, the micelle sizes were maintained at approximately 150 nm over 24 hrs. At pH 5, however, the micelle sizes drastically increased to approximately 800 nm and 1000 nm

within 24 hrs for **AM-1** and **AM-2**, respectively, with noticeable cloudiness in the solutions (Figure 2.7). It is hypothesized that pH-sensitive AMs degrades to compound **4** and **PEG-CHO**. Physical mixtures containing **4** and **PEG-CHO** at 1:1 and 1:2 molar ratios, end points of **AM-1** and **AM-2** degradation, were found at 4510 and 4310 nm, respectively. The sizes of **AM-1** and **AM-2** at pH 5 within 24 hrs are smaller than the physical mixtures, indicating compound **4** did not completely precipitate and cleavage of hydrazone lead to larger aggregate formation. Overall these data suggest that the AMs can form stable micelles with a favorable size range (150 to 200 nm) for cell uptake at physiological pH. However, the AMs rapidly degrade under acidic conditions, disrupting the micelles.

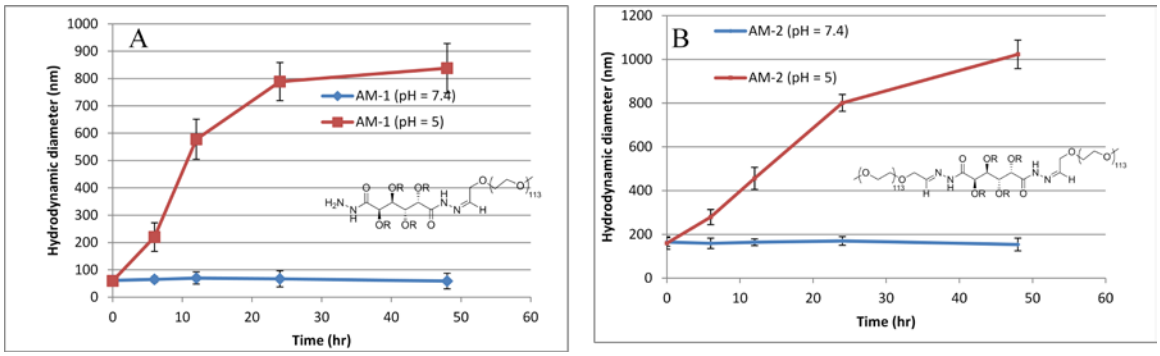

Figure 2.7 Hydrodynamic sizes of AMs as function of pH: (A) **AM-1** and (B) **AM-2** Data represent mean ± standard error (n=3).

2.2.3 DOX loading and pH-dependent release from AM micelles

To evaluate the pH-sensitivity of AMs, DOX was introduced as an anticancer drug with logP value of 1.41 to ascertain the AMs' potential in cancer therapy. The DOX weight loadings in AMs were **AM-1**, 15.1% and **AM-2**, 8.9% which are lower than DOX in other systems such as PLGA-PEG (17.8%) [36], PCL-PEG (20.3%) [37], Pluronic (16.9% - 25.1%) [38-40]. The

observed lower DOX loading in AMs is possibly due to limited hydrophobicities as other amphiphilic polymers possess larger hydrophobic polymer chain. Thus, **AM-2** has lower DOX loading than **AM-1** as the extra PEG chain decreased the relative hydrophobicity. Notably, the micelle size did not dramatically change after DOX encapsulation and maintained an appropriate size range (10 – 200 nm) for cellular uptake [41-44].

Table 2.3 DOX-loaded micelle properties. Data represent mean ± standard error (n=3).

AM	**Micelle size (nm)**	**DOX weight loading%**	**Encapsulation Efficiency%**	**DOX loaded micelle size (nm)**
AM-1	75 ± 7.2	15.1 ± 1.1	24.3 ± 0.8	89 ± 6.1
AM-2	165 ± 9.8	8.9 ± 0.7	15.8 ± 1.1	196 ± 15.8

The *in vitro* release of DOX was carried out at both physiological pH (7.4) and acidic pH (5) conditions. Approximately 20% of DOX was released after 7 days at pH 7.4 for both AMs. However, at pH 5 the DOX release was accelerated, starting at 8 hr (30% for **AM-1** and 20% **AM-2**) and nearly complete by 7 days (90% for **AM-1** and 80% for **AM-2**) (Figure 2.8). The enhanced release of DOX at pH 5 is due to the cleavage of the acid-labile hydrazone bond, leading to micelle disruption. The pH-dependent release profile of DOX indicates that the AMs may maintain the DOX integrity in physiological pH, yet release the drug in acidic pH. This finding suggests that these pH-sensitive AMs have potential use for anticancer drug delivery tumor tissue express acidic environment.

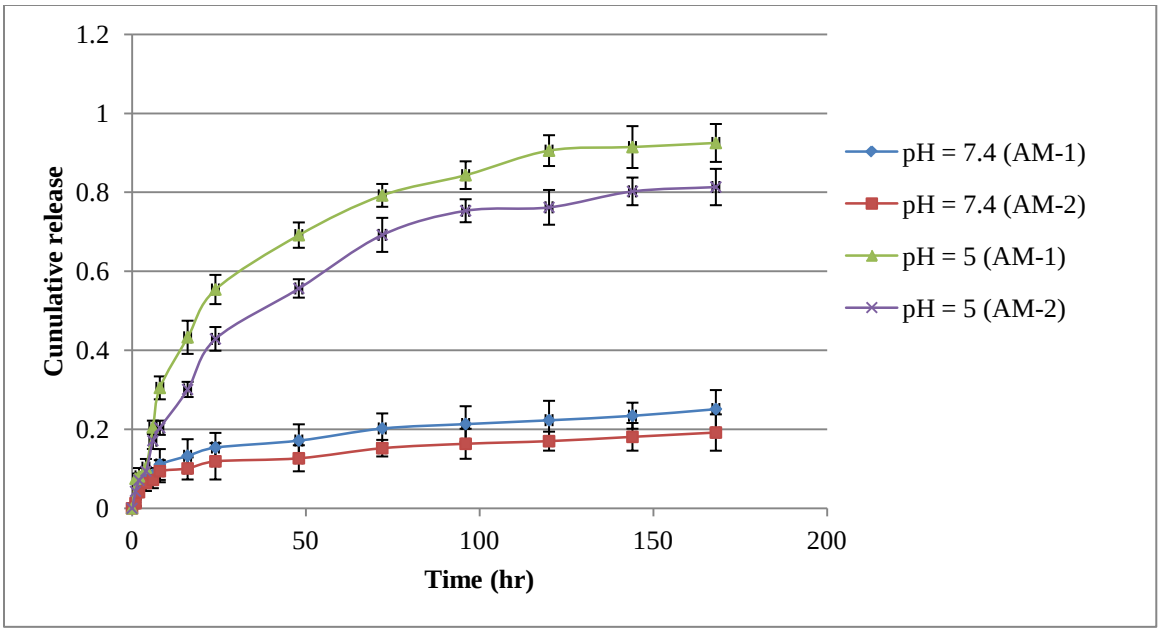

Figure 2.8 DOX release from drug-loaded micelles at different pHs: physiological pH 7.4 and representative intracellular pH 5. Data represent mean ± standard error (n=3).

2.2.4 *In vitro* cytotoxicity assay of DOX-loaded micelles *(Performed by Leora Nusblat)*

MDA-MB-231 cell line is a breast cancer cell line that is readily targeted by DOX [45-47]. Thus cytotoxicity against MDA-MB-231 cells was conducted with DOX-loaded micelles (pH-sensitive AMs and M12P5 as the non-responsive control) and free DOX. Over 48 hrs, **AM-1**/DOX and **AM-2**/DOX decreased cell viability compared to the control, M12P5/DOX (Figure 2.9). The lower efficiency of M12P5/DOX is likely due to the fact that M12P5 is not pH-sensitive to lower pH values and does not release sufficient DOX. In contrast, **AM-1** and **AM-2** can degrade at lower pH and release the DOX. The free DOX showed 70% cell viability due to the insufficient intracellular uptake, as suggested by literature precedence [48-50].

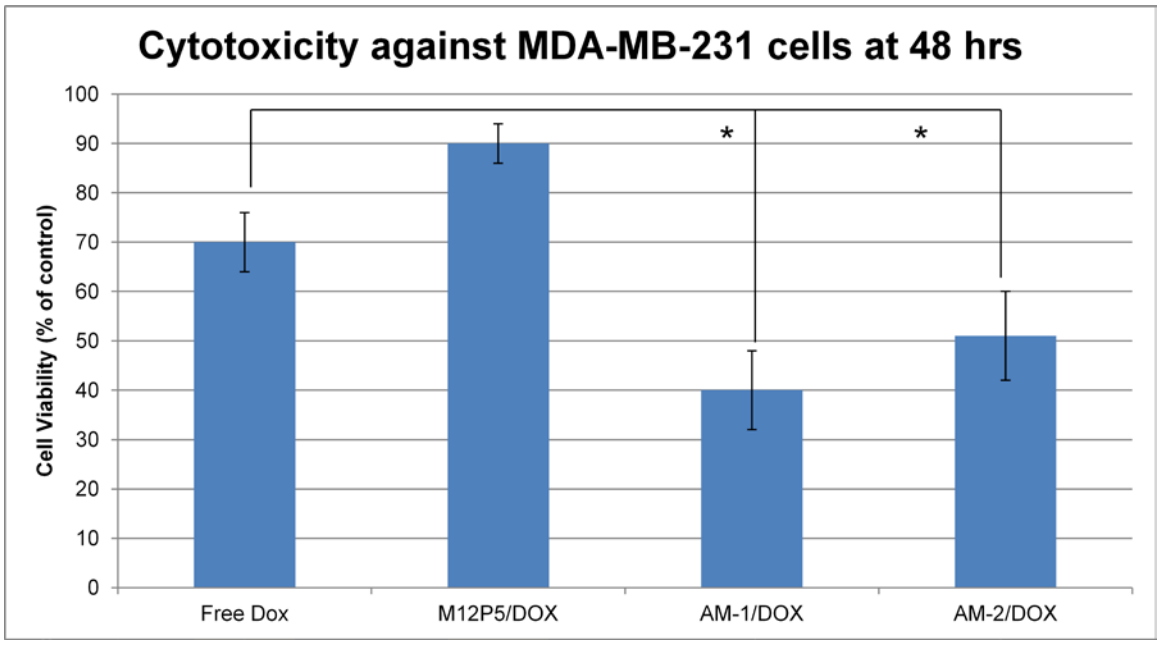

Figure 2.9 Cytotoxicity of DOX-loaded micelles against MDA-MB-231 breast cancer cell lines at 48 hrs using free DOX as the control. Asterisks indicate that both **AM-1**/DOX and **AM-2**/DOX significantly decrease cell viability relative to free DOX ($p < 0.05$). Data represent mean ± standard error (n=3).

2.3 Conclusion

Two pH-sensitive AMs were synthesized with a hydrazone linkage to adjoin the hydrophobic and hydrophilic segments. ^{1}H NMR spectra and MALDI data were used to characterize the AMs' chemical structures. Hydrodynamic diameters of the AMs are within an optimal range for cellular uptake (100 – 200 nm), and CMC values are 10^{-8}-10^{-6}M indicating that micelles should be stable upon dilution. The degradation products of the AMs after incubation in acidic conditions were identified using MS, ^{1}H NMR and DLS methods. As an anticancer drug, DOX was encapsulated in AMs and a pH-dependent drug release profile observed. Cytotoxicity studies against MDA-MB-231 breast cancer cells showed that pH-sensitive AMs decreased cell viability

compared to the controll AM and free DOX. The *in vitro* data indicates that pH-sensitive AMs may be an effective anticancer drug carrier as it may resolve the dilemma between stability in physiological conditions and rapid drug release at tumor sites.

2.4 Experimental procedures

2.4.1 Materials

Spectra/Por dialysis tubing (MWCO 3500 Da and MWCO 7000 Da) were purchased from Fisher Scientific (Atlanta, GA). Dialysis cassettes (MWCO 7000 Da) were purchased from Thermo Scientific (Rockford, IL). Syringes were purchased from Beckton Dickinson (Franklin Lakes, NJ). Compound **1** (Scheme 1) was synthesized via a previously reported method [51]. mPEG-OH was purchased from Creative PEGworks (Winston-Salem, NC). Molecular sieves were activated by heating at 300 ºC for 4 hrs before use. All other reagents were purchased from Sigma-Aldrich (St. Louis, MO) and used without further purification.

2.4.2 Methods

2.4.2.1 Physicochemical characterization methods

^{1}H NMR spectra measurements were taken at 25 ºC on a Varian 400 MHz spectrometer using deuterated chloroform ($CDCl_3$) as a solvent and tetramethylsilane as an internal standard. Mass spectra were obtained on a Finnigan LDQ-DUO equipped with an adjustable atmospheric pressure ionization-electrospray ionization (API-ESI) Ion source. FTIR spectra were recorded on a Thermo Nicolet/Avatar 360 spectrometer using sample discs compressed with potassium bromide (KBr). Molecular weights of the polymers were determined by MALDI mass spectrometry using an ABI-MDS SCIEX 4800 MALDI-TOF/TOF mass spectrometer. CMC

measurements were carried out on a Spex FluoroMax pectrofluorometer (Piscataway, NJ) at 25^{o}C using pyrene as the probe molecule. Hydrodynamic diameters of the micelle were measured by DLS with a Malvern Zetasizer Nano ZS90. DLS measurements were conducted in a 1.0 mL quartz cuvette using a diode laser of 800 nm at 25 ºC and a scattering angle of 90º. Buffer solutions were prepared at pH 7.4 (phosphate buffered saline) and 5.0 (phosphate citrate buffer), and were filtered through 0.45 µm polytetrafluoroethylene filters. Centrifugation was carried out in EBA12 Zentrifugen (Hettich, Germany) centrifuge with 3000 rpm for 5 mins.

2.4.2.2 Synthesis of mPEG-CHO (1, Figure 2.3)

mPEG-OH (1.00 g, 0.200 mmol) and Dess-Martin Periodinane (DMP) (0.424 g, 1.00 mmol) were dissolved in anhydrous dichloromethane (DCM) (15 mL) and anhydrous dimethylformamide (DMF) (5.0 mL). The reaction mixture was allowed to stir for 72 hrs under argon at room temperature then filtered to remove precipitates using vacuum filtration. The filtrate was washed once with hydrochloric acid (HCl) (0.1 M, 100 mL) and twice with brine. Organic layer was dried over magnesium sulfate ($MgSO_4$), filtered, and the filtrate was collected and dried to obtain crude product as viscous oil using rotary evaporation. The crude product was dissolved in ~3 mL DCM and transferred to a 50 mL centrifuge tube. The final product was precipitated by adding diethyl ether (~47 mL) to the centrifuge tube and collected by centrifugation at 3000 rpm for 5 min. The supernatant was decanted and the remaining white product washed twice with diethyl ether. The product was then dried under ambient conditions overnight, then overnight again under high vacuum. Yield% = 71.4% (white powder, 0.709 g). ^{1}H-NMR (400 MHz, $CDCl_3$): (δ) 9.60 (t, 1H, CHO), 4.03 (d, 2H, CH_2), 3.60 (m, ~500H, CH_2),

3.23 (t, 3H, CH_3). GPC: Mw = 5300, PDI = 1.09. Calculated Mw = 4998. IR (KBr, cm^{-1}): 1725 (vs C=O aldehyde).

2.4.2.3 Synthesis of NHS-functionalized M12 (3, Figure 2.3)

Precursor **2** (0.500 g, 0.532 mmol) and NHS (0.612 g, 5.32 mmol) were dissolved in DCM (20 mL) and DMF (5 mL). The reaction mixture was stirred for 30 minutes to complete dissolution. DCC solution (1.50 mL, 1.50 mmol) was then added drop-wise to the reaction mixture. The resulting solution was allowed to stir for 24 hrs at room temperature under argon. The filtrate was washed once with hydrochloric acid (HCl) (0.1 M, 100 mL) and twice with brine. Organic layer was dried over magnesium sulfate ($MgSO_4$), filtered, and the filtrate was collected and dried to obtain final product as white solid using rotary evaporation. The product **3** was then dried under ambient conditions for one night followed by another night under high vacuum. Yield% = 56.0% (white solid, 0.338 g). ^{1}H-NMR (400 MHz, CDCl3): (δ) 5.67 (s, 2H, CH), 5.13 (s, 2H, CH), 2.80 (t, 8H, CH_2), 2.45 (t, 4H, CH_2), 2.23 (t, 4H, CH_2), 1.65 (m, 4H, CH_2), 1.57 (m, 4H, CH_2), 1.31 (m, 64H, CH_2), 0.91 (t, 12H, CH_3). IR (KBr, cm^{-1}): 1750 (vs C=O ester), 1730 (vs C=O ester). ESI-MS: *m/z* 1128.4 (M+H). Calculated Mw = 978.34.

2.4.2.4 Synthesis of hydrazide-functionalized precursor 4 (Figure 2.3)

NHS-functionalized precursor **3** (0.200 g, 0.177 mmol) was dissolved in DCM (10 mL) and DMF (5 mL). Anhydrous hydrazine (0.0310 mL, 1.00 mmol) was then added to the reaction mixture. After 24 hrs, the reaction mixture was washed once with hydrochloric HCl (0.1 M, 50 mL) and twice with brine (50 mL) for two times. The organic layer was dried over magnesium sulfate ($MgSO_4$), filtered, and the filtrate was collected and dried to obtain the final product as

yellow solid using rotary evaporation. The product **4** was then dried under ambient conditions for one night followed by another night under high vacuum. Yield% = 61.4% (yellow solid, 0.117 g). ^{1}H-NMR (400 MHz, CDCl3): (δ) 5.80 (s, 2H, CH), 5.23 (s, 2H, CH), 2.45 (t, 4H, CH_2), 2.23 (t, 4H, CH_2), 1.65 (m, 4H, CH_2), 1.57 (m, 4H, CH_2), 1.31 (m, 64H, CH_2), 0.91 (t, 12H, CH_3). IR (KBr, cm^{-1}): 1750 (vs C=O ester), 1680 (vs C=O hydrazide). ESI-MS: *m/z* 967.8 (M+H). Calculated Mw: 966.8.

2.4.2.5 Synthesis of pH-sensitive AM-1 (5, Figure 2.3)

Hydrazide-functionalized precursor **4** (Figure 2.2) (0.080 g, 0.082 mmol) was dissolved in DCM (10 mL) and DMF (3 mL) with mPEG-CHO (138 mg, 0.0280 mmol). Activated molecular sieves and 0.1% TFA (6.3 µL, 0.082 µmol) were then added to the solution, and the reaction was stirred for 24 hrs at room temperature under argon. The molecular sieves were then removed via vacuum filtration and the filtrate was concentrated *in vacuo*. The resulting viscous oil was dissolved in ~3 mL DCM and transferred to a 50 mL centrifuge tube. Product **4** was precipitated by adding diethyl ether (~47 mL) to the centrifuge tube and collected by centrifugation at 3000 rpm for 5 min. The supernatant was decanted and the remaining white product was washed twice with diethyl ether. AM-1 (**5**) was then dried under ambient conditions one night, then another night under high vacuum. Yield% = 65.0 % (white powder, 106 mg). ^{1}H-NMR (400 MHz, CDCl3): (δ) 5.82 (s, 2H, CH), 5.26 (s, 2H, CH), 3.60 (m, ~500H, CH_2), 2.43 (t, 4H, CH_2), 2.24 (t, 4H, CH_2), 1.67 (m, 4H, CH_2), 1.59 (m, 4H, CH_2), 1.34 (m, 64H, CH_2), 0.91 (t, 12H, CH_3). IR (KBr, cm^{-1}): 1610 (s C=N hydrazone).GPC: Mw = 6800, PDI = 1.11. Calculated Mw = 5904.32

2.4.2.6 Synthesis of pH-sensitive AM-2 (6, Figure 2.3)

Hydrazide-functionalized precursosr **4** (Figure 2.2.1.1) (0.080 g, 0.082 mmol) was dissolved in DCM (10 mL) and DMF (3 mL) with mPEG aldehyde (0.820 g, 0.164 mmol). Activated molecular sieves and 0.1% TFA (12.6 µL, 0.164 µmol) were then added to reaction mixture, and stirred for 24 hrs at room temperature under argon. The molecular sieves were removed via vacuum filtration and the filtrate was concentrated *in vacuo*. The resulting viscous oil was dissolved in ~3 mL DMF and dialyzed (MWCO 7000) against deionized water for 48 hrs. The white product **6** was collected by lyophilization. Yield% = 56.2% (white powder, 0.504 g). ^{1}H-NMR (400 MHz, $CDCl_3$): (δ) 5.80 (s, 2H, CH), 5.23 (s, 2H, CH), 3.63 (m, ~1100H, CH2), 2.45 (t, 4H, CH2), 2.25 (t, 4H, CH2), 1.69 (m, 4H, CH2), 1.57 (m, 4H, CH2), 1.31 (m, 64H, CH2), 0.91 (t, 12H, CH3). IR (KBr, cm^{-1}): 1610 (s C=N hydrazone). GPC: Mw = 12300, PDI = 1.12. Calculated Mw = 11076.34

2.4.3 CMC measurements

A solution of pyrene, the fluorescence probe molecule, was made up to a concentration of 5×10^{-6} M in acetone. Samples were prepared by adding 1 mL of pyrene solution to a series of vials and allowing the acetone to evaporate so that the final concentration of pyrene in all of the samples was 5×10^{-7} M. AMs were dissolved in HPLC grade water and diluted to a series of concentrations from 1×10^{-3} M to 1×10^{-10} M. AM-pyrene solutions (10 mL) were incubated overnight at 37 °C with agitation at 60 rpm using a controlled environment incubator shaker (New Brunswick Scientific Co., Edison, NJ) to allow partition of the pyrene into the micelles. Excitation was performed from 300 to 360 nm, with 390 nm as the emission wavelength. The maximum absorption of pyrene shifted from 332 to 334.5 nm on micelle formation. The

fluorescent intensity ratios of 334.5 nm to 332 nm were calculated and plotted against the logarithm of AM concentrations.

2.4.4 AM degradation in acidic condition

AM was dissolved with $CDCl_3$ (0.75 mL) in the NMR tube, and ^1H NMR was recorded. PBS buffer (0.5mL) with pH 5 was added to the AM/CDCl3 solution. The solution was allowed to incubate for 24 hrs at 37^oC with agitation at 60 rpm using a controlled environment incubator shaker (New Brunswick Scientific Co. Edison, NJ). ^1H NMR was recorded for the solution again.

2.4.5 Micelle formulation and DOX encapsulation

AM (10 mg) was first dissolved in DMF (10 mL), and deionized water (2 mL) was then added drop wise to the polymer solution with vigorous stirring. The resulting solution was dialyzed against deionized water for 48 hrs using cellulose dialysis membranes (MWCO 3500 Da). Deionized water was replaced every 2 hrs for the first 12 hrs and every 6 hrs thereafter. To prepare DOX-loaded micelles, polymer was co-dissolved with DOX (5 mg) in a similar fashion as with the blank micelles. The resulting solutions were dialyzed against deionized water for 48 hrs using cellulose dialysis membranes (MWCO 3500 Da). To measure the weight loading of DOX, the lyophilized micelle samples were dissolved in THF/Methanol (1/1 V/V) and analyzed by high-performance liquid chromatography (HPLC). The mobile phase was comprised of 100% acetonitrile and run at 1 mL/min flow rate at 35 ^oC. Samples were filtered using 0.45 μm PTFE syringe filters and subsequently injected (20 μL) using an autosampler. DOX absorbed at 349 nm with a retention time of 3.8 min. No absorption of AMs or relevant degradation products was

observed. DOX concentration was calculated from a calibration curve of known DOX standard solutions. The experiment was carried out in triplicate.

2.4.6 DOX release from the micelles

Dialysis cassettes (MWCO 7000) loaded with 2.5 mL of DOX-encapsulated micelles were placed in a sealed container with 60 mL of buffer (pH 7.4 or pH 5) and incubated at 37 ºC with agitation at 60 rpm using a controlled environment incubator-shaker (New Brunswick Scientific Co., Edison, NJ). 20 mL of release media was collected and replaced with 20 mL of fresh media at desired time intervals. The collected release media was lyophilized and dissolved in 1 mL THF/Methanol (1/1 V/V) for HPLC analysis. An XTerra® RP18 5 μm 4.6x150 mm column (Waters, Milford, MA) on a Waters 2695 Separations Module equipped with a Waters 2487 Dual λ Absorbance Detector was used to analyze and quantify vitamin E release. The mobile phase was comprised of 100% acetonitrile and run at 1 mL/min flow rate at 25 ^{o}C. Samples were filtered using 0.45 μm PTFE syringe filters and subsequently injected (20 μL) using an autosampler. DOX absorbed at 348 nm with a retention time of 3.8 min. No absorption of AMs or relevant degradation products was observed. DOX release was calculated from a calibration curve of known DOX standard solutions. The release study was carried out in triplate.

2.4.7 Cytotoxicity studies *(Performed by Leora Nusblat)*

MDA-MB-231 cells were plated in 96-well plates at a density of 10^4 cells per well in Dulbecco modified eagle's media (DMEM) + 10% fetal bovine serum (FBS) and incubated overnight in a 37^oC, 5% CO_2 incubator. AMs were prepared at a concentration of 2 mg/ml with 40 ug/ml DOX

loaded. Cells were transfected with AMs at a concentration of 2 nM in PBS. After 48 hrs, an MTS (3-(4,5-dimethylthiazol-2-yl)-5-(3-carboxymethoxyphenyl)-2-(4-sulfophenyl)-2H-tetrazolium) assay was performed and the absorbance at 450 nm was measured by a DTX880 Multimode Detector microplate reader (Beckman Coulter). Cell viability was normalized to that of MDA-MB-231 cells with PBS treatment. The experiment was carried out in biological triplicate.

2.5 References

[1] W. Steiner. Therapy of Hypopharyngeal Cancer. Part I. Review of the Literature: Surgery and/or Radiotherapy. *HNO* **1994** *42* 4-13.
[2] M. Tsubokura, Y. Miura, T. Itokawa, N. Takei, T. Higaki, T. Amaki, Y. Ishida, M. Kusama, S. Ono, H. Narimatsu, M. Kami, T. Komatsu. Failure of Liver Function Tests in Predicting Drug Clearance of Chemotherapeutic Agents in a Patient Who Had Recovered from Hepatic Congestion. *Br J Clin Pharmacol* **2010** *70* 277-279.
[3] Y. Iitsuka, Y. Tanaka, T. Hosono-Fukao, T. Hosono, T. Seki, T. Ariga. Relationship between Lipophilicity and Inhibitory Activity against Cancer Cell Growth of Nine Kinds of Alk(En)Yl Trisulfides with Different Side Chains. *Oncol Res* **2010** *18* 575-582.
[4] G. Aubel-Sadron, D. Londos-Gagliardi. Daunorubicin and Doxorubicin, Anthracycline Antibiotics, a Physicochemical and Biological Review. *Biochimie* **1984** *66* 333-352.
[5] A. Trouet, D. Deprez-De Campeneere. Daunorubicin-DNA and Doxorubicin-DNA. A Review of Experimental and Clinical Data. *Cancer Chemother Pharmacol* **1979** *2* 77-79.
[6] S.T. Duggan, G.M. Keating. Pegylated Liposomal Doxorubicin: A Review of Its Use in Metastatic Breast Cancer, Ovarian Cancer, Multiple Myeloma and Aids-Related Kaposi's Sarcoma. *Drugs* **2011** *71* 2531-2558.
[7] J. Greidanus, P.H. Willemse, D.R. Uges, E.T. Oremus, Z.J. De Langen, E.G. De Vries. Continuous Infusion of Low-Dose Doxorubicin, Epirubicin and Mitoxantrone in Cancer Chemotherapy: A Review. *Pharm Weekbl Sci* **1988** *10* 237-245.
[8] M.L. Tan, P.F. Choong, C.R. Dass. Review: Doxorubicin Delivery Systems Based on Chitosan for Cancer Therapy. *J Pharm Pharmacol* **2009** *61* 131-142.
[9] C.E. Ashley, E.C. Carnes, G.K. Phillips, D. Padilla, P.N. Durfee, P.A. Brown, T.N. Hanna, J. Liu, B. Phillips, M.B. Carter, N.J. Carroll, X. Jiang, D.R. Dunphy, C.L. Willman, D.N. Petsev, D.G. Evans, A.N. Parikh, B. Chackerian, W. Wharton, D.S. Peabody, C.J. Brinker. The Targeted Delivery of Multicomponent Cargos to Cancer Cells by Nanoporous Particle-Supported Lipid Bilayers. *Nat Mater* **2011** *10* 389-397.
[10] C. Oerlemans, W. Bult, M. Bos, G. Storm, J.F. Nijsen, W.E. Hennink. Polymeric Micelles in Anticancer Therapy: Targeting, Imaging and Triggered Release. *Pharm Res* **2010** *27* 2569-2589.

[11] Y. Matsumura, K. Kataoka. Preclinical and Clinical Studies of Anticancer Agent-Incorporating Polymer Micelles. *Cancer Sci* **2009** *100* 572-579.
[12] L.Y. Tian, L.; Zhou, N.; Tat, H.; Uhrich, K. E. Amphiphilic Scorpion-Like Macromolecules: Design, Synthesis, and Characterization. *Macromolecules* **2004** *37* 5-11.
[13] B. Bhhatarai, P. Gramatica. Prediction of Aqueous Solubility, Vapor Pressure and Critical Micelle Concentration for Aquatic Partitioning of Perfluorinated Chemicals. *Environ Sci Technol* **2011** *45* 8120-8128.
[14] K.C. Huang, C.M. Lin, H.K. Tsao, Y.J. Sheng. The Interactions between Surfactants and Vesicles: Dissipative Particle Dynamics. *J Chem Phys* **2009** *130* 245101-245108.
[15] J.D.R. Djordjevic, L.; Wang, J.; Uhrich, K.E. Amphiphilic Scorpion-Like Macromolecules as Micellar Nanocarriers. *Journal of Bioactive and Compatible Polymers* **2008** *23* 20-28.
[16] S.R. Croy, G.S. Kwon. Polymeric Micelles for Drug Delivery. *Curr Pharm Des* **2006** *12* 4669-4684.
[17] L.S. del Rosario, B. Demirdirek, A. Harmon, D. Orban, K.E. Uhrich. Micellar Nanocarriers Assembled from Doxorubicin-Conjugated Amphiphilic Macromolecules (Dox-Am). *Macromol Biosci* **2010** *10* 415-423.
[18] E.S. Lee, Z. Gao, Y.H. Bae. Recent Progress in Tumor Ph Targeting Nanotechnology. *J Control Release* **2008** *132* 164-170.
[19] I.F. Tannock, D. Rotin. Acid Ph in Tumors and Its Potential for Therapeutic Exploitation. *Cancer Res* **1989** *49* 4373-4384.
[20] J. Hu, S. Miura, K. Na, Y.H. Bae. Ph-Responsive and Charge Shielded Cationic Micelle of Poly(L-Histidine)-Block-Short Branched Pei for Acidic Cancer Treatment. *J Control Release* **2013** *172* 69-76.
[21] H. Yin, Y.H. Bae. Physicochemical Aspects of Doxorubicin-Loaded Ph-Sensitive Polymeric Micelle Formulations from a Mixture of Poly(L-Histidine)-B-Poly(Ethylene Glycol)/Poly(L-Lactide)-B-Poly(Ethylene Glycol) [Corrected]. *Eur J Pharm Biopharm* **2009** *71* 223-230.
[22] T. Jiang, Y.M. Li, Y. Lv, Y.J. Cheng, F. He, R.X. Zhuo. Amphiphilic Polycarbonate Conjugates of Doxorubicin with Ph-Sensitive Hydrazone Linker for Controlled Release. *Colloids Surf B Biointerfaces* **2013** *111C* 542-548.
[23] R. Liu, Y. Zhang, X. Zhao, A. Agarwal, L.J. Mueller, P. Feng. Ph-Responsive Nanogated Ensemble Based on Gold-Capped Mesoporous Silica through an Acid-Labile Acetal Linker. *J Am Chem Soc* **2010** *132* 1500-1501.
[24] A. Schlossbauer, C. Dohmen, D. Schaffert, E. Wagner, T. Bein. Ph-Responsive Release of Acetal-Linked Melittin from Sba-15 Mesoporous Silica. *Angew Chem Int Ed Engl* **2011** *50* 6828-6830.
[25] M. Gumusderelioglu, D. Kesgin. Release Kinetics of Bovine Serum Albumin from Ph-Sensitive Poly(Vinyl Ether) Based Hydrogels. *Int J Pharm* **2005** *288* 273-279.
[26] J. Shin, P. Shum, J. Grey, S. Fujiwara, G.S. Malhotra, A. Gonzalez-Bonet, S.H. Hyun, E. Moase, T.M. Allen, D.H. Thompson. Acid-Labile Mpeg-Vinyl Ether-1,2-Dioleylglycerol Lipids with Tunable Ph Sensitivity: Synthesis and Structural Effects on Hydrolysis Rates, Dope Liposome Release Performance, and Pharmacokinetics. *Mol Pharm* **2012** *9* 3266-3276.
[27] H.S. Yoo, E.A. Lee, T.G. Park. Doxorubicin-Conjugated Biodegradable Polymeric Micelles Having Acid-Cleavable Linkages. *J Control Release* **2002** *82* 17-27.
[28] R. Tang, W. Ji, D. Panus, R.N. Palumbo, C. Wang. Block Copolymer Micelles with Acid-Labile Ortho Ester Side-Chains: Synthesis, Characterization, and Enhanced Drug Delivery to Human Glioma Cells. *J Control Release* **2011** *151* 18-27.

[29] R. Tang, W. Ji, C. Wang. Amphiphilic Block Copolymers Bearing Ortho Ester Side-Chains: Ph-Dependent Hydrolysis and Self-Assembly in Water. *Macromol Biosci* **2010** *10* 192-201.
[30] J.X. Xu, J.B. Tang, L.H. Zhao, Y.Q. Shen. Advances in the Study of Tumor Ph-Responsive Polymeric Micelles for Cancer Drug Targeting Delivery. *Yao Xue Xue Bao* **2009** *44* 1328-1335.
[31] A.A. Kale, V.P. Torchilin. Design, Synthesis, and Characterization of Ph-Sensitive Peg-Pe Conjugates for Stimuli-Sensitive Pharmaceutical Nanocarriers: The Effect of Substitutes at the Hydrazone Linkage on the Ph Stability of Peg-Pe Conjugates. *Bioconjug Chem* **2007** *18* 363-370.
[32] G.R. Braslawsky, K. Kadow, J. Knipe, K. McGoff, M. Edson, T. Kaneko, R.S. Greenfield. Adriamycin(Hydrazone)-Antibody Conjugates Require Internalization and Intracellular Acid Hydrolysis for Antitumor Activity. *Cancer Immunol Immunother* **1991** *33* 367-374.
[33] J.L. Buss, P. Ponka. Hydrolysis of Pyridoxal Isonicotinoyl Hydrazone and Its Analogs. *Biochim Biophys Acta* **2003** *1619* 177-186.
[34] M. Gandomkar, R. Najafi, M. Shafiei, S.E. Ebrahimi. Confirmation of Hydrazone Formation in Hynic-Peptide Conjugate Preparation, and Its Hydrolysis During Labeling with (99m)Tc. *Appl Radiat Isot* **2007** *65* 805-808.
[35] C.C. Lee, A.T. Cramer, F.C. Szoka, Jr., J.M. Frechet. An Intramolecular Cyclization Reaction Is Responsible for the in Vivo Inefficacy and Apparent Ph Insensitive Hydrolysis Kinetics of Hydrazone Carboxylate Derivatives of Doxorubicin. *Bioconjug Chem* **2006** *17* 1364-1368.
[36] S.M. Mo, I.J. Oh. Release of Adriamycin from Poly(Lactide-Co-Glycolide)-Polyethylene Glycol Nanoparticles. *J Nanosci Nanotechnol* **2011** *11* 1795-1798.
[37] Y.Y. Diao, H.Y. Li, Y.H. Fu, M. Han, Y.L. Hu, H.L. Jiang, Y. Tsutsumi, Q.C. Wei, D.W. Chen, J.Q. Gao. Doxorubicin-Loaded Peg-Pcl Copolymer Micelles Enhance Cytotoxicity and Intracellular Accumulation of Doxorubicin in Adriamycin-Resistant Tumor Cells. *Int J Nanomedicine* **2011** *6* 1955-1962.
[38] G.A. Husseini, D.A. Christensen, N.Y. Rapoport, W.G. Pitt. Ultrasonic Release of Doxorubicin from Pluronic P105 Micelles Stabilized with an Interpenetrating Network of N,N-Diethylacrylamide. *J Control Release* **2002** *83* 303-305.
[39] Y. Tian, P. Ravi, L. Bromberg, T.A. Hatton, K.C. Tam. Synthesis and Aggregation Behavior of Pluronic F87/Poly(Acrylic Acid) Block Copolymer in the Presence of Doxorubicin. *Langmuir* **2007** *23* 2638-2646.
[40] M. Ugarenko, C.K. Chan, A. Nudelman, A. Rephaeli, S.M. Cutts, D.R. Phillips. Development of Pluronic Micelle-Encapsulated Doxorubicin and Formaldehyde-Releasing Prodrugs for Localized Anticancer Chemotherapy. *Oncol Res* **2009** *17* 283-299.
[41] Z.G. Gao, D.H. Lee, D.I. Kim, Y.H. Bae. Doxorubicin Loaded Ph-Sensitive Micelle Targeting Acidic Extracellular Ph of Human Ovarian A2780 Tumor in Mice. *J Drug Target* **2005** *13* 391-397.
[42] J.H. Jeong, S.H. Kim, S.W. Kim, T.G. Park. Intracellular Delivery of Poly(Ethylene Glycol) Conjugated Antisense Oligonucleotide Using Cationic Lipids by Formation of Self-Assembled Polyelectrolyte Complex Micelles. *J Nanosci Nanotechnol* **2006** *6* 2790-2795.
[43] V.A. Sethuraman, M.C. Lee, Y.H. Bae. A Biodegradable Ph-Sensitive Micelle System for Targeting Acidic Solid Tumors. *Pharm Res* **2008** *25* 657-666.
[44] J. Wang, D. Mongayt, V.P. Torchilin. Polymeric Micelles for Delivery of Poorly Soluble Drugs: Preparation and Anticancer Activity in Vitro of Paclitaxel Incorporated into Mixed Micelles Based on Poly(Ethylene Glycol)-Lipid Conjugate and Positively Charged Lipids. *J Drug Target* **2005** *13* 73-80.

[45] J.M. Escoffre, J. Piron, A. Novell, A. Bouakaz. Doxorubicin Delivery into Tumor Cells with Ultrasound and Microbubbles. *Mol Pharm* **2011** *8* 799-806.
[46] S.M. Lee, R.W. Ahn, F. Chen, A.J. Fought, T.V. O'Halloran, V.L. Cryns, S.T. Nguyen. Biological Evaluation of Ph-Responsive Polymer-Caged Nanobins for Breast Cancer Therapy. *ACS Nano* **2010** *4* 4971-4978.
[47] S. Leong, M.J. McKay, R.I. Christopherson, R.C. Baxter. Biomarkers of Breast Cancer Apoptosis Induced by Chemotherapy and Trail. *J Proteome Res* **2012** *11* 1240-1250.
[48] M. Huan, B. Zhang, Z. Teng, H. Cui, J. Wang, X. Liu, H. Xia, S. Zhou, Q. Mei. In Vitro and in Vivo Antitumor Activity of a Novel Ph-Activated Polymeric Drug Delivery System for Doxorubicin. *PLoS One* **2012** *7* e44116.
[49] C. Kojima, T. Suehiro, K. Watanabe, M. Ogawa, A. Fukuhara, E. Nishisaka, A. Harada, K. Kono, T. Inui, Y. Magata. Doxorubicin-Conjugated Dendrimer/Collagen Hybrid Gels for Metastasis-Associated Drug Delivery Systems. *Acta Biomater* **2013** *9* 5673-5680.
[50] Y.X. Zhao, A. Shaw, X. Zeng, E. Benson, A.M. Nystrom, B. Hogberg. DNA Origami Delivery System for Cancer Therapy with Tunable Release Properties. *ACS Nano* **2012** *6* 8684-8691.
[51] L. Tian, L. Yam, N. Zhou, H. Tat, K.E. Uhrich. Amphiphilic Scorpion-Like Macromolecules: Design, Synthesis, and Characterization. *Macromolecules* **2004** *37* 538-543.

3 Cationic Amphiphilic Macromolecule - Lipid for siRNA Delivery

3.1 Introduction

3.1.1 siRNA therapy

Short interfering ribonucleic acid (siRNA) was first discovered in 1998 [1] as an important molecule for suppression of protein expression in the RNA interference (RNAi) pathway [1-4]. The robustness of the siRNA approach has motivated a large amount of work in the development of different classes of therapeutic agents [5-8]. siRNA has two RNA strands, a sense strand and an anti-sense strand, each consisting of 21-23 base pairs [9-11] that bind to each other in a complementary fashion. siRNAs are derived from either long double-stranded RNA (dsRNA) or short hairpin RNA that have been introduced into the cell [12-15].

In the first step of the RNAi pathway (Figure 3.1), a long dsRNA is cleaved into siRNA by the Dicer enzyme [1, 2, 9]. The siRNA is then incorporated into the nuclease to form the RNAi silencing complex (RISC). RISC facilitates the unwinding of the siRNA duplex and helps deliver the anti-sense strand of the siRNA duplex to a complementary sequence found on messenger RNA (mRNA). This interaction causes mRNA to be cleaved by RISC, leading to the “silencing” of a specific gene [16-19]. Current research suggests that a significant benefit of siRNA is that it is more efficient at gene suppression and less toxic than other nucleotide therapeutics [20, 21].

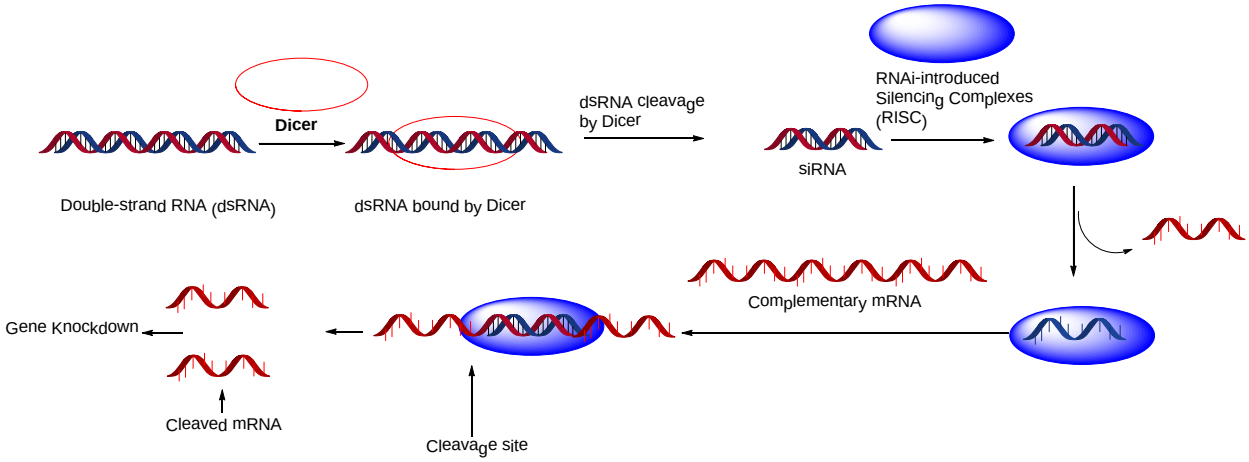

Figure 3.1 General mechanism for siRNA down-regulation via the RNAi pathway[22]

3.1.2 siRNA delivery

In siRNA delivery to the cytosol, there are two types of challenges. The first type is extracellular requirements, which include stable circulation in the blood stream, penetration into the blood vessel walls, and specific recognition by target cells [23]. The second type is intracellular barriers, which include endocytotic internalization, endosomal escape, and cytosol release [24-26] (Figure 3.2). Naked siRNA has a very short half life [27] in the blood stream due to the degradation by RNase and adsorption by serum protein [28]. With its high molecular weight (13100 – 14000 g/mol) and negative charge [5], siRNA has a low chance of crossing the cellular membrane [29]. Once the siRNA is internalized in cells, it can be trapped in endosomes and degraded by lysosomes [22]. Therefore, a method to deliver siRNA to the target cell is needed.

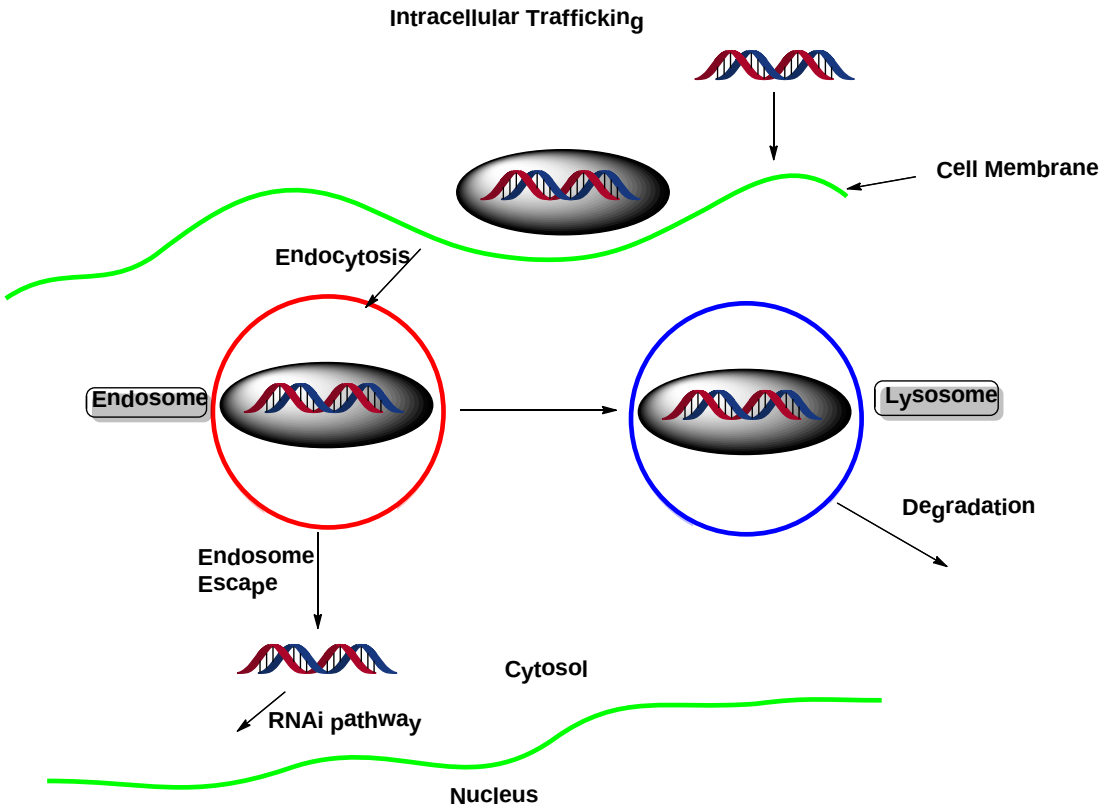

Figure 3.2 Intracellular barriers of intracellular trafficking: endocytosis, endosome escape, and lysosome degradation[22]

3.1.3 Current siRNA delivery vehicles

Both viral and non-viral vectors have been used as siRNA carriers. Many viral vectors have high gene-silencing efficacy, but often have high toxicity and can cause immunogenic responses [30]. In the past decade, the motivation of creating safe vectors has led to many developments in non-viral vectors. Non-viral vectors are generally characterized as siRNA conjugated systems and siRNA non-conjugated systems. siRNA conjugated systems are prepared by coupling siRNA with selected molecules through cross-linking (Figure 3.3a). The molecules conjugated to siRNA can improve the stability of siRNA in blood stream, enhance the cellular uptake, and allow

siRNA to escape endosomes [31, 32]. Aptamer-siRNA conjugates can enhance the cell recognition and cellular uptake of the siRNA conjugates via interaction of aptamers with cells (Figure 3.3b) [33]. siRNA non-conjugated systems mainly consist of siRNA encapsulated nanoparticles. Typical nanoparticles for siRNA are constructed by cationic assemblies, such as micelles and liposomes. PEG is widely incorporated into such lipid assemblies to prevent non-specific binding of proteins and increase circulation time; targeting groups can also be conjugated to the outer layer for an enhanced cellular uptake (Figure 3.3c) [34, 35]. Cationic dendrimers can also condense negatively charged siRNA and form a polyplex to protect siRNA from degradation and deliver the cargo to desired sites (Figure 3.3d) [36-38].

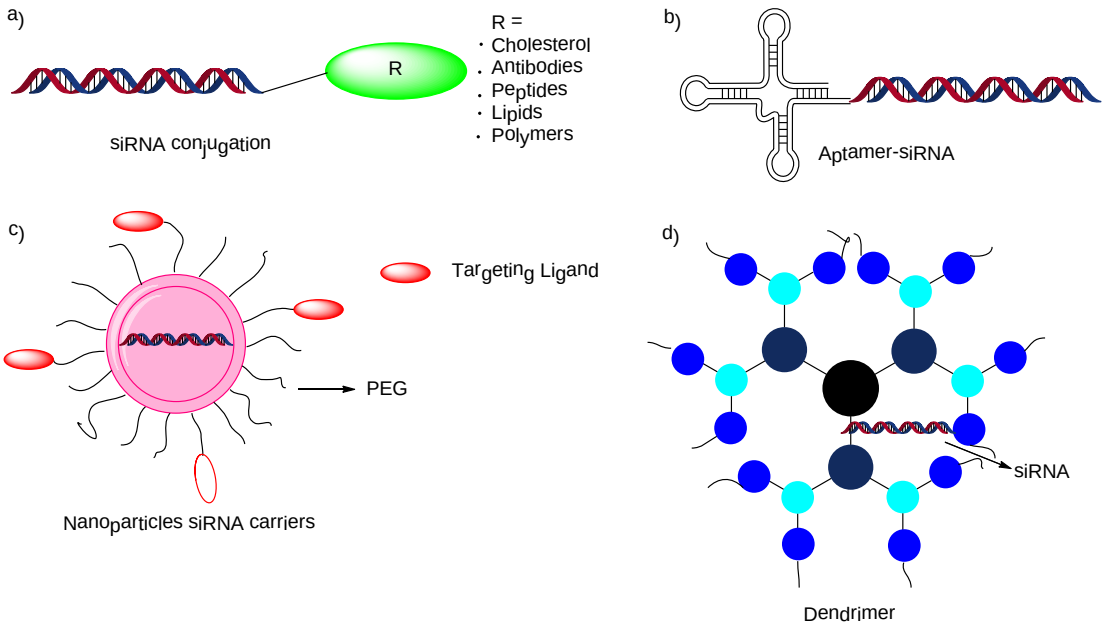

Figure 3.3: Examples of siRNA delivery systems: A) siRNA conjugation with selected molecules; B) Aptamer-siRNA chimeras; C) Nanoparticles siRNA carriers with targeting ligand and PEG; D) Dendrimers with interior encapsulation of siRNA [31, 35]

3.1.4 Cationic amphiphilic macromolecule – lipid complexes for siRNA delivery

As discussed in Chapter 2, polymeric micelles are a class of nanocarriers with long circulation in blood stream, enhanced uptake in tumor tissue, and controlled drug release at target sites [39]. Besides applications in cancer therapy, polymeric micelles are also investigated as non-viral vectors for siRNA delivery [40].

In this chapter, we evaluate the properties of cationic delivery vehicles with amphiphilic macromolecules (AMs). AMs composed of alkylated sugar-based backbone and PEG tail have been studied to transport drugs into cancer cells [41-43]. By incorporating cationic oligoethylene imine units into the backbone of AM structures, cationic amphiphilic macromolecules (CAMs) were developed and demonstrated moderate siRNA transfection efficiencies with low cytotoxcities [44]. While CAMs show promise as a siRNA nanocarrier, the transfection efficiencies still require improvements.

Cationic lipids have been broadly studied as siRNA delivery reagents, as their permanent cationic charges can complex anionic siRNA and their lipid fusion properties can enhance endosomal escape [45-47]. However, lipid-based systems usually have poor stability in blood stream and suffer relatively high cytotoxicity [26]. As discussed in Chapter 1, liposomes are nanoscale assemblies with a hydrophilic core and hydrophobic bilayer. As CAM delivery systems are stable in the physiological condition and demonstrated biocompatiblity, we hypothesized that complexes containing both CAMs and lipids will yield a more efficient siRNA delivery system. Two species of CAMs, differing by the number of amine groups in their backbone (Figure 3.4, **7N** and **9N**), were chosen as they demonstrated relatively high transfection efficiencies compared to other CAMs with fewer amine groups [44]. The lipid system is composed of 1,2-dioleoyl-sn-glycero-3-phosphoethanolamine (DOPE) and 1,2-dioleoyl-3-trimethylammonium-propane (DOTAP) (Figure 3.4) in a weight ratio of 1:1. Composite systems

containing CAM (**7N** or **9N**) and lipid was first established by evaluating non-covalent interactions. Then, to evaluate the potential of the CAM-lipid complexes as siRNA carrier, a series of physicochemical and biological experiments were conducted.

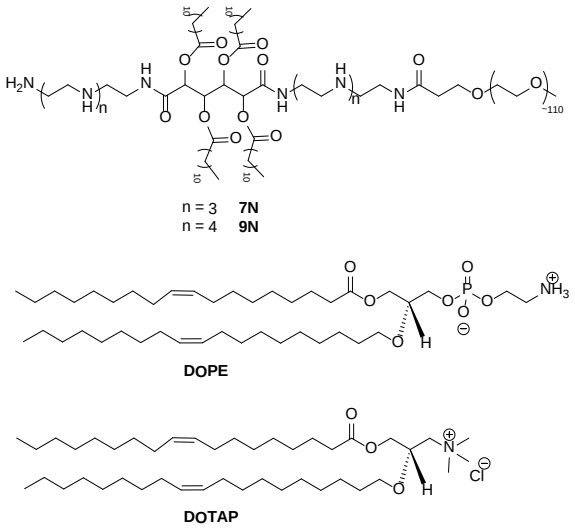

Figure 3.4 Chemical structure of CAMs (**7N** and **9N**) (top), DOPE (middle), and DOTAP (bottom)

3.2 Results and discussions

3.2.1 Isothermal compression (*Performed by Evan Mintzer in Yeshiva University*)

The two CAMs (**7N** and **9N**) were synthesized and characterized as described in a previously published paper [44]. In this work, the CAMs were formulated into CAM-lipid complexes by addition of lipids (DOPE and DOTAP in a 1:1 weight ratio). The interactions between CAM and lipid are dictated both by electrostatic repulsions and hydrophobic attractions. The electrostatic repulsion is caused by the positive amines of CAM and cationic DOTAP, whereas the hydrophobic attraction is due to the alkyl chains of the CAMs and lipids. Langmuir monolayers were created to study this net interaction, where there is a delicate balance between electrostatic repulsions and hydrophobic interactions between CAMs and lipids.

Compressing films of surface-active compounds at the air-aqueous (i.e., hydrophobic – hydrophilic) interface is a well-established method for examining mixing [48]. The condensation effect, in which the observed molecular area is decreased from that predicted molecular area (assuming ideality), is an indication of attractive interactions [48]. To evaluate miscibility, films of various CAM-lipid weight ratios were compressed and the resulting isotherms compared with each pure component (i.e., CAM alone and lipid alone). High water-solubility of both CAMs (**7N**, left panel and **9N**, Figure 3.5 right panel) caused the films to collapse at ~10 mN/m (Figure 3.5A). Thus, molecular areas were compared with values at 5 mN/m and compared to isotherms of **7N** and **9N** with increasing amounts of lipid (Figure 3.5B). The large condensation effect observed for all compositions indicates strong attractive interactions of similar magnitude (except at 90% CAM). This effect is noted by the large negative deviation from ideality (Figure 3.5B) and illustrates intimate CAM-lipid mixing. The stabilizing effect of even small lipid amounts is demonstrated by the increase in collapse pressures (i.e. much lower molecular areas) when lipid is included in the films. Taken together, these results show that the combination of the CAM species (**7N** and **9N**) and lipids form stable mixtures. Though similar compression trends were observed within cationic lipids [49], this work is the first example showing the compression isotherms between cationic macromolecule and lipids.

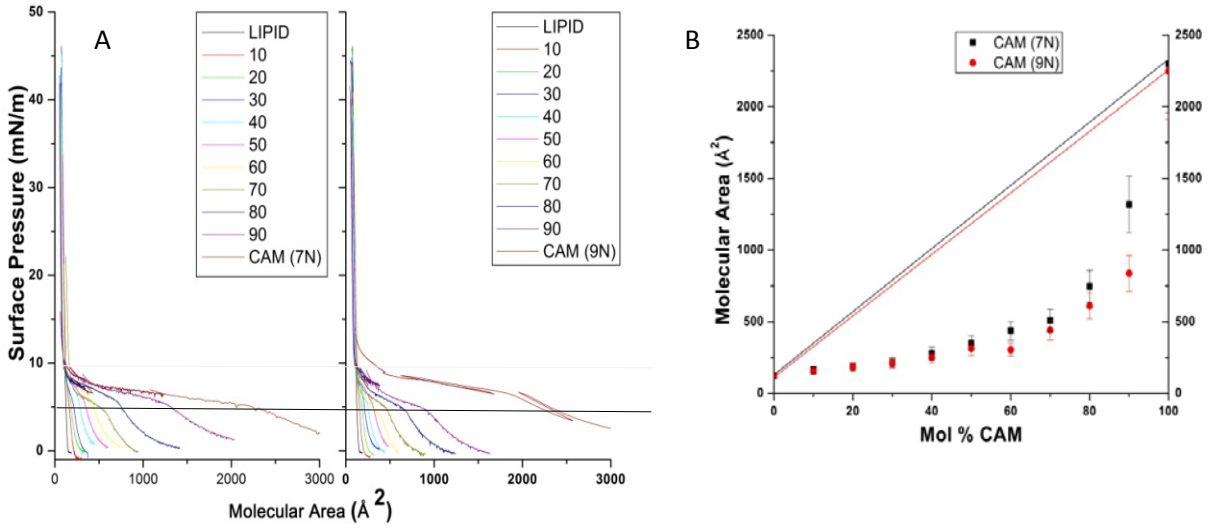

Figure 3.5 (A) Compression isotherms of **7N**-lipid (left panel) and **9N**-lipid films (right panel) on pure water. Compositions are expressed as mol % CAM (inset). (B) Area-composition plots for **7N** (black) and **9N** (red). Data were derived from compression isotherms at 5 mN/m.

3.2.2 Isothermal titration calorimetry (ITC) (*Performed by Evan Mintzer in Yeshiva University*)

To quantify the affinities of each CAM species to lipid, we followed the ITC protocol of Tsamaloukas et al. and titrate DOPE/DOTAP liposomes into CAMs [50]. The resulting heats of binding derived from titration of **7N** or **9N**, and the corresponding optimized global fits are shown (Figure 3.6). The curve-fitting routine assumes CAM interactions with either the outer lipid-layer only or with both lipid and aqueous layer. Using the former assumption (i.e., lipid only), slightly improved global fits were obtained. The results show that **7N** binds lipids with ~7-fold higher affinity compared to **9N**, based on partition coefficients (7.9 mM^{-1} for **7N** and 1.2 mM^{-1} for **9N**). The binding is endothermic, indicating hydrophobic interaction, an entropy

increase originating from water displacement in hydrophobic region. CAMs dissociate from micelle and partition into liposomes during titration. Entropy is decreased during the CAM dissociation process, thus entropy is increased during CAM partitioning into liposomes to obtain the net entropy increase. This data suggests that the interactions involve membrane penetration of CAM into liposomes rather than association of CAM with the liposome surface.

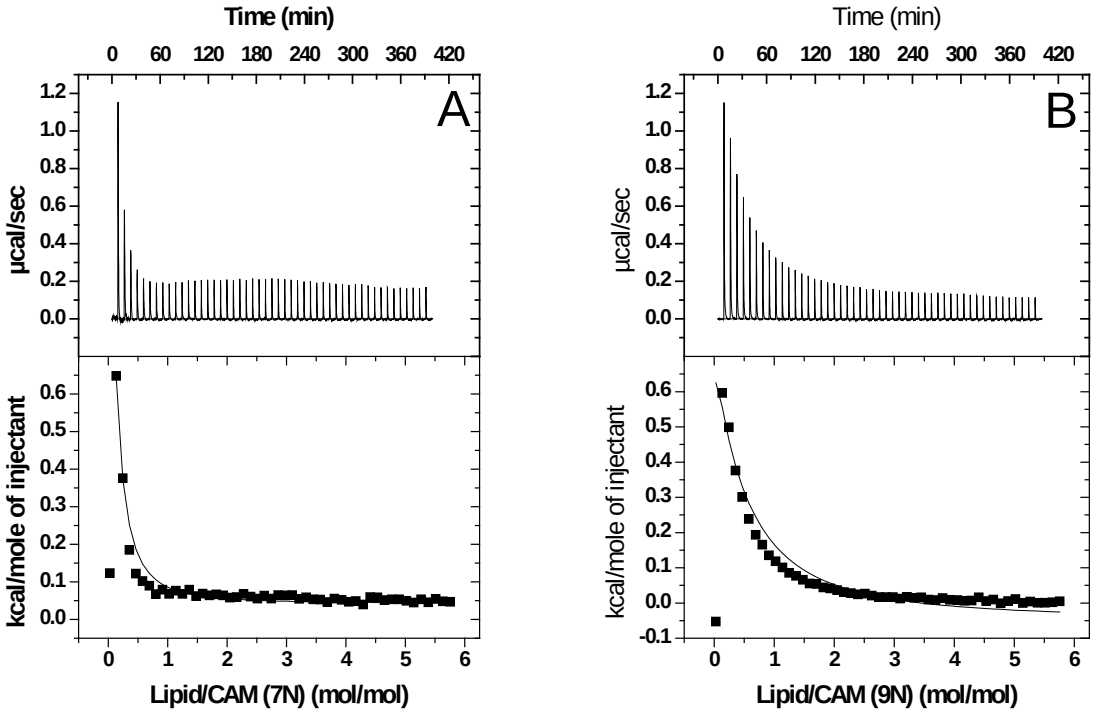

Figure 3.6 Results from ITC "uptake" experiments for 0.5 mM **7N** (A) and **9N** (B) dispersions titrated with 20 mM DOPE/DOTAP liposomes at 25 °C, pH 7. Top panels: Raw data. Bottom panels: Integrated heats of binding (squares) and linear regression analysis of integrated heats (lines).

3.2.3 Physicochemical characterization of CAM-lipid

After CAM-lipid complexes of various compositions were formulated [20], their sizes were characterized using DLS. CAM-lipid complexes for all compositions were between 130 to 160 nm in diameter (Figure 3.7A), which is within the optimal range for both cellular uptake and systemic circulation [40, 51, 52]. Generally, DLS histograms show a single peak with narrow distribution indicating that a distinct mono-dispersed complex was formed (data not shown). No aggregation was observed with any composition of the CAM-lipid complexes, indicating that stable hybrid complexes were constructed. The stable formation of the complexes was also supported by Langmuir monolayer and ITC studies (Figure 3.5 and 3.6). CAM-lipid complex zeta potentials at pH 7.4 varied monotonically between that for CAM alone (~10 mV) and for lipid alone (~50 mV) (Figure 3.7B). The zeta potential difference between CAM and lipid is due to the nature of the cationic charges. CAM possesses primary (pKa 10.7) and secondary amines (pKa 9.7) such that protonation is not complete at pH 7.4 due to electrostatic repulsion, while DOTAP possesses the quaternary ammonium cation which is pH-independen and DOPE is neutral. When forming the CAM-lipid complexes, the PEG tail of the CAM may shield the surface charge and lower the zeta potential as the CAM composition increases.

Gel electrophoresis was then used to monitor siRNA complexation with the CAM-lipid complexes (Figure 3.7C). As for CAMs alone[44], an N/P ratio of 50 was necessary for efficient siRNA complexation with CAM-lipid mixtures. At an N/P ratio of 50, only a minor fraction of siRNA migrated on the gel, indicating complete complexation of siRNA to **9N**-lipid for all compositions (Figure 3.7C). Similar results were observed when **7N**-lipid was used (data not shown). A representative TEM images of **9N**-lipid complex with weight ratio of 1:1 is shown

(Figure 3.7D). The size measured by TEM (120 nm) correlated with the DLS observations (150 nm), the smaller particles observed in TEM may be lipid assemblies or CAM alone.

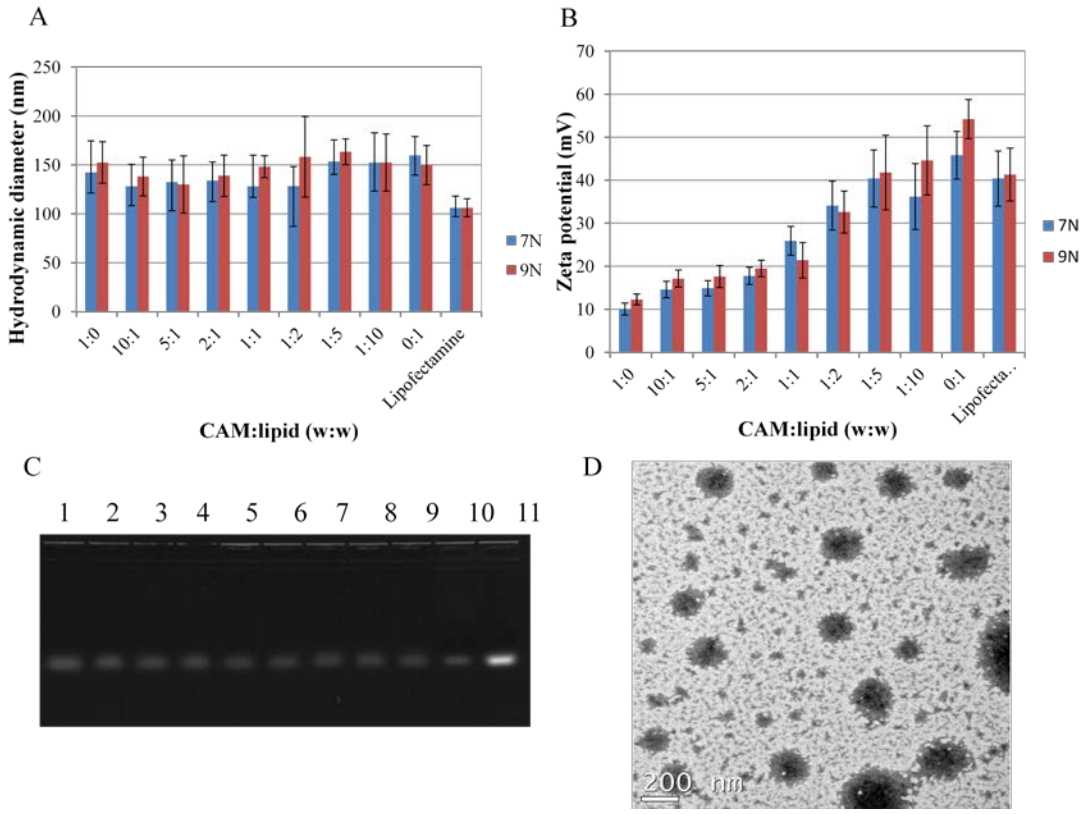

Figure 3.7 (A) Hydrodynamic diameter of CAM-lipid complexes in HEPES (10 mM, pH 7.4) buffer with different weight ratios using DLS. (B) Zeta potentials of CAM-lipid complexes in HEPES (10 mM, pH 7.4) with different weight ratios. Lipofectamine was used as control, data represent mean ± standard deviation (n=3). (C) Electrophoresis gel, lanes 1-9 correspond to 9N-lipid weight ratios of 1:0, 10:1, 5:1, 2:1, 1:1, 1:2, 1:5, 1:10, 0:1 at N/P ratio of 50, lane 10 is Lipofectamine, lane 11 is siRNA alone. (D) TEM image of CAM (**9N**)-lipid at 1:1 weight ratio. Data represent mean ± standard deviation (n=3)

The sizes of the CAM-lipid after siRNA complexation were also measured (Figure 3.8). These results indicate that the CAM-lipid/siRNA complex diameters remained at approximately 100-200 nm, suggesting that the complex size is not significantly affected by siRNA complexation.

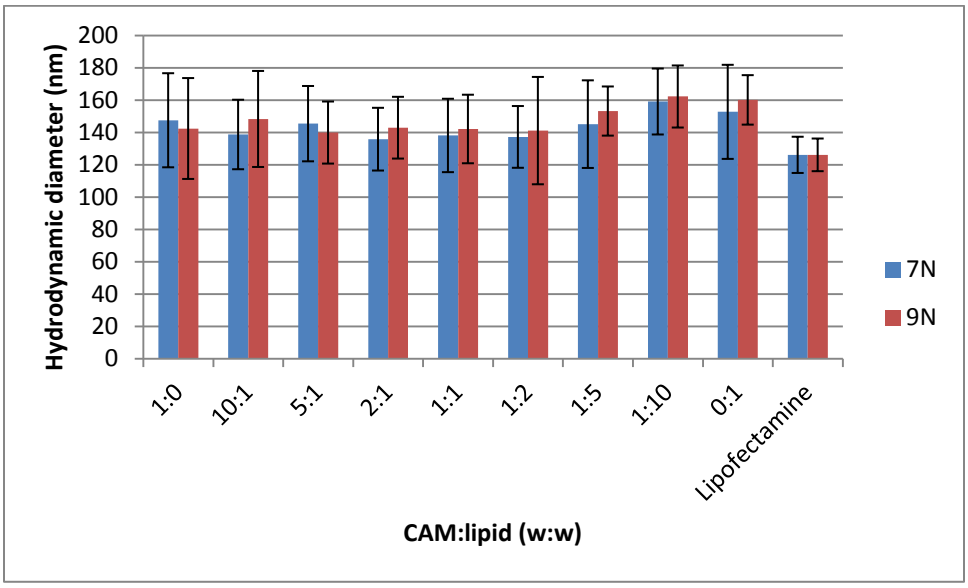

Figure 3.8 Hydrodynamic sizes of CAM-lipid/siRNA complexes with N/P ratio of 50 in HEPES (10 mM, pH 7.4) buffer, measured by DLS. Lipofectamine was used as control. Data represent mean ± standard deviation (n=3)

Zeta potentials of CAM-lipid structures after complexation with siRNA (Figure 3.9) decreased as compared to CAM-lipid complexes alone, this effect is due to the neutralization of cationic surface charge from anionic siRNA. Despite this decrease, all CAM-lipid/siRNA complexes maintained a net cationic charge, rendering a favorable intracellular uptake of the complexes.

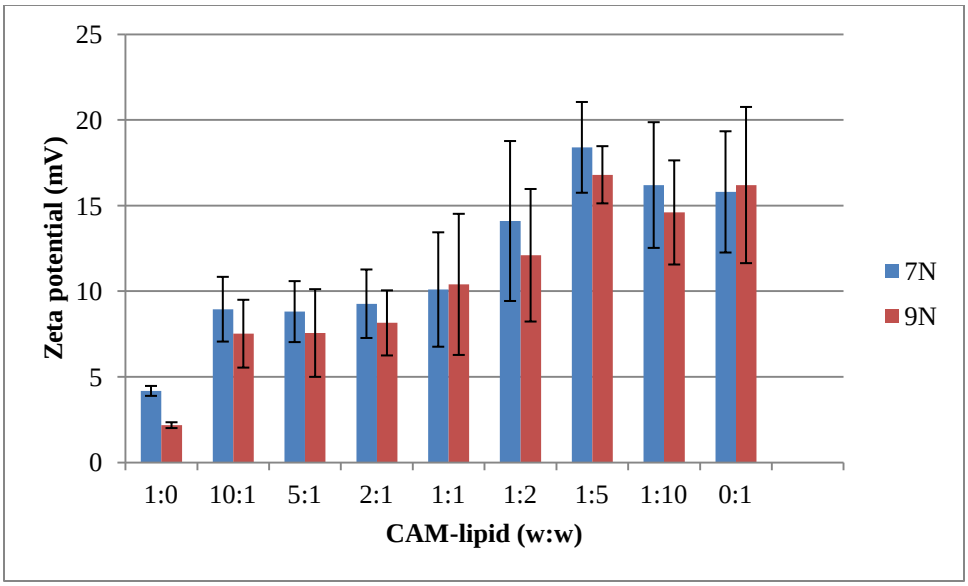

Figure 3.9: Zeta potentials of CAM-lipid complexes in HEPES (10 mM, pH 7.4) with different weight ratios. Lipofectamine was used as control. Data represent mean ± standard deviation (n=3).

The stability of the CAM-lipid/siRNA complexes under serum-containing condition was monitored by the complex size up to one week in the presence of 10% fetal bovine serum (FBS) (Figure 3.10). The complexes with higher CAM weight ratios maintained 100-200 nm size range; with decreasing CAM weight ratios, the complex sizes increased. For complexes without CAMs, immediate visual aggregation was observed. This data suggests that CAM-lipid complex can maintain the integrity of siRNA from degradation and aggregation under the serum-containing conditions.

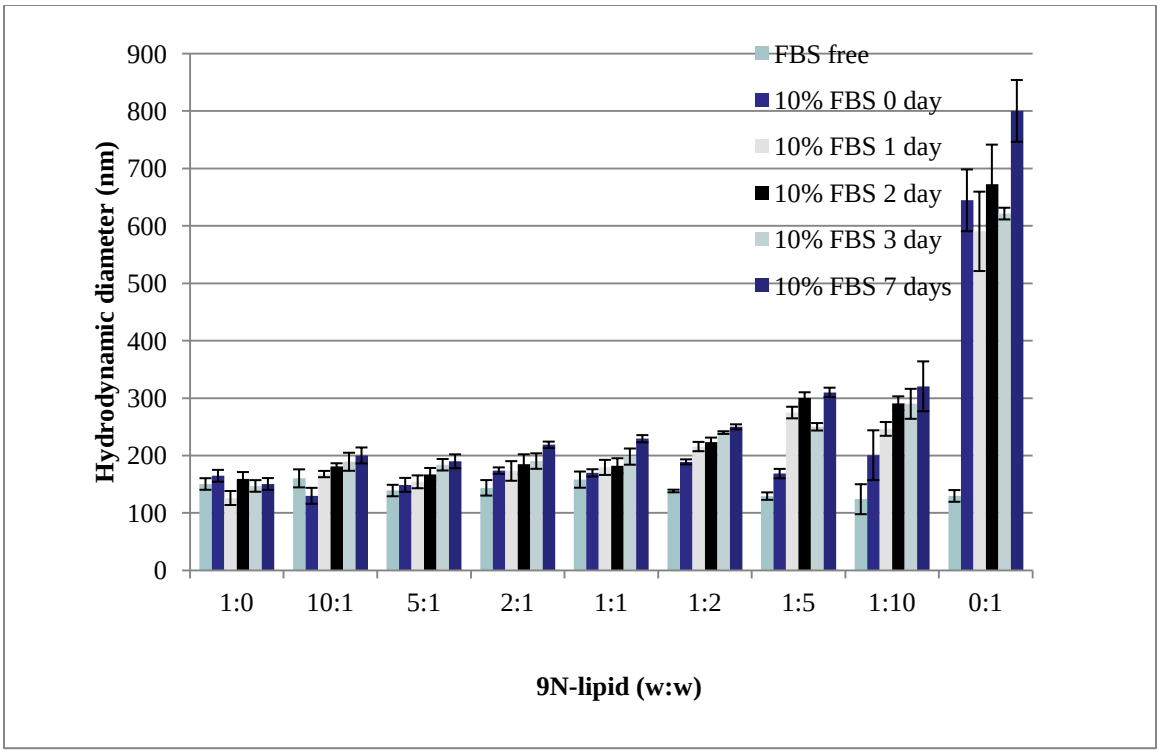

Figure 3.10 Hydrodynamic diameters of **9N**-lipid/siRNA complex in the presence of serum over one week. Data represent mean ± standard deviation (n=3)

3.2.4 siRNA delivery using CAM-lipid *(Performed by Leora Nusblat)*

To evaluate the gene silencing efficiency of CAM-lipid systems, the delivery of anti-luciferase siRNA to U87-Luc cells expressing luciferase was monitored. Nearly no silencing was observed with a scrambled siRNA control, indicating that gene knockdown was specifically induced by anti-luciferase siRNA alone. Similar transfection efficiencies were found both CAM alone and lipid alone (Figure 3.11). CAM-lipid complexes with weight ratios of 10:1, 5:1, and 2:1 showed decreased transfection efficiencies compared to the CAM or lipid alone. In contrast, the transfection efficiencies of CAM-lipid complexes with weight ratios of 1:1, 1:2, 1:5, and 1:10 were improved and statistically comparable to Lipofectamine. Thus, increasing the CAM ratio in

the CAM-lipid complex decreases transfection efficiency. Based on literature precedence, we believe increasing CAM ratio leads to a higher PEG percentage in the CAM-lipid complex which may impede the cellular uptake of the complex [17]. However, CAM alone showed higher efficiencies than the CAM-lipid complexes with weight ratio of 5:1, 2:1, and 10:1. This data suggests that synergistic effects between the CAM and lipid play an important role in the process. To examine the synergistic effect between CAM and lipid, sequential studies were performed using **9N**-lipid with weight ratio of 1:10, as the **9N**-lipid at 1:10 ratio showed a higher transfection efficiency than other formulations.

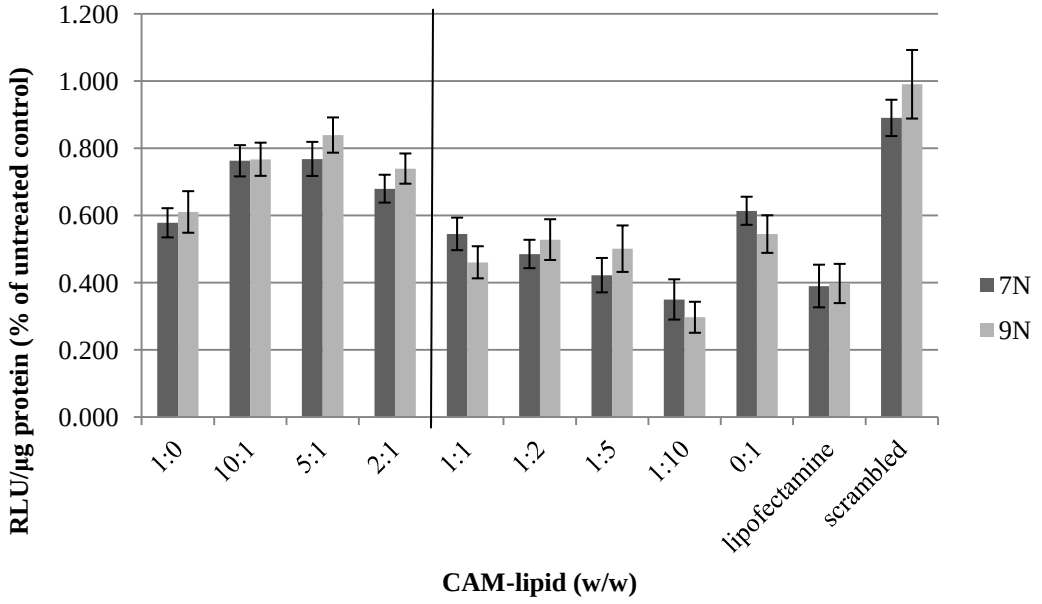

Figure 3.11 Luciferase reporter gene down-regulation assay over 48 hrs performed with U87 luciferase cell line using complexes formulated from CAM-lipid complexes and anti-luciferase siRNA at N/P ratio of 50. Lipofectamine and scrambled siRNA were used as siRNA controls. No significant statistical difference was observed between CAM-lipid at weight ratio 1:1, 1:2, 1:5, 1:10 and Lipofectamine. Data represent mean ± standard error (n=3).

3.2.5 siRNA binding to CAM-lipid *(Performed by Leora Nusblat)*

ITC has been applied in drug discovery to understand affinity and thermodynamics of the binding between ligands and proteins. Yet, limited literature is available that utilize ITC to probe siRNA binding to delivery vehicles [53, 54]. As one example, Keller et al. used ITC to illustrate siRNA binding to chitosan [53]. To our knowledge, our work is the first that uses ITC to characterize siRNA binding to polymer-lipid complexes. Herein, ITC was used to monitor the thermodynamics of siRNA binding to **9N**-lipid mixtures at both physiological and endosomal pH conditions (7.4 and 5, respectively). The siRNA binding to the **9N**-lipid system at pH 7.4 resulted in a large endothermic heat signal (Figure 3.12A). However, siRNA titration to the same **9N**-lipid system at pH 5 yielded a significantly reduced heat signal, similar to that observed from siRNA titration into the buffer alone (Figure 3.12C). The reduced signal can originate from two situations: siRNA binds to **9N**-lipid complexes with greater affinity at pH 7.4 than pH 5; siRNA is only diluted in solution due to precipitation of **9N**-lipid complexes. Both situations may indicate that once the siRNA complex enters the more acidic intracellular environment, siRNA is released from the CAM-lipid system. Therefore, the complexation of siRNA to CAM-lipid is altered by pH changes, such that siRNA can be bound at neutral pH (e.g., in bloodstream) and then released under acidic conditions (i.e., within the cellular endosomes). Unfortunately, monitoring the siRNA binding under serum conditions is not feasible due to the large heat signal imposed by the serum protein.

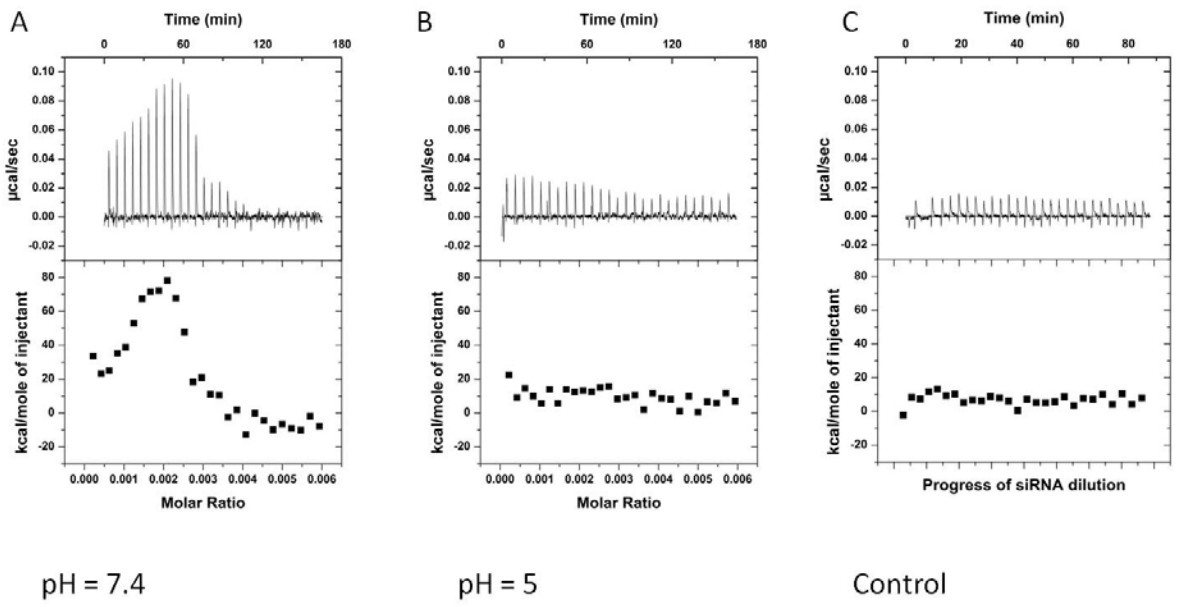

Figure 3.12 Comparison of data from isothermal titration of 0.128 mM **9N**-lipid complex (1/10) with 3.8 μM siRNA at pH 7.4 (A) and pH 5 (B). Panel C is siRNA only as a control. Top panels: raw heat signals. Lower panels: Integrated areas corresponding to each titration.

3.2.6 pH-dependent characteristics of CAM-lipid

To understand this difference in siRNA binding affinity at pH 7.4 and 5, zeta potentials of **9N**-lipid complexes were measured at both pH values. Zeta potentials of **9N**-lipid with 1:10 weight ratio decreased drastically from 48 mV (pH 7.4) to 5 mV (pH 5) (Figure 3.13A). The descending trend of the zeta potential from pH 7.4 to pH 5 was also observed at 1:5, 1:2, and 1:1 weight ratios. The decreased binding affinity at pH 5 can be anticipated by the decreased zeta potential of **9N**-lipid complexes. To further study the decrease in zeta potential of the complexes, the complex sizes were measured to probe the colloidal stabilities at pH 5. The **9N**-lipid with 1:10 weight ratio showed a steep size increase from 150 nm to 770 nm (Figure 3.13B). Turbidities of the complexes were measured to illustrate that **9N**-lipid with 1:10 ratio has less than 20%

transmission (Figure 3.13C). Visual cloudiness in the dispersion (**9N**-lipid 1:1 weight ratio) suggested the formation of precipitates, which is likely due to the complex instability at pH 5 (Figure 3.13D). It suggests that **9N**-lipid with weight ratio of 1:10 were instable at pH 5. Notably, both the **9N** and lipid alone were stable and maintain their sizes at pH 5. **9N** displayed an increase zeta potential at pH 5 compared to pH 7.4; when mixed with cationic lipid at pH 5, the electrostatic repulsion appears to overcome the hydrophobic attraction, yielding an instable complex that crashes out of solution. Hence, the pH-responsive effect between **9N** and lipid at weight ratio 1:10 and pH 5 was observed. Given that **9N**-lipid at weight ratio 1:10 crashes out of solution at pH 5, the previously observed weak binding (Figure 3.12B) may be due to the minimal concentration of CAM and/or lipids are in solution.

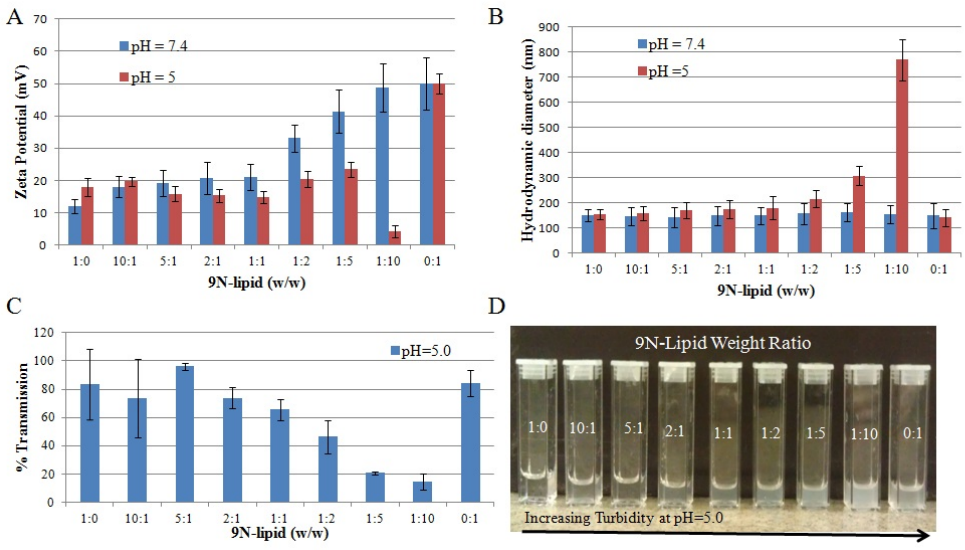

Figure 3.13 Stability studies of **9N**-lipid complexes: (A) Zeta potentials of **9N**-lipid complexes at pH 7.4 and 5; (B) hydrodynamic volumes of **9N**-lipid complexes at pH 7.4 and 5; (C) turbidities of **9N**-lipid complexes at pH 5; and (D) visual appearances of **9N**-lipid complexes at pH 5. Data represent mean ± standard deviation (n=3)

3.2.7 Intracellular trafficking of siRNA complexes *(Performed by Leora Nusblat)*

The intracellular trafficking of **9N**-lipid was examined using confocal microscopy. **9N**-lipid/Cy5-siRNA (**9N**-lipid at weight ratio 1:10) was evaluated with LysoTracker Red which accumulates in endosomes after 4 h of incubation (Figure 3.14). The data indicates that the complexes were internalized but not yet released from endosomes or early lysosomes by 4 h. After 24 h, only minimal co-localization of the complex in the endosomes was observed and more extensive siRNA distribution was observed in the cytoplasm (data not shown), suggesting that Cy5-siRNA had undergone endosomal/lysosomal escape. Based on the previous pH-dependent data, the endosomal escape is explained by the pH-responsive feature of the **9N**-lipid at weight ratio of 1:10. When the complexes are internalized in acidic endosomes, they collapse and cause the release of lipid, CAM, and siRNA. Then, the lipid serves as a destabilizing agent that disrupts the endosome membrane [55]. The CAM also introduces endosome disruption likely via the well-studied proton sponge effect [56, 57]. The siRNA is released into the cytoplasm to trigger the RNAi process. The same trends were observed when using Lipofectamine as the carrier. For the less effective carrier (**9N**-lipid with weight ratio of 10:1), siRNA appeared to aggregate on the cell surface after 4 h. After 24 h, some CAM-lipid complexes were internalized; however, significantly more CAM-lipid complex remained on the cell surface as compared to the 1:10 formulation. These results suggest that siRNA efficiency is impaired at 10:1 weight ratio due to insufficient cell uptake and decreased intracellular release of siRNA. Therefore, cytotoxicity studies were conducted to determine CAM-lipid complexes of optimized composition have potential non-viral carriers for siRNA delivery.

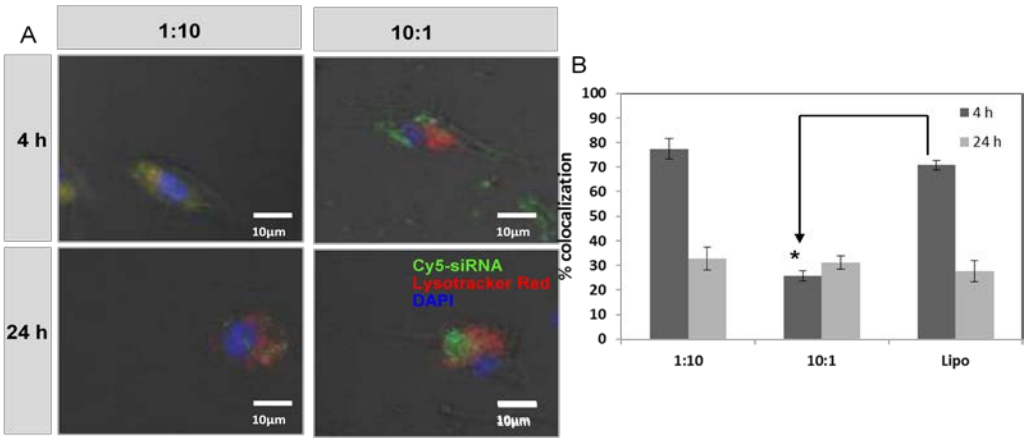

Figure 3.14 (A) Confocal microscope images of Cy5-siRNA (green) and endosomal (red) distribution in U87 cells when delivered by the 9N-lipid complexes at two formulations (1:10 and 10:1), at 4 h (top panel) and 24 h (bottom panel) post-transfection. (B) Colocalization was quantified using ImageJ. The percent colocalization of Lysotracker Red and Cy5-siRNA was calculated as mean gray value from colocalized points divided by mean gray value from sum of points using Image J. Data represent mean ± standard error (n = 3).

3.2.8 Cytotoxicity studies *(Performed by Leora Nusblat)*

Given the previous observation that CAM/siRNA complexes displayed low cytotoxicity[17], we hypothesized that CAM-lipid/siRNA complexes would also be relatively nontoxic to cells. To determine the effect of the concentration of **9N**-lipid with weight ratio of 1:10 on cytotoxicity, an MTS assay was performed in U87 cells. No statistical significant difference in cytotoxicity was observed between **9N**-lipid/siRNA and Lipofectamine/siRNA at CAM-lipid concentrations less than $1x10^{-5}$ M (Figure 3.15). At **9N**-lipid complex concentrations of $1x10^{-5}$ M and $1x10^{-4}$ M, the viability was improved compared to Lipofectamine, although in both cases, a significant decrease in viability was observed compared to lower complex concentrations. As the concentration used for transfection was 2×10^{-5} M **9N**-lipid, it can be inferred that the enhanced

endosomal escape and gene silencing ability of the **9N**-lipid/siRNA (1:10 w/w) complexes compared to Lipofectamine is not due to cell toxicities. The CAM-lipid system presented in this study demonstrates a high transfection efficiency and low cytotoxicity which can solve the dilemma between efficiency and cytotoxicity [3-5] in non-viral delivery systems for *in vivo* applications.

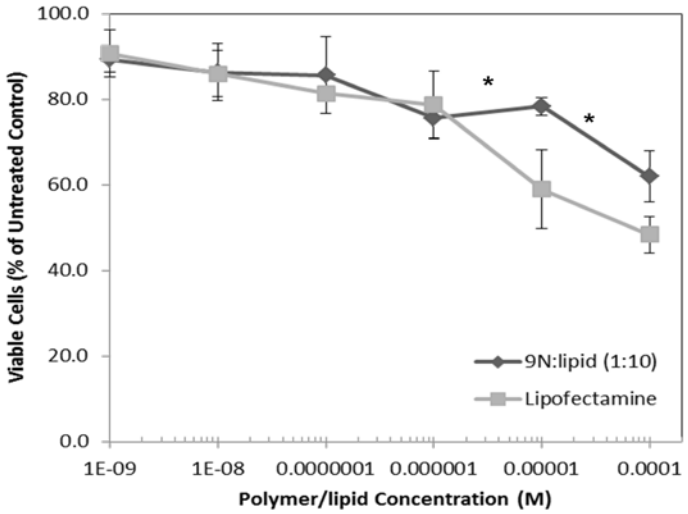

Figure 3.15 Cytotoxicity of **9N**-lipid/siRNA (1:10 w/w) complexes as compared to Lipofectamine/siRNA in U87 glioma cells after 72 h of exposure. Data represent mean ± standard error (n = 3). Asterisks represent concentrations at which CAM-lipid complexes elicited a statistically significant lower cytotoxicity than Lipofectamine ($p < 0.05$).

3.3 Conclusions

We developed a novel composite system that physically combines polymer and lipid. Compression isotherm and ITC were used to confirm the formation of stable CAM-lipid complexes and the interaction mechanism. Size and zeta potential measurements validate that CAM-lipid complexes are stable and suitable for *in vivo* delivery. *In vitro* siRNA delivery

experiments demonstrated that CAM-lipid complexes at specific CAM-lipid weight ratios have comparable gene silencing efficiencies compared to Lipofectamine. Intracellular trafficking and additional ITC studies revealed that siRNA can escape from endosomes and are released from CAM-lipid complexes to down-regulate genes. The differential binding affinities of siRNA to the complexes at pH 7.4 and 5 demonstrated the pH-responsive feature of the complexes (i.e., complexes are unstable under acidic condition). These studies strongly suggest that CAM-lipid complexes can serve as efficient siRNA delivery vehicles. Although not investigated in the study, the hydrophobic portion of the CAM-lipid complexes can allow encapsulation of hydrophobic drugs or diagnostic tags. Herein, it is conceivable that CAM-lipid can be utilized as a multifunctional delivery system to achieve more therapeutic and diagnostic effects.

3.4 Experimental procedures

3.4.1 Materials

DOPE and DOTAP were purchased from Avanti Polar Lipid (Alabaster, AL). The anti-luciferase siRNA (sense sequence: 5′-CUUACGCUGAGUACUUCGAdTdT-3′; antisense sequence: 5′-UCGAAGUACUCAGCGUAAGdTdT-3′) and Cy5 labeled negative control siRNA were purchased from Qiagen (Valencia, CA). All cell culture media and Lipofectamine were purchased from Invitrogen (Carlsbad, CA). The Luciferase assay kit and BCA protein assay kit were purchased from Promega (Madison, WI). U87-LUC, a human primary glioblastoma cell line with constitutive expression of firefly luciferase, was generously provided by Dr. Xu-Li Wang (Pharmaceutics and Pharmaceutical Chemistry, University of Utah). All other reagents were purchased from Sigma-Aldrich (St. Louis, MO) and used as received without further purification, except where noted.

3.4.2 Methods

3.4.2.1 Isothermal compression *(Performed by Evan Mintzer, Yeshiva University)*

Surface properties of CAM and mixed CAM-lipid monolayers were evaluated at the air-water interface using a Langmuir surface balance from KSV-Nima (Espoo, Finland) on a subphase of pure water (resistivity ≥ 18.2 MΩ · cm) at ambient temperature (~ 22 °C). CAM and lipid were dissolved in HPLC-grade chloroform to concentrations of ~1 mg/mL and mixtures were prepared by adding appropriate volumes of each from stock solutions. Between each experiment, the Teflon trough (Biolin Scientific, MD) (total subphase volume = 109 mL) and barriers were cleaned with methanol and then rinsed repeatedly with ultra-pure water. Contaminants were removed from the platinum Wilhelmy plate (Biolin Scientific, MD) with an open fire from a Bunsen burner. All glassware was thoroughly cleaned with chloroform and methanol. The subphase surface was cleaned by aspirating during repeated sweeps of the computer-controlled barriers while monitoring the surface pressure and continued until the change in pressure was negligible. CAM and CAM-lipid films were spread onto the subphase surface using a digital Hamilton syringe (Reno, NV). After a 10 min delay to allow for complete solvent evaporation, the films were compressed at a rate of 10 cm^2/min. Data were collected by KSV-Nima's LB Control software (v. 3.60) and analyzed using Origin (Northampton, MA).

3.4.2.2 Isothermal calorimetry titration *(Performed by Evan Mintzer, Yeshiva University)*

Mixing of the CAMs with the lipids were further examined with the "uptake" ITC protocol as described by Heerklotz et. al [50] using a VP-ITC from Microcal (GE Healthcare, Northampton,

MA). Briefly, CAM dispersions were titrated with lipid vesicle suspensions at 25 °C in 10 µL aliquots at 6 min intervals during stirring (280 rpm). The data were collected with Microcal's dedicated Origin software program and the resulting heat signals were fitted using an Excel (Microsoft, CA) spreadsheet available for download.

3.4.2.3 Preparation of CAM-lipid complexes

Complexes of various CAM-lipid ratios were prepared by a co-evaporation technique previously described [58]. Briefly, the lipid component was comprised of a 1:1 (w/w) mixture of DOPE and DOTAP. CAM and lipid (DOPE/DOTAP) were co-dissolved in chloroform at various CAM to lipid weight ratios. The chloroform was removed by rotary evaporation. The resulting films were hydrated with 10 mM 4-(2-hydroxyethyl)-1-piperazineethanesulfonic acid (HEPES) buffer at pH 7.4 overnight at room temperature. The complex suspensions were then extruded 21 times with the 100 nm pore size polycarbonate filter (Avanti Lipid, AL) through a mini-extruder (Avanti Lipid, AL) to give nanoscale CAM-lipid complexes. Formation of CAM-lipid-siRNA complexes was performed by mixing CAM-lipid formulations with siRNA for 60 min at room temperature.

3.4.2.4 Size and zeta potential measurements of CAM-lipid complexes

CAM-lipid complexes (1 mg/mL in HEPES) with or without siRNA were analyzed using a NanoZS90 instrument (Malvern Instruments, UK) at room temperature. Each sample was run three separate times with 20 measurements per run to obtain the size and zeta potential.

3.4.2.5 Electropherotic mobility assay

CAM-lipid/siRNA complexes were prepared as previously described for CAM/siRNA complexes [44]. Dispersions were briefly vortexed and incubated for 60 min at room temperature to allow for complex formation. Prior to electrophoresis, 2 μL of 10X BlueJuice gel loading buffer was added to each sample. Gel electrophoresis was performed using 0.8 % agarose E-gels containing ethidium bromide for DNA visualization and a PowerBase electrophoretic chamber (Invitrogen, CA). Gels were imaged using BioDoc-It Imaging System (UVP, CA).

3.4.2.6 Transmission electronic microscopy

A drop of CAM-lipid complex dispersion (0.05 mg/mL) with or without siRNA and a drop of uranyl acetate (0.5 mg/mL) were both placed on a carbon film-coated copper grid. Excess solution was removed by tapping the edge of grid with filter paper. The grid was then dried for 30 min in a desiccator at room temperature. Images were taken on a TEM-Topcon 002B (TOPOCON, Japan).

3.4.2.7 Cell culture *(Performed by Leora Nusblat)*

U87 and U87-LUC cells were maintained in DMEM medium supplemented with 10% fetal bovine serum (FBS) and 1% penicillin/streptomycin. Cells were incubated at 37 °C in a 5% CO_2 incubator (VWR, PA). For the U87-LUC cell line, which stably expresses luciferase, expression was maintained under selective pressure by G418 (500 μg/mL).

3.4.2.8 siRNA delivery assay *(Performed by Leora Nusblat)*

U87 cells were plated at a density of 5000 cells/well in 96-well plates approximately 20 h prior to transfection. Immediately prior to transfection, CAM-lipid/siRNA complexes were prepared in 20 μL of HEPES (N/P 50). Lipofectamine was used as a positive control whereas scrambled siRNA was used as a negative control. A 100 nM siRNA solution was used, while CAM-lipid stock dispersions were prepared at 20 nM. The CAM-lipid/siRNA complexes were brought to a total volume of 100 μL in OptiMEM medium. The serum-containing culture medium was aspirated from the cells and each well treated with 100 μL of CAM-lipid/siRNA complexes in OptiMEM medium. After a 4 h incubation period, cells were washed 3 times with HEPES and the transfection mixture replaced with a serum-containing growth medium and maintained under normal growth conditions. After 48 h, the cells were assayed for firefly luciferase expression using a luminometer (Turner Biosystems, WI), and the values were normalized to total protein expression using a BCA assay kit (Promega, WI).

3.4.2.9 siRNA binding assay *(Performed by Evan Mintzer, Yeshiva University)*

*ITC was used to compare CAM-lipid complex binding to siRNA. For these experiments, 10 μL aliquots of 3.8 μM (0.05 mg/mL) siRNA were injected into the calorimetry cell containing 64 μM (0.05 mg/mL total concentration) CAM-lipid complex at 25 °C at 2 min intervals. The experiments were repeated with both CAM species (**7N** and **9N**) at pH 7.4 and pH 5.5. Data analysis was performed using Microcal's "one-binding site" model on Origin. Prior to analysis, heat of dilution, obtained from titrating siRNA into respective buffers, was subtracted from each*

run, and the baselines manually adjusted to the average noise level between injections. Heat changes from titration of CAM-lipid complexes with buffer were confirmed to be insignificant prior to data collection.

3.4.2.10 Intracellular trafficking *(Performed by Leora Nusblat)*

U87 cells were seeded in 24-well plates at 70% confluency and allowed to adhere overnight. Uptake and release of a fluorescently labeled siRNA (Dharmacon, Lafayette, CO) sequence into U87 cells was evaluated using fluorescence microscopy. After 4 h or 24 h of incubation with Cy5-scrambled-siRNA (Dharmacon, CO) and 1:10 CAM-lipids, 10:1 CAM-lipids, or Lipofectamine control, U87 cells were washed twice with HEPES and stained with LysoTracker Red (Molecular Probes, OR). After fixation in 4 % paraformaldehyde for 15 min and counterstaining with 4',6-diamidino-2-phenylindole (DAPI), images were taken on an IX81 motorized inverted confocal microscope (Olympus, PA) to view siRNA localization within the cells. Colocalization was evaluated by merging images and quantifying their overlapping areas in ImageJ.

3.4.2.11 Cytotoxicity studies *(Performed by Leora Nusblat)*

The cytotoxicity of CAM-lipid/siRNA complexes with varying fractions of lipid and CAM was assessed with an MTS assay (Promega, WI) in U87 cells. Cells were seeded in 96-well plates for 24 h. Following transfection with the various CAM-lipids for 4 h, cells were washed 3 times and cultured in serum-containing media. After 48 h, an MTS assay was performed and the absorbance at 450 nm was measured by a DTX880 Multimode Detector microplate reader

(Beckman Coulter, NJ). Cell viability was normalized to that of U87 cells with HEPES treatment.

3.4.2.12 Statistical analysis

Statistical analyses were carried out using a one-way ANOVA test with a Fisher's all-pairs post hoc comparison test. (Synergy Software, PA). The significance criteria assumed a 95% confidence level ($P < 0.05$). Standard error of the mean is reported in the form of error bars on the graphs of the final data.

3.5 References

[1] A. Fire, S. Xu, M.K. Montgomery, S.A. Kostas, S.E. Driver, C.C. Mello. Potent and Specific Genetic Interference by Double-Stranded Rna in Caenorhabditis Elegans. *Nature* **1998** *391* 806-811.
[2] G.J. Hannon. Rna Interference. *Nature* **2002** *418* 244-251.
[3] A.P. McCaffrey, L. Meuse, T.T. Pham, D.S. Conklin, G.J. Hannon, M.A. Kay. Rna Interference in Adult Mice. *Nature* **2002** *418* 38-39.
[4] H. Ngo, C. Tschudi, K. Gull, E. Ullu. Double-Stranded Rna Induces Mrna Degradation in Trypanosoma Brucei. *Proc Natl Acad Sci U S A* **1998** *95* 14687-14692.
[5] Y. Dorsett, T. Tuschl. Sirnas: Applications in Functional Genomics and Potential as Therapeutics. *Nat Rev Drug Discov* **2004** *3* 318-329.
[6] G. Meister, M. Landthaler, Y. Dorsett, T. Tuschl. Sequence-Specific Inhibition of Microrna- and Sirna-Induced Rna Silencing. *RNA* **2004** *10* 544-550.
[7] M.B. Wang, Z. Cheng, P. Keese, M.W. Graham, P.J. Larkin, P.M. Waterhouse. Comparison of the Coat Protein, Movement Protein and Rna Polymerase Gene Sequences of Australian, Chinese, and American Isolates of Barely Yellow Dwarf Virus Transmitted by Rhopalosiphum Padi. *Arch Virol* **1998** *143* 1005-1013.
[8] P.M. Waterhouse, M.W. Graham, M.B. Wang. Virus Resistance and Gene Silencing in Plants Can Be Induced by Simultaneous Expression of Sense and Antisense Rna. *Proc Natl Acad Sci U S A* **1998** *95* 13959-13964.
[9] D.A. Braasch, S. Jensen, Y. Liu, K. Kaur, K. Arar, M.A. White, D.R. Corey. Rna Interference in Mammalian Cells by Chemically-Modified Rna. *Biochemistry* **2003** *42* 7967-7975.
[10] J. Kurreck. Sirna Efficiency: Structure or Sequence-That Is the Question. *J Biomed Biotechnol* **2006** *2006* 83757-83768.
[11] M. Overhoff, M. Alken, R.K. Far, M. Lemaitre, B. Lebleu, G. Sczakiel, I. Robbins. Local Rna Target Structure Influences Sirna Efficacy: A Systematic Global Analysis. *J Mol Biol* **2005** *348* 871-881.

[12] Y. Dorsett, T. Tuschl. Sirnas: Applications in Functional Genomics and Potential as Therapeutics. *Nature Reviews Drug Discovery* **2004** *3* 318-329.
[13] A.P. Aalto, L.P. Sarin, A.A. van Dijk, M. Saarma, M.M. Poranen, U. Arumae, D.H. Bamford. Large-Scale Production of Dsrna and Sirna Pools for Rna Interference Utilizing Bacteriophage Phi6 Rna-Dependent Rna Polymerase. *RNA* **2007** *13* 422-429.
[14] Y. Nakazawa, A. Hiraguri, H. Moriyama, T. Fukuhara. The Dsrna-Binding Protein Drb4 Interacts with the Dicer-Like Protein Dcl4 in Vivo and Functions in the Trans-Acting Sirna Pathway. *Plant Mol Biol* **2007** *63* 777-785.
[15] G.S. Parker, D.M. Eckert, B.L. Bass. Rde-4 Preferentially Binds Long Dsrna and Its Dimerization Is Necessary for Cleavage of Dsrna to Sirna. *RNA* **2006** *12* 807-818.
[16] J.W. Hewett, F.C. Nery, B. Niland, P. Ge, P. Tan, P. Hadwiger, B.A. Tannous, D.W. Sah, X.O. Breakefield. Sirna Knock-Down of Mutant Torsina Restores Processing through Secretory Pathway in Dyt1 Dystonia Cells. *Hum Mol Genet* **2008** *17* 1436-1445.
[17] A.C. Hsieh, R. Bo, J. Manola, F. Vazquez, O. Bare, A. Khvorova, S. Scaringe, W.R. Sellers. A Library of Sirna Duplexes Targeting the Phosphoinositide 3-Kinase Pathway: Determinants of Gene Silencing for Use in Cell-Based Screens. *Nucleic Acids Res* **2004** *32* 893-901.
[18] K. Miyawaki-Shimizu, D. Predescu, J. Shimizu, M. Broman, S. Predescu, A.B. Malik. Sirna-Induced Caveolin-1 Knockdown in Mice Increases Lung Vascular Permeability Via the Junctional Pathway. *Am J Physiol Lung Cell Mol Physiol* **2006** *290* L405-413.
[19] Y.R. Yuan, Y. Pei, H.Y. Chen, T. Tuschl, D.J. Patel. A Potential Protein-Rna Recognition Event Along the Risc-Loading Pathway from the Structure of A. Aeolicus Argonaute with Externally Bound Sirna. *Structure* **2006** *14* 1557-1565.
[20] G. Beale, A.J. Hollins, M. Benboubetra, M. Sohail, S.P. Fox, I. Benter, S. Akhtar. Gene Silencing Nucleic Acids Designed by Scanning Arrays: Anti-Egfr Activity of Sirna, Ribozyme and DNA Enzymes Targeting a Single Hybridization-Accessible Region Using the Same Delivery System. *J Drug Target* **2003** *11* 449-456.
[21] A. Kwok, S.L. Hart. Comparative Structural and Functional Studies of Nanoparticle Formulations for DNA and Sirna Delivery. *Nanomedicine* **2011** *7* 210-219.
[22] M. Dominska, D.M. Dykxhoorn. Breaking Down the Barriers: Sirna Delivery and Endosome Escape. *J Cell Sci* **2010** *123* 1183-1189.
[23] K. Chaturvedi, K. Ganguly, A.R. Kulkarni, V.H. Kulkarni, M.N. Nadagouda, W.E. Rudzinski, T.M. Aminabhavi. Cyclodextrin-Based Sirna Delivery Nanocarriers: A State-of-the-Art Review. *Expert Opin Drug Deliv* **2011** *8* 1455-1468.
[24] S.H. Kim, J.H. Jeong, S.H. Lee, S.W. Kim, T.G. Park. Local and Systemic Delivery of Vegf Sirna Using Polyelectrolyte Complex Micelles for Effective Treatment of Cancer. *J Control Release* **2008** *129* 107-116.
[25] D.L. Lewis, J.A. Wolff. Systemic Sirna Delivery Via Hydrodynamic Intravascular Injection. *Adv Drug Deliv Rev* **2007** *59* 115-123.
[26] Y.C. Tseng, S. Mozumdar, L. Huang. Lipid-Based Systemic Delivery of Sirna. *Adv Drug Deliv Rev* **2009** *61* 721-731.
[27] A. Sato, S.W. Choi, M. Hirai, A. Yamayoshi, R. Moriyama, T. Yamano, M. Takagi, A. Kano, A. Shimamoto, A. Maruyama. Polymer Brush-Stabilized Polyplex for a Sirna Carrier with Long Circulatory Half-Life. *J Control Release* **2007** *122* 209-216.
[28] J.J. Turner, S.W. Jones, S.A. Moschos, M.A. Lindsay, M.J. Gait. Maldi-Tof Mass Spectral Analysis of Sirna Degradation in Serum Confirms an Rnase a-Like Activity. *Mol Biosyst* **2007** *3* 43-50.

[29] X.L. Wang, S. Ramusovic, T. Nguyen, Z.R. Lu. Novel Polymerizable Surfactants with Ph-Sensitive Amphiphilicity and Cell Membrane Disruption for Efficient Sirna Delivery. *Bioconjug Chem* **2007** *18* 2169-2177.
[30] F.F. Yang, W. Huang, Y.F. Li, Z.G. Gao. Current Status of Non-Viral Vectors for Sirna Delivery. *Yao Xue Xue Bao* **2011** *46* 1436-1443.
[31] J.H. Jeong, H. Mok, Y.K. Oh, T.G. Park. Sirna Conjugate Delivery Systems. *Bioconjug Chem* **2009** *20* 5-14.
[32] A. Muratovska, M.R. Eccles. Conjugate for Efficient Delivery of Short Interfering Rna (Sirna) into Mammalian Cells. *FEBS Lett* **2004** *558* 63-68.
[33] T.C. Chu, K.Y. Twu, A.D. Ellington, M. Levy. Aptamer Mediated Sirna Delivery. *Nucleic Acids Res* **2006** *34* e73.
[34] W. Gao, Z. Xiao, A. Radovic-Moreno, J. Shi, R. Langer, O.C. Farokhzad. Progress in Sirna Delivery Using Multifunctional Nanoparticles. *Methods Mol Biol* **2010** *629* 53-67.
[35] Y. Gao, X.L. Liu, X.R. Li. Research Progress on Sirna Delivery with Nonviral Carriers. *Int J Nanomedicine* **2011** *6* 1017-1025.
[36] J. Liu, C. Gu, E.B. Cabigas, K.D. Pendergrass, M.E. Brown, Y. Luo, M.E. Davis. Functionalized Dendrimer-Based Delivery of Angiotensin Type 1 Receptor Sirna for Preserving Cardiac Function Following Infarction. *Biomaterials* **2013** *34* 3729-3736.
[37] O.M. Merkel, M. Zheng, M.A. Mintzer, G.M. Pavan, D. Librizzi, M. Maly, H. Hoffken, A. Danani, E.E. Simanek, T. Kissel. Molecular Modeling and in Vivo Imaging Can Identify Successful Flexible Triazine Dendrimer-Based Sirna Delivery Systems. *J Control Release* **2011** *153* 23-33.
[38] Y. Zhang, C. Zhou, K.J. Kwak, X. Wang, B. Yung, L.J. Lee, Y. Wang, P.G. Wang, R.J. Lee. Efficient Sirna Delivery Using a Polyamidoamine Dendrimer with a Modified Pentaerythritol Core. *Pharm Res* **2012** *29* 1627-1636.
[39] S.R. Croy, G.S. Kwon. Polymeric Micelles for Drug Delivery. *Curr Pharm Des* **2006** *12* 4669-4684.
[40] A.J. Convertine, C. Diab, M. Prieve, A. Paschal, A.S. Hoffman, P.H. Johnson, P.S. Stayton. Ph-Responsive Polymeric Micelle Carriers for Sirna Drugs. *Biomacromolecules* **2010**.
[41] L.S. del Rosario, B. Demirdirek, A. Harmon, D. Orban, K.E. Uhrich. Micellar Nanocarriers Assembled from Doxorubicin-Conjugated Amphiphilic Macromolecules (Dox-Am). *Macromol Biosci* **2010** *10* 415-423.
[42] J.D.R. Djordjevic, ; J. Wang,; K.E. Uhrich, Amphiphilic Scorpion-Like Macromolecules as Micellar Nanocarriers. *Journal of Bioactive and Compatible Polymers* **2008** *23* 20-28.
[43] L.Y. Tian, L.; Zhou, N.; Tat, H.; Uhrich, K. E. Amphiphilic Scorpion-Like Macromolecules: Design, Synthesis, and Characterization. *Macromolecules* **2004** *37* 5.
[44] S.M. Sparks, C.L. Waite, A.M. Harmon, L.M. Nusblat, C.M. Roth, K.E. Uhrich. Efficient Intracellular Sirna Delivery by Ethyleneimine-Modified Amphiphilic Macromolecules. *Macromol Biosci* **2011** *11* 1192-1200.
[45] A.L. Bailey, P.R. Cullis. Membrane Fusion with Cationic Liposomes: Effects of Target Membrane Lipid Composition. *Biochemistry* **1997** *36* 1628-1634.
[46] N. Duzgunes, J.A. Goldstein, D.S. Friend, P.L. Felgner. Fusion of Liposomes Containing a Novel Cationic Lipid, N-[2,3-(Dioleyloxy)Propyl]-N,N,N-Trimethylammonium: Induction by Multivalent Anions and Asymmetric Fusion with Acidic Phospholipid Vesicles. *Biochemistry* **1989** *28* 9179-9184.

[47] J. Monkkonen, A. Urtti. Lipid Fusion in Oligonucleotide and Gene Delivery with Cationic Lipids. *Adv Drug Deliv Rev* **1998** *34* 37-49.
[48] D. Chapman, N.F. Owens, M.C. Phillips, D.A. Walker. Mixed Monolayers of Phospholipids and Cholesterol. *Biochim Biophys Acta* **1969** *183* 458-465.
[49] M. Subramanian, J.M. Holopainen, T. Paukku, O. Eriksson, I. Huhtaniemi, P.K. Kinnunen. Characterisation of Three Novel Cationic Lipids as Liposomal Complexes with DNA. *Biochim Biophys Acta* **2000** *1466* 289-305.
[50] A.D. Tsamaloukas, S. Keller, H. Heerklotz. Uptake and Release Protocol for Assessing Membrane Binding and Permeation by Way of Isothermal Titration Calorimetry. *Nat Protoc* **2007** *2* 695-704.
[51] L. Nuhn, M. Hirsch, B. Krieg, K. Koynov, K. Fischer, M. Schmidt, M. Helm, R. Zentel. Cationic Nanohydrogel Particles as Potential Sirna Carriers for Cellular Delivery. *ACS Nano* **2012** *6* 2198-2214.
[52] X.L. Wang, R. Xu, Z.R. Lu. A Peptide-Targeted Delivery System with Ph-Sensitive Amphiphilic Cell Membrane Disruption for Efficient Receptor-Mediated Sirna Delivery. *J Control Release* **2009** *134* 207-213.
[53] P. Holzerny, B. Ajdini, W. Heusermann, K. Bruno, M. Schuleit, L. Meinel, M. Keller. Biophysical Properties of Chitosan/Sirna Polyplexes: Profiling the Polymer/Sirna Interactions and Bioactivity. *J Control Release* **2012** *157* 297-304.
[54] L.B. Jensen, K. Mortensen, G.M. Pavan, M.R. Kasimova, D.K. Jensen, V. Gadzhyeva, H.M. Nielsen, C. Foged. Molecular Characterization of the Interaction between Sirna and Pamam G7 Dendrimers by Saxs, Itc, and Molecular Dynamics Simulations. *Biomacromolecules* **2010** *11* 3571-3577.
[55] A. El Ouahabi, M. Thiry, V. Pector, R. Fuks, J.M. Ruysschaert, M. Vandenbranden. The Role of Endosome Destabilizing Activity in the Gene Transfer Process Mediated by Cationic Lipids. *FEBS Lett* **1997** *414* 187-192.
[56] S. Yang, S. May. Release of Cationic Polymer-DNA Complexes from the Endosome: A Theoretical Investigation of the Proton Sponge Hypothesis. *J Chem Phys* **2008** *129* 185-195.
[57] Y. Hattori, Y. Maitani. Low-Molecular-Weight Polyethylenimine Enhanced Gene Transfer by Cationic Cholesterol-Based Nanoparticle Vector. *Biol Pharm Bull* **2007** *30* 1773-1778.
[58] A.M. Harmon, M.H. Lash, S.M. Sparks, K.E. Uhrich. Preferential Cellular Uptake of Amphiphilic Macromolecule-Lipid Complexes with Enhanced Stability and Biocompatibility. *J Control Release* **2011** *153* 233-239.

4. Stability of Amphiphilic Macromolecules in Commercial Sterilization

4.1 Introduction

Amphiphilic macromolecules (AMs) can self-assemble into micelles in aqueous media due to their amphiphilicity. Given the micellization behavior of AMs, they are capable of encapsulating hydrophobic molecules in the micelle inner core and transporting the molecular cargo within the aqueous environment [1-7]. An amphiphilic macromolecule (AM) (Figure 4.1) previously developed by Uhrich et al. is composed of a hydrophobic, alkylated mucic acid backbone and hydrophilic poly(ethylene glycol) (PEG) coupled to the hydrophobic core via an ester bond [8].

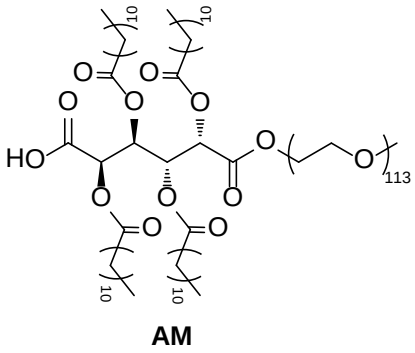

Figure 4.1 Structure of AM [8]

This AM has been demonstrated as a nano carrier for water-insoluble drugs and *in vitro* evaluation for systemic delivery was also performed [9-11]. The AM has also been incorporated into liposomes by electrostatic and hydrophobic interactions with lipids. The formulation of these AM-lipid complexes results in increased biocompatibility, ability to load and deliver anti-cancer therapeutics, and allow for preferential uptake in cancer cells [12]. By chemically incorporating oligoethylenimines into the AM backbone, cationic AMs can be obtained with capabilities to complex with and deliver siRNA *in vitro* [13]. In addition to these drug delivery

applications, AMs have also demonstrated unique properties in managing atherosclerosis, a main trigger for cardiovascular disease [14]. The AM has been tested as a therapeutic agent to inhibit the atherosclerotic cascade by inhibiting the uptake of oxLDL in macrophages. To optimize the inhibition effectiveness, other AMs with modified structures have also been synthesized and tested [14-18]. Due to the broad biomedical applications of these AMs, they could potentially be developed into a medical device or drug and therefore, must be rendered sterile.

Common sterilization methods include heat sterilization [19-21], chemical sterilization [22, 23], sterile filtration [24-26], and ionizing sterilization[27-32]. Heat sterilization usually requires high temperatures (120^{o}C) which could possibly lead to decomposition or degradation of AMs [19-21]. Chemical sterilization requires high concentrations of reactive sterilants, such as hydrogen peroxide, or ozone, which could lead to potential oxidative reaction with the AM [22, 23]. Sterile filtration is a convenient and efficient way to sterilize samples; however, it requires a filtration membrane which will absorb highly viscous drug components or nanoparticles [24-26]. Ionizing sterilization includes electron beam (e-beam) and gamma radiation. Gamma radiation uses Cobalt-60 to continuously emit gamma rays with a high penetrating effect. Electron beam radiation is generated as electrons from a high-energy accelerator, and has a higher dose rate but less penetration than gamma radiation [27, 30]. As both e-beam and gamma sterilization methods use ionizing energy to irradiate samples without inducing high temperature or using chemical sterilants, these methods were chosen to test the stability of AMs to typical sterilizing conditions. Despite their positive attributes, both e-beam and gamma radiation exposure can cause slight degradation due to the high energy of the ionizing source [29-31, 33].

In this work, both e-beam and gamma radiation are used to irradiate the AM in powder form to study the effect of both sterilization methods on the AM properties. The AM was exposed to

each irradiation process at target doses of 25 kGy and 50 kGy, as 25 kGy is a typical sterilization dose and 50 kGy is a typical maximum processing dose [32]. After the exposures, proton nuclear magnetic resonance (^{1}H-NMR) spectroscopy was performed to determine the impact on chemical structure of the AM. Gel permeation chromatography (GPC) was used to investigate changes in molecular weight. Dynamic light scattering (DLS) was utilized to determine the impact on micelle behavior of AM. *In vitro* oxLDL uptake inhibition studies were then performed to determine the impact on the inhibiting activity of AMs in macrophages.

4.2 Results and discussion

4.2.1 Physicochemical characterization of AMs after sterilization

The AM powder remained a white solid after both radiation processes. To determine the impact of the ionizing radiation (e-beam and gamma radiation) on the physicochemical properties and bioactivity of the AM, ^{1}H NMR, GPC, and DLS were used to measure the changes in chemical structure, molecular weight and micelle behavior, respectively.

Weight-average molecular weight (M_w) is a parameter to determine polymer degradation or intermolecular cross-linking after the radiation processes. The M_w of irradiated AMs showed no significant differences against the control, indicating no degradation or intermolecular cross-linking caused by irradiation (Table 4.1).^{1}H NMR spectroscopy was used to determine changes in the chemical structure. The main peaks of the mucic acid backbone, PEG, and alkyl chains appeared identical to controls after the radiation exposure. Based on the ^{1}H NMR and M_w data the chemical structure and molecular weight of AM were not affected by radiation exposure. Micellar size is an important property when using AMs as therapeutic delivery vehicles. Micelles of non-treated AMs are about 11.5 nm in size, which is usually within the ideal range for drug

delivery [5, 34, 35]. No significant differences ($p<0.05$) were discovered between the irradiated samples and control, indicating that neither of the e-beam and gamma radiation methods had significant impact on the micellar size of the AM (Table 4.1). The zeta potential of the micellar AM correlates to the anionic nature of AM, which plays an important role when AM inhibits the oxLDL uptake in macrophages [15, 16]. Hence, zeta potential is a key parameter when predicting activity of AMs in treating atherosclerosis. Zeta potentials of irradiated AM samples display no significant differences compared to control ($p<0.05$) (Table 4.1). According to the DLS data of irradiated and non-treated AMs, neither e-beam nor gamma irradiation affect the micellar behavior of AM in aqueous media.

Table 4.1 Molecular weight and micelle behavior of AM (mean ± standard deviation)

	Control	**e-beam 25kGy**	**e-beam 50kGy**	**gamma 25kGy**	**gamma 50kGy**
M_w (Da)	6300±200	6200±120	6100±110	6000±150	6400±190
Sizes (nm)	11.5±0.92	12.2±2.2	10.9±1.6	11.6±1.2	12.0±1.2
Zetapotential (mV)	-19.8±3.1	-19.0±2.8	-18.5±2.0	-19.6±2.7	-20.2±3.4

4.2.2 Bioactivity evaluation after sterilization *(Performed by Kyle Zablocki)*

Besides the physicochemical properties of AMs, the ability of AMs to inhibit oxLDL uptake in macrophages were also studied. PBMC macrophages were co-incubated with oxLDL and AMs for 24 h. Basal condition (Figure 4.2) was performed as incubation without oxLDL or AMs, whereas the oxLDL condition (Figure 4.2) was performed as incubation with oxLDL only. Both of these conditions are shown as controls along with the untreated AMs. oxLDL uptake in

PBMC for radiated AMs was quantified and normalized to the cell counts of oxLDL conditions (Figure 4.2). Both untreated AMs and irradiated AMs inhibited around 70% oxLDL uptake in macrophages, showing no significant differences between untreated and irradiated AMs (Figure 4.2). Hence, the abilities of all radiated AMs to inhibit oxLDL uptake in macrophages were not altered through the radiation exposure. This finding also demonstrates that the overall AM properties were not impacted by the exposure to both radiation processes.

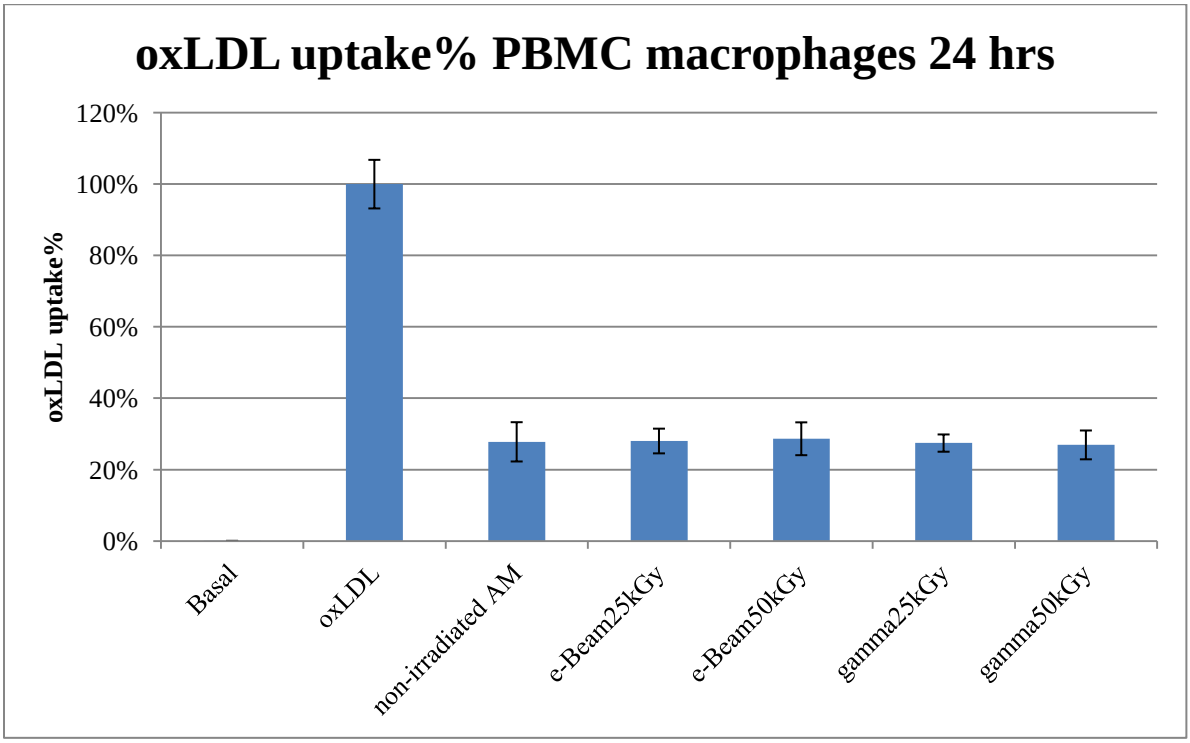

Figure 4.2 oxLDL uptake in PBMC macrophages after radiation exposure at 25 kGy and 50 kGy. No significant differences were observed against the non-irradiated controls ($p < 0.05$).

4.3 Conclusion

The potential of developing AM into an implantable device dictates that AM should be compatible with a sterilization process such as ionizing radiation. In this study, the AM composition, molecular weight, micelle behavior, and biological activity are not substantially affected by exposure to e-beam and gamma radiation (25 and 50 kGy). Therefore, e-beam or gamma radiation with doses up to 50 kGy can be suitable for sterilizing AM.

4.4 Experimental

4.4.1 Materials

All other chemicals and reagents were purchased from Sigma-Aldrich (Milwaukee, WI) and used as received.

4.4.2 Sample preparation

AM (Figure 4.1) was synthesized based on previously published method [8]. In short, mucic acid was acylated with lauroyl chloride followed by coupling with mono-hydroxy PEG. The AM powder (2.5g) was divided into five BD Falcon 5 mL polystyrene round-bottom tubes (12 × 75 mm style; BD Bioscience Discovery Labware, Bedford, MA), one was for the untreated control and another four were for the radiation exposures. All the samples were stored at 4 ^{o}C for 24 h prior to being sent to Johnson & Johnson Sterile Process Technology (SPT) for radiation processing. After exposure, samples were stored at 4^{o}Cfor 24 h until physicochemical and biological characterization studies were performed in triplicate.

4.4.3 Radiation exposure *(Performed by Sterile Process Technology of J & J)*

Gamma irradiation was conducted in a Cobalt 60 source MDS Nordion Gamma Cell 220 Research irradiator at Sterile Process Technology of Johnson & Johnson. The temperature during exposure ranged from 30^{o}C to 37^{o}C with a dose rate of approximately 0.002kGy/s for a maximum of 9 h. Samples for e-beam irradiation were processed under ambient conditions in the Mevex 5 MeV, 2kW electron beam linear accelerator. Samples were placed upright in an Ethafoam® jig and presented single-sided to the beam. Doses for both of the radiation processes were 25 kGy and 50k Gy. The dose rate for e-beam was approximately 12.5 kGy/s. The temperature ranged from 38^{o}C (25 kGy) to 55^{o}C (50 kGy) during the e-beam exposures. Samples designated as controls were not exposed to ionizing radiation.

4.4.4 Physicochemical characterization

Proton nuclear magnetic resonance (^{1}H NMR) spectra were obtained using a Varian 500 MHz spectrometer. AM samples (10-15 mg) were dissolved in deuterated chloroform. Each spectrum was an average of 16 scans. Molecular weights (M_w) were determined using gel permeation chromatography (GPC) with respect to PEG standards (Sigma-Aldrich) on a Waters Stryagel® HR 3 THF column (7.8 × 300 mm). The Waters LC system (Milford, MA) was equipped with a 2414 refractive index detector, a 1515 isocratic HPLC pump, and 717plus autosampler. Samples (10 mg/mL) were prepared in THF and filtered using 0.23μm pore PTFE syringe filters (Fisher Scientific).Dynamic light scattering (DLS) analysis was carried out on a Zetasizer nanoseries

nano ZS90 (Malvern instruments). Samples (1-2 mg/mL) were prepared in HPLC water and filtered using 0.23µm pore size PTFE syringe filters (Fisher Scientific).

4.4.5 Cell culture *(Performed by Kyle Zablocki)*

Peripheral blood mononuclear cells (PBMC) were isolated from human buffy coats (Blood Center of New Jersey, East Orange, NJ) by density gradient centrifugation over Ficoll-Paque. Monocytes were selected by plastic adherence as follows. PBMCs suspended in Roswell Park Memorial Institute (RPMI) 1640 medium (ATCC) with 10% fetal bovine serum were incubated in 96-well plates for 4 h. Non-adherent cells were removed by washing three times with phosphate buffer saline, and adherent cells were cultured for 7 days in RPMI supplemented with 10% fetal bovine serum, 1% penicillin/streptomycin and 50 ng/mL macrophage colony-stimulating factor (M-CSF) (PeproTech) for differentiation into macrophages. Media was changed every 2-3 days.

4.4.6 oxLDL uptake by PBMC macrophages *(Performed by Kyle Zablocki)*

PBMC macrophages were co-incubated with 10µg/mL of 3,3'-dioctadecyloxacarbocyanine (DiO) labeled oxLDL (Kalen Biomedical; Montgomery Village, MD) and AM(10^{-6}M) for 24 h in RPMI 1640. Cells were fixed with and counterstained with Hoechst 33342 prior to epifluorescent imaging on a Nikon Eclipse TE2000-S. oxLDL uptake was quantified using ImageJ and normalized to cell count. Results are the average of three experiments performed in biological triplicate.

4.4.7 Statistical analysis

Statistical analysis was performed with Student t-tests using SigmaStata software. Differences were considered significant at $p<0.05$ by pairwise comparison with Dunnett's post hoc test.

4.5 References

[1] M.L. Adams, D.R. Andes, G.S. Kwon. Amphotericin B Encapsulated in Micelles Based on Poly(Ethylene Oxide)-Block-Poly(L-Amino Acid) Derivatives Exerts Reduced in Vitro Hemolysis but Maintains Potent in Vivo Antifungal Activity. *Biomacromolecules* **2003** *4* 750-757.
[2] M.F. Francis, M. Piredda, F.M. Winnik. Solubilization of Poorly Water Soluble Drugs in Micelles of Hydrophobically Modified Hydroxypropylcellulose Copolymers. *J Control Release* **2003** *93* 59-68.
[3] A.K. Iyer, K. Greish, T. Seki, S. Okazaki, J. Fang, K. Takeshita, H. Maeda. Polymeric Micelles of Zinc Protoporphyrin for Tumor Targeted Delivery Based on Epr Effect and Singlet Oxygen Generation. *J Drug Target* **2007** *15* 496-506.
[4] J.X. Xu, J.B. Tang, L.H. Zhao, Y.Q. Shen. Advances in the Study of Tumor Ph-Responsive Polymeric Micelles for Cancer Drug Targeting Delivery. *Yao Xue Xue Bao* **2009** *44* 1328-1335.
[5] W. Xu, P. Ling, T. Zhang. Polymeric Micelles, a Promising Drug Delivery System to Enhance Bioavailability of Poorly Water-Soluble Drugs. *J Drug Deliv* **2013** *2013* 340315.
[6] H. Yin, Y.H. Bae. Physicochemical Aspects of Doxorubicin-Loaded Ph-Sensitive Polymeric Micelle Formulations from a Mixture of Poly(L-Histidine)-B-Poly(Ethylene Glycol)/Poly(L-Lactide)-B-Poly(Ethylene Glycol) [Corrected]. *Eur J Pharm Biopharm* **2009** *71* 223-230.
[7] C.Y. Zhang, Y.Q. Yang, T.X. Huang, B. Zhao, X.D. Guo, J.F. Wang, L.J. Zhang. Self-Assembled Ph-Responsive Mpeg-B-(Pla-Co-Pae) Block Copolymer Micelles for Anticancer Drug Delivery. *Biomaterials* **2012** *33* 6273-6283.
[8] L.Y. Tian, L.; N. Zhou,; H. Tat,; K. E. Uhrich, Amphiphilic Scorpion-Like Macromolecules: Design, Synthesis, and Characterization. *Macromolecules* **2004** *37* 538-545.
[9] J.D.R. Djordjevic, L.; J. Wang,; K.E. Uhrich, Amphiphilic Scorpion-Like Macromolecules as Micellar Nanocarriers. *Journal of Bioactive and Compatible Polymers* **2008** *23* 20-28.
[10] A.M. Harmon, K.E. Uhrich. In Vitro Evaluation of Amphiphilic Macromolecular Nanocarriers for Systemic Drug Delivery. *Journal of Bioactive and Compatible Polymers* **2009** *24* 185-197.
[11] L. Tao, K.E. Uhrich. Novel Amphiphilic Macromolecules and Their in Vitro Characterization as Stabilized Micellar Drug Delivery Systems. *J Colloid Interface Sci* **2006** *298* 102-110.
[12] A.M. Harmon, M.H. Lash, S.M. Sparks, K.E. Uhrich. Preferential Cellular Uptake of Amphiphilic Macromolecule-Lipid Complexes with Enhanced Stability and Biocompatibility. *J Control Release* **2011** *153* 233-239.

[13] S.M. Sparks, C.L. Waite, A.M. Harmon, L.M. Nusblat, C.M. Roth, K.E. Uhrich. Efficient Intracellular Sirna Delivery by Ethyleneimine-Modified Amphiphilic Macromolecules. *Macromol Biosci* **2011** *11* 1192-1200.
[14] N.M. Iverson, S.M. Sparks, B. Demirdirek, K.E. Uhrich, P.V. Moghe. Controllable Inhibition of Cellular Uptake of Oxidized Low-Density Lipoprotein: Structure-Function Relationships for Nanoscale Amphiphilic Polymers. *Acta Biomater* **2010** *6* 3081-3091.
[15] E. Chnari, H.B. Lari, L. Tian, K.E. Uhrich, P.V. Moghe. Nanoscale Anionic Macromolecules for Selective Retention of Low-Density Lipoproteins. *Biomaterials* **2005** *26* 3749-3758.
[16] E. Chnari, J.S. Nikitczuk, K.E. Uhrich, P.V. Moghe. Nanoscale Anionic Macromolecules Can Inhibit Cellular Uptake of Differentially Oxidized Ldl. *Biomacromolecules* **2006** *7* 597-603.
[17] J. Wang, N.M. Plourde, N. Iverson, P.V. Moghe, K.E. Uhrich. Nanoscale Amphiphilic Macromolecules as Lipoprotein Inhibitors: The Role of Charge and Architecture. *Int J Nanomedicine* **2007** *2* 697-705.
[18] A.W. York, K.R. Zablocki, D.R. Lewis, L. Gu, K.E. Uhrich, R.K. Prud'homme, P.V. Moghe. Kinetically Assembled Nanoparticles of Bioactive Macromolecules Exhibit Enhanced Stability and Cell-Targeted Biological Efficacy. *Adv Mater* **2012**.
[19] G. Alexandrou, K. Chrissafis, L. Vasiliadis, E. Pavlidou, E.K. Polychroniadis. Effect of Heat Sterilization on Surface Characteristics and Microstructure of Mani Nrt Rotary Nickel-Titanium Instruments. *Int Endod J* **2006** *39* 770-778.
[20] P.R. Chaturvedi, N.M. Patel, S.A. Lodhi. Effect of Terminal Heat Sterilization on the Stability of Phospholipid-Stabilized Submicron Emulsions. *Acta Pharm Nord* **1992** *4* 51-55.
[21] C.Y. Yeung, H.C. Lee, S.P. Lin, Y.C. Yang, F.Y. Huang, C.K. Chuang. Negative Effect of Heat Sterilization on the Free Amino Acid Concentrations in Infant Formula. *Eur J Clin Nutr* **2006** *60* 136-141.
[22] W.S. Pietrzak. Effects of Ethylene Oxide Sterilization on 82: 18 Plla/Pga Copolymer Craniofacial Fixation Plates. *J Craniofac Surg* **2010** *21* 177-181.
[23] F. Bounoure, H. Fiquet, P. Arnaud. Comparison of Hydrogen Peroxide and Peracetic Acid as Isolator Sterilization Agents in a Hospital Pharmacy. *Am J Health Syst Pharm* **2006** *63* 451-455.
[24] M.W. Jornitz, P.G. Soelkner, T.H. Meltzer. Sterile Filtration--a Review of the Past and Present Technologies. *PDA J Pharm Sci Technol* **2002** *56* 192-195.
[25] J.R. Lakey, M.E. Smith, T.J. Fetterhoff, T.J. Cavanagh, M.J. Wright, F.E. Dwulet. Sterile Filtration of Collagenase Solution: Effect of Filter Membrane Composition on Enzyme Recovery. *Transplant Proc* **1998** *30* 347.
[26] H.G. Schroeder. Sterile Filtration: Process Optimization through Real Compliance. *PDA J Pharm Sci Technol* **2003** *57* 393-398.
[27] V. Erokhin, T. Berzina, M.P. Fontana. Electron Beam Irradiation for Structuring of Molecular Assemblies. *IEEE Trans Nanobioscience* **2004** *3* 6-15.
[28] E. Karadag, O.B. Uzum, D. Saraydin, O. Guven. Dynamic Swelling Behavior of Gamma-Radiation Induced Polyelectrolyte Poly(Aam-Co-Ca) Hydrogels in Urea Solutions. *Int J Pharm* **2005** *301* 102-111.
[29] S.C. Loo, C.P. Ooi, Y.C. Boey. Influence of Electron-Beam Radiation on the Hydrolytic Degradation Behaviour of Poly(Lactide-Co-Glycolide) (Plga). *Biomaterials* **2005** *26* 3809-3817.

[30] A. Merkli, J. Heller, C. Tabatabay, R. Gurny. Gamma Sterilization of a Semi-Solid Poly(Ortho Ester) Designed for Controlled Drug Delivery--Validation and Radiation Effects. *Pharm Res* **1994** *11* 1485-1491.
[31] G. Valdes-Diaz, S. Rodriguez-Calvo, A. Perez-Gramatges, M. Rapado-Paneque, F.A. Fernandez-Lima, C.R. Ponciano, E.F. da Silveira. Effects of Gamma Radiation on Phase Behaviour and Critical Micelle Concentration of Triton X-100 Aqueous Solutions. *J Colloid Interface Sci* **2007** *311* 253-261.
[32] P.D. Zygoura, E.K. Paleologos, M.G. Kontominas. Effect of Ionising Radiation Treatment on the Specific Migration Characteristics of Packaging-Food Simulant Combinations: Effect of Type and Dose of Radiation. *Food Addit Contam Part A Chem Anal Control Expo Risk Assess* **2011** *28* 686-694.
[33] H. Fujii, K. Sakata, Y. Katsumata, R. Sato, M. Kinouchi, M. Someya, S. Masunaga, M. Hareyama, H.M. Swartz, H. Hirata. Tissue Oxygenation in a Murine Scc Vii Tumor after X-Ray Irradiation as Determined by Epr Spectroscopy. *Radiother Oncol* **2008** *86* 354-360.
[34] S.R. Croy, G.S. Kwon. Polymeric Micelles for Drug Delivery. *Curr Pharm Des* **2006** *12* 4669-4684.
[35] J. Wang, D. Mongayt, V.P. Torchilin. Polymeric Micelles for Delivery of Poorly Soluble Drugs: Preparation and Anticancer Activity in Vitro of Paclitaxel Incorporated into Mixed Micelles Based on Poly(Ethylene Glycol)-Lipid Conjugate and Positively Charged Lipids. *J Drug Target* **2005** *13* 73-80.

5 Summary and Future Direction

5.1 Dissertation summary

As many potent chemotherapeutics are water-insoluble, drug delivery vehicles are of most importance. Some AMs have been evaluated for anticancer drug delivery, however, the drug release is mediated by diffusion [1, 2] and not suitable for quick, triggered drug release. pH is a typical stimulus in cancer therapy owing to the acidic nature of tumor and intracellular environments [3]. In this dissertation, a pH-sensitive hydrazone bond was incorporated into the backbone of the parent AM. Two AMs bearing different numbers of PEG tails were successfully synthesized and their chemical structures characterized. With hydrazone bond cleavage occurring at acidic pH, AM micelles would undergo disruption. A typical anticancer drug, doxorubicin (DOX) was encapsulated; DOX release at acidic pH was also enhanced significantly compared to physiological pH. Cytotoxicity against cancer cells using DOX-loaded micelles was monitored against the parent AM (M12P5) and free DOX. DOX-loaded parent AMs showed less cytotoxicity against cancer cells, reducing cell viability to 90%. In contrast pH-sensitive AMs with either one or two PEG tails showed enhanced cytotoxicity, reducing cell viability to 40% which is higher than free DOX. As previously demonstrated in the pH-dependent release profile, hydrazone cleavage can accelerate drug release in intracellular conditions leading to enhanced cytotoxicity.

siRNA is a very important drug candidate as it is effective at silencing target protein, however, safe and effective carriers for siRNA are needed. A pH-responsive AM-lipid complex describe based on previous work [4], that showed cationic AMs have moderate delivery efficiencies with

excellent biocompatibility compared to polyethylenimine (PEI). To develop more efficient siRNA carriers, composite systems containing cationic AM and lipids were formulated. Thermodynamic studies (isotherm compression and isothermal titration calorimetry) were conducted to probe the interactions between cationic AM and lipid. Attractive net interactions between the AM and lipid was observed, in the presence of both electrostatic repulsion and hydrophobic attraction. *In vitro* siRNA delivery experiments demonstrated that certain compositions had comparable efficiency to Lipofectamine, gold standard in siRNA transfection. To probe the synergistic effect between AM and lipids, a series of experiments were conducted with the most effective AM-lipid composite system. Isothermal titration calorimetry was again used to measure the siRNA binding affinity to the system at both physiological and intracellular pH. Favorable binding between siRNA and complexes was observed at physiological pH. Though lower pH values typically protonate amines and increase cationic charges, no binding was observed at acidic pH condition. Further measurements involving complex stability at lower pH values indicated that the most effective composite system showed no cationic charge and decreased stability. This pH-responsive feature of the composite formulation provides a protective environment for siRNA at physiological pH yet releases siRNA at acidic pH. Intracellular trafficking of siRNA showed endosomal escape after 24 hrs. The composite formulation can respond to environmental pH changes: they are stable at physiological pH and unstable at acidic pH. Mechanistic studies indicated that CAM-lipid complexes can be an efficient and practical solution to the current siRNA delivery obstacle.

In summary, the dissertation describes AM-based drug delivery systems for anticancer drug and siRNA delivery. The common feature of the AM-based drug delivery systems is the pH-responsive characteristic: AMs micelles described in Chapter 2 undergo disruption at pH 5 based

on the hydrazone bond cleavage and CAM-lipid complexes in Chapter 3 are unstable and release siRNA at pH 5. Initial *in vitro* studies in both systems showed promise for delivery due to the pH-responsive feature.

5.2 Future directions

Although the pH-sensitive AMs show promise as anticancer drug delivery vehicles *in vitro*, *in vivo* data is lacking. Specifically, An animal model with tumor cell injections that develop tumor tissues is recommended. The drug-loaded micelles can be administered in two ways: local and systemic. As local delivery to tumor site will render the micelles in acidic condition right after the administration, drug will be release immediately. However, systemic injection will require stability in the circulation and accumulation in tumor tissue. Through incorporating targeting ligand to the AMs, both accumulation in tumor tissue and stability in physiological circulation can be achieved.

Instead of moving forward with the investigated systems, additional improvements are suggested. For example, the AMs described in Chapter 2 have relatively low weight loading (up to 15%) of doxorubicin compared to commercially available systems, such as Pluronic (up to 25%). AMs have a long PEG tail and a relatively small hydrophobic segment, yielding a small hydrophobic core. To improve the drug weight loading, methods to increase hydrophobicity can include increasing the alkyl chain length coupled to mucic acid and coupling another hydrophobic segment.

Another approach to prepare degradable AMs is proposed (Figure 5.1). In the proposed structure (Figure 5.1), hydrazide-functionalized AMs are attached to a dendrimer core bearing aldehyde

groups via pH-sensitive hydrazone bonds. Due to the amphiphilic feature of AM, the unimer can be considered as a unimolecular micelle (Figure 5.1). Hydrophobic drug can be loaded into core of the unimer (Figure 5.1) or the unimer can further self-assemble into a larger aggregate and encapsulate hydrophobic drugs to improve drug loading. Once the unimolecular micelles are in acidic condition, the cleavage of hydrazone bond will lead to drug release. The unimolecular micelle may be more stable than individual unimer-assembled micelles which are in thermodynamic equilibrium with the unimers. Additionally, targeting ligands can be incorporated into the unimer through PEG functionalization (Figure 5.1). Clustered ligands in each unimer can increase the ligand density in self-assembled larger micelles, yielding an enhanced intracellular uptake.

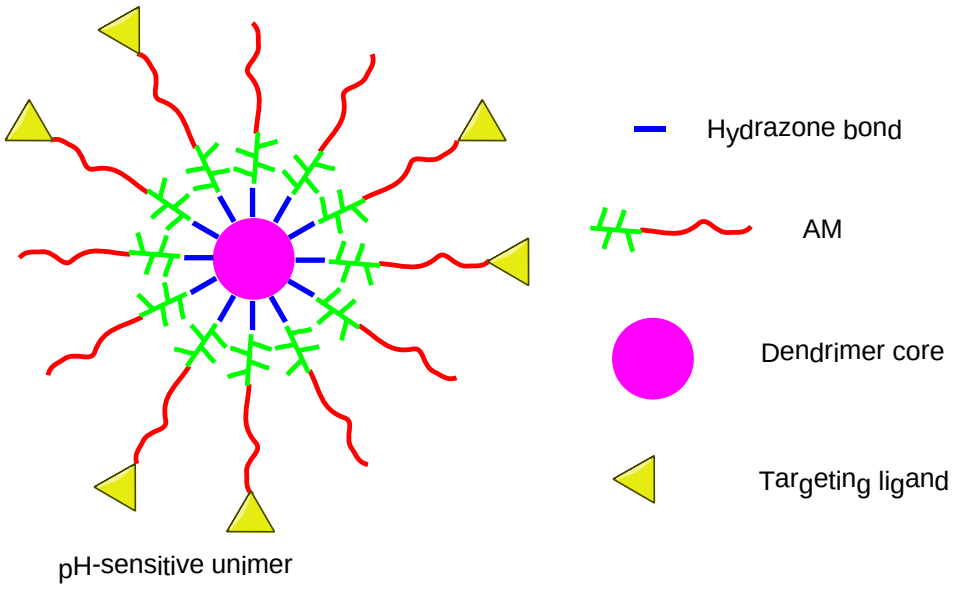

Figure 5.1 Schematic illustration of pH-sensitive unimolecular micelle bearing AM as the arm via hydrazone bonds

As described in Chapter 3, CAM-lipid complexes showed instability at lower pH. Performing isotherm compression at lower pH value will indentify the repulsive interaction between CAM

and lipid. CAM-lipid complexes show interesting differential binding affinities to siRNA at different pHs using ITC. Carrying out the binding studies in a more physiological-like condition, such as adding RNase and serum protein, would be insightful. Another future direction is to evaluate the transfection efficiencies using *in vivo* models. As the efficient CAM-lipid complexes show high transfection efficiency and low cytotoxicity, *in vivo* investigation of the aforementioned systems would better evaluate their potential in delivering siRNA. Based on the non-covalent interactions between CAM and lipid, stability in the actual physiological condition could be an issue leading to decreased *in vivo* transfection efficiency. However, the idea of triggering the endosomal escape and siRNA release based on pH change is still a viable approach. As such, a covalently adjoined pH-responsive and lipid features could lead to a more stable carrier while retaining the aforementioned endosomal escape and pH-triggered siRNA release (Figure 5.2). To achieve siRNA release in cytosol, the pH-cleavable linkages can be used to link the CAM cationic and lipid features, then cleaved to release siRNA. If necessary, a pH-cleavable linkage can also be added to remove the PEG tail and yield a higher siRNA release rate.

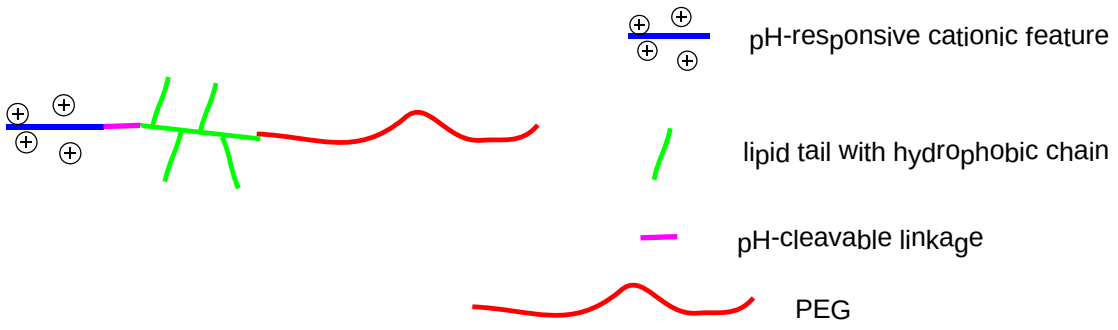

Figure 5.2 Schematic illustration of novel AMs bearing pH-responsive cationic feature, pH-cleavable linkage, lipid feature, and PEG for enhanced siRNA delivery

5.3 References

[1] L.S. del Rosario, B. Demirdirek, A. Harmon, D. Orban, K.E. Uhrich. Micellar Nanocarriers Assembled from Doxorubicin-Conjugated Amphiphilic Macromolecules (Dox-Am). *Macromol Biosci* **2010** *10* 415-423.
[2] Djordjevic,J.; J. Wang,; K.E. Uhrich, Amphiphilic Scorpion-Like Macromolecules as Micellar Nanocarriers. *Journal of Bioactive and Compatible Polymers* **2008** *23* 20-28.
[3] Y. Shen, H. Tang, M. Radosz, E. Van Kirk, W.J. Murdoch. Ph-Responsive Nanoparticles for Cancer Drug Delivery. *Methods Mol Biol* **2008** *437* 183-216.
[4] S.M. Sparks, C.L. Waite, A.M. Harmon, L.M. Nusblat, C.M. Roth, K.E. Uhrich. Efficient Intracellular Sirna Delivery by Ethyleneimine-Modified Amphiphilic Macromolecules. *Macromol Biosci* **2011** *11* 1192-1200.

6 Appendix 1: Synthesis of AMs for Atherosclerosis Treatment

6.1 Introduction

Atherosclerosis has acquired much attention due to its role in triggering cardiovascular disease, a leading cause of death in society [1-5]. Escalated oxidized low density lipoprotein (oxLDL) uptake in macrophages in the artery wall converts the macrophages to foam cells of which uncontrolled accumulation leads to atherosclerotic plaque formation [6-9]. The treatment of atherosclerosis has largely been focused on inhibiting cholesterol synthesis in the blood; for example, statin families lower the cholesterol level [10-17]. Other therapeutic efforts have been focused on intervening in the atherosclerotic cascade such as monocyte recruitment inhibition [18, 19], deletion of macrophage receptors responsible for oxLDL binding and uptake [20], and macrophage differentiation suppression and foam cell reduction [21].

In collaboration with Moghe's Lab in the Biomedical Engineering department of Rutgers University, AMs have shown promise in preventing the atherosclerotic progression via inhibiting oxLDL uptake in macrophages [22-24]. Previous efforts have been focused in identifying specific architectural features that impact inhibition of oxLDL uptake. First, a series of AMs were synthesized to investigate the influence of PEG chain length, alkyl chain length attached to the mucic acid, carboxylic acid location, type and number of anionic charges, anionic group rotational motion, and PEG architecture on oxLDL inhibition [24, 25]. Overall, the parent AM (Figure 6.1) has demonstrated the highest efficiency in preventing oxLDL uptake in macrophages [24]. The importance of charge and the presence of a rigid hydrophobic carboxylic acid for oxLDL inhibitory ability was also elucidated [24]. Molecular modeling studies have

shown that the higher calculated binding affinity of the AMs for the receptor, the better the inhibitory ability they possess [26].

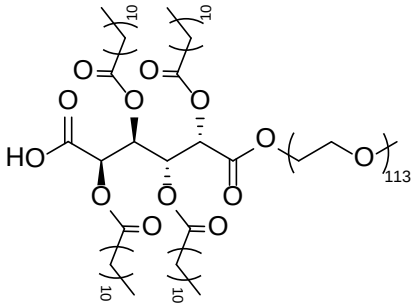

Parent AM: M12P5

Figure 6.1 Chemical structure of parent AM: M12P5 where M represents mucic acid backbone, 12 represents 12-carbon chain attached to the hydroxyl group of mucic acid, P represents PEG, 5 represents 5 kDa molecular weight of PEG [27]

Despite systematically altering the charge, alkyl chain length, and PEG length, the role of rigidity in AM activity has not been investigated. In this work, an aromatic ring-based AM was synthesized through alteration of the hydrophobic backbone. To optimize binding affinity to the scavenger receptor, we hypothesized that increasing the rigidity of the AM core can result in higher binding affinity to scavenger receptor and more efficient oxLDL inhibitory activity

6.2 Results and discussion

6.2.1 Synthesis and characterization of aromatic ring-based AM (Ar12P5, Figure 6.2)

Aromatic compounds are structurally more rigid than aliphatic compounds and, as previously mentioned, studies show that increased carboxylic acid rigidity is desirable for enhanced inhibitory activity [24, 26]. In this work, 2,5-dihydroxy terephthalic acid was chosen as the

building block, as it contains both two carboxylate and two hydroxyl groups for functionalization. Similar to the synthesis of parent AM [27], the aromatic ring-based AM (**Ar12P5**, Figure 6.2) was synthesized in two steps (Figure 6.2). The 2,5-dihydroxy terephthalic acid was first modified with lauroyl chloride in the presence of zinc chloride to yield the hydrophobic core (**Ar12**, Figure 6.2). Final product **Ar12P5** (Figure 6.2) was prepared by conjugating hydroxyl terminated-PEG (5 kDa) to the **Ar12** (Figure 6.2) via DCC. The chemical structure and molecular weight of **Ar12P5** were confirmed by ^{1}H NMR spectroscope and GPC.

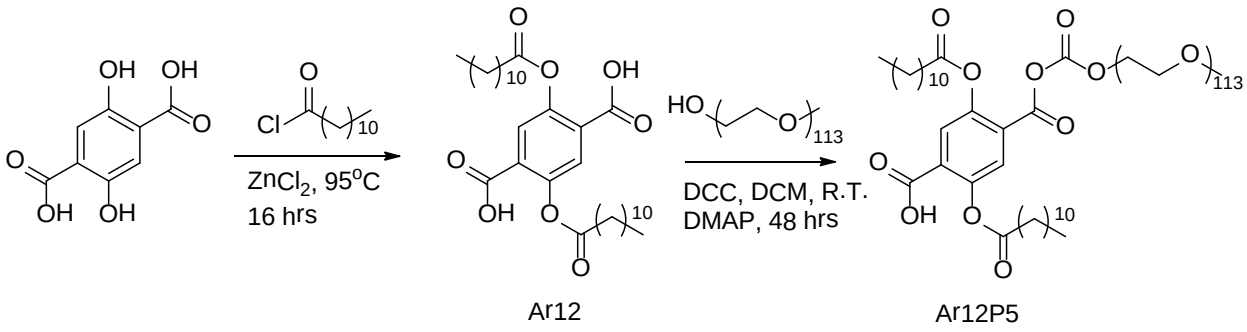

Figure 6.2 Synthetic scheme of aromatic ring-based AM: **Ar12P5**, Ar represents aromatic ring, 12 represents 12 carbon chain attached to the hydroxyl group, P represents PEG, 5 represents 5kDa molecular weight of PEG

As the aromatic terephthalic acid may alter the conformation of the AMs' core from a linear sugar backbone to a partially rigid aromatic backbone, micelles formed from **Ar12P5** were twice the size (40 nm) of micelle formed by **M12P5** (15 nm) [27]. This increase in size was anticipated, as terephthalic acid is more sterically bulky than an extended chain such as mucic acid. Furthermore, the CMC value of **Ar12P5** is significantly higher than that of the extended chain AMs, 10^{-4} M as opposed to 10^{-6} M, respectively. The T_m value was not significantly affected, as both were in the range of 60 °C.

6.2.2 oxLDL uptake inhibition in macrophages *(Performed by Nicole Plourde)*

The modified AMs were evaluated for their ability to inhibit oxLDL internalization through *in vitro* structure-activity relationship studies with human embryonic kidney – scavenger receptor (HEK-SRA) cells. Experiments were carried out via incubation of the HEK-SRA cells with 10^{-6} M polymers and fluorescently labeled oxLDL for 24 hr at 37 °C. The 24-hr time point allows for saturation of the cells with oxLDL. As controls, the basal uptake of oxLDL when SRA-expression was not induced and the basal uptake of oxLDL when no polymer was present were both evaluated. Incorporation of a rigid aromatic ring in the AM gave a similar oxLDL inhibition efficiency (~80%) to compared to previously determined, "gold standard" of M12P5 (Figure 6.3). This finding correlates with previous results that indicate constraining the motion of charge can enhance the oxLDL inhibition. The following modeling was carried out to illustrate the structural relation with binding to SRA receptors.

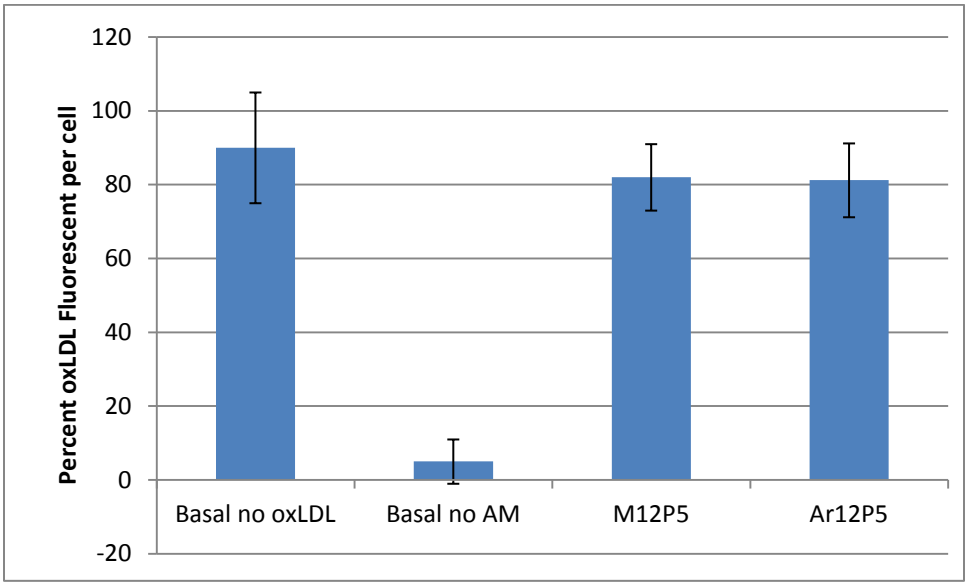

Figure 6.3 oxLDL uptake inhibition efficiencies of HEK-SRA cells in the presence of AMs at 24

hr. Data represent mean ± standard error (n = 3).

6.2.3 Binding affinity to SRA receptor *(Performed by Nicole Plourde)*

For molecular modeling, the polymers were evaluated according to their chemical structures and scaled to contain only 20 ethylene glycol repeat units instead of 110. We previously observed that the PEG chain has little interaction with the collagen-like domain [26], and scaling allows for optimization of computational time. The aliphatic arms were modeled at full alkyl chain length to fully assess the role of the hydrophobic domain. The modeled polymers were docked to an SR-A collagen-like domain homology model using GOLD v.3.2 [28] and ranked based on its GoldScore. The **M12P5** possesses a favorable binding energy (-29 kcal/mol) as the four aliphatic arms remain in close contact with the SR-A model, indicating a significant amount of hydrophobic interactions. Incorporation of a rigid aromatic hydrophobic component (**Ar12P5**) resulted in binding comparable to **M12P5**. Although it has only half the number of aliphatic arms, **Ar12P5** demonstrated comparable binding in both *in vitro* and molecular modeling experiments, inhibiting ~80% oxLDL uptake in HEK-SRA cells while showing a favorable binding energy (-26 kcal/mol) in modeling studies. This data correlates with previous findings that suggest increased rigidity positively affects oxLDL inhibition [29].

6.3 Conclusion

An aryl-based AM was designed to investigate the influence of a rigid hydrophobic domain on aggregation and biological properties. While seemingly small with respect to the overall polymer

compositions, this slight alteration in backbone architecture resulted in significant differences in properties, particularly in micelle size and solution stability. *In vitro* and molecular modeling experiments also demonstrated that minute changes in the polymer structure significantly affect SR-A binding affinities and consequently modulate the competitive inhibition of oxLDL uptake. Incorporation of an aromatic backbone (**Ar12P5**) results in oxLDL inhibition comparable to that of the previously published "gold standard", M12P5. These findings establish that the rigidity of the hydrophobic domain is a critical design factor influencing the biological and physicochemical properties of these polymers.

6.4 Experimental

6.4.1 Materials

All reagents and solvents were purchased from Sigma-Aldrich as used as received.

6.4.2 Characterization methods

^{1}H-NMR spectra were obtained using a Varian 400 MHz or 500 MHz spectrophotometer with TMS as internal reference. Samples were dissolved in $CDCl_3$, or $CDCl_3$ with a few drops of DMSO-d_6 if necessary. Molecular weights (Mw) were determined using gel permeation chromatography (GPC) with respect to PEG standards (Sigma-Aldrich) on a Waters Stryagel® HR 3 THF column (7.8 x 300 mm). The Waters LC system (Milford, MA) was equipped with a 2414 refractive index detector, a 1515 isocratic HPLC pump, and 717plus autosampler. Samples (10 mg/mL) were dissolved in THF and filtered using 0.45 μm pore size nylon or PTFE syringe filters (Fisher Scientific). Dynamic light scattering (DLS) analysis was carried out on a Zetasizer

nanoseries nano ZS90 (Malvern instruments). CMC studies were carried out on a Spex fluoromax-3 spectrofluorometer (Jobin Yvon Horiba) at 25 ºC. Melting points were determined by DSC on a TA DSC Q2000. TA Universal Analysis 2000 software was used for data collection on a Dell Dimension 3000 computer. Samples (4-8 mg) were heated under dry nitrogen gas. Data were collected at heating and cooling rates of 10 °C min^{-1} with a two-cycle minimum.

6.4.3 Synthesis of Ar12

2,5-Dihydroxyteraphthalic acid (5.00 g, 25.0 mmol) and zinc chloride (0.81 g, 5.9 mmol) were stirred with lauroyl chloride (87 ml, 380 mmol). The solution was heated to 95 °C in a temperature-controlled oil bath and stirred under argon overnight. Diethyl ether (100 ml) and DI water (30 ml) were added and the solution was allowed to stir for 45 minutes. The organic phase was washed with water (5 x 100 ml) and then concentrated via rotary evaporation. The concentrated solution was precipitated from hexanes (2.5 L) yielding Ar12 as a yellow solid**.** Yield% = 68% (10.1 g). ^{1}H NMR ($CDCl_3$): δ = 0.80-0.93 (t, 6H, CH_3), 1.20-1.45 (m, 32H, CH_2), 1.70-1.81 (m, 4H, CH_2), 2.51-2.65 (m, 4H, CH_2), 7.70 (s, 2H, Ar-CH); ^{13}C NMR (CDC_{l3}): 14.32, 22.87, 29.34, 29.53, 29.67, 29.80, 29.82, 32.10, 34.37, 127.37, 128.74, 147.84, 165.27, 172.42; IR (NaCl cm^{-1}): 2847, 1768, 1690 (C=O), 1268, 1177, 935, 897; Tm = 71 °C

6.4.4 Synthesis of Ar12P5

Hydroxy-terminated PEG (2.7 g, 0.53 mmol) was azeotropically distilled with toluene. Ar12P5 (1.5 g, 1.6 mmol) and DMAP (0.15 g 0.48 mmol) were dissolved in anhydrous DCM (15 ml).

PEG was cooled to room temperature under argon and the solution of Ar12P5 and DMAP was added. Once the PEG had dissolved, dicyclohexylcarbodiimide (DCC) (1.7 ml, 1.7 mmol) was added dropwise. The reaction mixture was stirred under argon for 48 hours, cooled and the resulting white solid precipitate (dicyclohexylurea) was removed by vacuum filtration. The filtrate was washed once with HCl (0.1N, 20 ml) and twice with brine (20 ml), dried over $MgSO_4$ and concentrated *via* rotary evaporation. The product was precipitated from DCM and diethyl ether yielding 2 as a white solid (2.6 g, 83%). 1H-NMR (CDCl3): d 0.85 (t, 6H, CH3), 1.30 (m, 32H, CH2), 1.71 (m, 4H, CH2), 2.21 (m, 4H, CH2), 2.36 (m, 4H, CH2), 3.63 (m, 500H, CH2), 7.65 (d, 1H, Ar-H), 8.10 (s, 1H, Ar-H); IR (NaCl cm^{-1}): 3426, 2879, 1650 (C=O), 1108, 949, 842; Tm = 56^{o}C; GPC : Mw = 6.3 kDa; PDI = 1.07

6.4.5 CMC measurements

A solution of pyrene, the fluorescence probe molecule, was made up to a concentration of 5 x 10^{-6} M in acetone. Samples were prepared by adding 1 mL of pyrene solution to a series of vials and allowing the acetone to evaporate so that the final concentration of pyrene in all of the samples was 5 x 10^{-7} M. AMs were dissolved in HPLC grade water and diluted to a series of concentrations from 1 x 10^{-3} M to 1 x 10^{-10} M. AM-pyrene solutions (10 mL) were shaken overnight at 37 °C to allow partition of the pyrene into the micelles. Emission was performed from 300 to 360 nm, with 390 nm as the excitation wavelength. The maximum absorption of pyrene shifted from 332 to 334.5 nm on micelle formation [30-32]. The ratio of absorption of encapsulated pyrene (334.5 nm) to pyrene in water (332 nm) was plotted as the logarithm of polymer concentrations. The inflection point of the curve was taken as the CMC value.

6.4.6 Cell culture *(Performed by Nicole Plourde)*

Studies of polymer interactions were conducted using a tet-inducible cell line with controlled expression of scavenger receptor A (SRA), human embryonic kidney (HEK) cells stably transfected with human SRA (gift from Dr. Steven R. Post), which are referred to as HEK-SRA. Cells were propagated in high glucose Dulbecco's Modified Eagle Medium (DMEM) (Invitrogen) supplemented with 10% fetal bovine serum (FBS), 1% penicillin/streptomycin, 15 µg/mL Blasticidin and 100 µg/mL HygromycinB at 37 °C in 5% CO_2. SRA expression was induced with addition of 0.5 µg/ml tetracycline overnight and throughout the experiment. Transfection was ensured via antibody bingding assays.

6.4.7 oxLDL uptake inhibition in HEK-SRA cells *(Performed by Nicole Plourde)*

The internalization of oxLDL by HEK-SRA cells was assayed by incubating boron-dipyrromethene (BODIPY)-labeled oxLDL (10 µg/ml) and 10^{-6} M polymers with cells for 24 hr at 37 °C and 5% CO_2 in serum containing DMEM. Conditions included a control of medium alone without polymer intervention, and non-induced cells. Cells were washed once with PBS, fixed with 4% formaldehyde, and imaged on a Nikon Eclipse TE2000-S fluorescent microscope to determine fluorescently tagged oxLDL accumulation. The images were analyzed with ImageJ 1.42q (NIH) and fluorescence data was normalized to cell count. The oxLDL uptake levels were normalized to those obtained in the absence of polymers.

6.4.8 AM and SR-A modeling *(Performed by Nicole Plourde)*

The AMs were modeled according to their chemical structures using the build module in molecular operating environment (MOE) (Chemical Computing Group, Inc., Montreal, Canada). The model polymer molecules were parameterized for Amber99 [33] force field and energy minimized until convergence (grad = 0.001) was attained. The creation of the SR-A homology model was previously described.[29] Briefly, the 3D homology model of the SR-A collagen-like domain was generated using the program MODELLER [34] with collagen type I chain A as template.

6.4.9 Docking and scoring *(Performed by Nicole Plourde)*

Selected polymer models were docked to the collagen-like domain of SR-A using GOLD v3.2 [28]. The GOLD program employs a genetic algorithm for docking flexible ligands into partially flexible receptor sites. The binding cavity was defined as residues Arg45 – Ser68 with an active site radius of 15 Å such that all major residues thought to be necessary for oxLDL binding were included. Dockings were performed with standard default settings; population size of 100, selection pressure of 1.1, number of operations at 100,000, number of islands at 5, and a niche size of 2. Twenty independent docking runs were performed for each polymer, which optimized the computational time required to dock and score non-redundant conformations. The docked pairs were ranked based on each GoldScore. The best ranking conformation of the polymer illustrated the most preferred conformation to interact with scavenger receptor and the binding energy was computed for the refined complexes using the following equation

$$\Delta E_{binding} = \Delta E_{complex} - \Delta E_{SR-A} - \Delta E_{Polymer}$$

Where $\Delta E_{complex}$ is the energy of the polymers docked to collagen-like domain of SR-A, ΔE_{SR-A} is the energy of the homology model of the scavenger receptor collagen-like domain, and $\Delta E_{Polymer}$ is the energy of the polymer. Each structure (polymer model, homology model of the SR-A collagen-like domain, and the docked conformation of the pair) was parameterized using Amber99 [33] force field and energy minimized until convergence (grad = 0.001) was attained. These minimized energies were used to estimate the binding energy.

6.4.10 Statistical analysis

Each *in vitro* experiment was performed at least twice and three replicate samples were investigated in each experiment. Five images per well were captured and analyzed. The results were then evaluated using analysis of variance (ANOVA). Significance criteria assumed a 95% confidence level ($P<0.05$). Standard error of the mean is reported in the form of error bars on the graphs of the final data.

6.5 References

[1] K.J. Williams, I. Tabas. Atherosclerosis--an Inflammatory Disease. *N Engl J Med* **1999** *340* 1928-1935.
[2] P. Libby, M. Aikawa, M.K. Jain. Vascular Endothelium and Atherosclerosis. *Handb Exp Pharmacol* **2006** 285-306.
[3] G.D. Sloop. Atherosclerosis--an Inflammatory Disease. *N Engl J Med* **1999** *340* 1928-1929.
[4] P.L. Weissberg, M.R. Bennett. Atherosclerosis--an Inflammatory Disease. *N Engl J Med* **1999** *340* 1928-1929.
[5] B. Zieden, J. Molgaard, A.G. Olsson. Low-Density Lipoprotein Oxidation and Coronary Atherosclerosis. *Lancet* **1992** *340* 727-728.

[6] V.R. Babaev, S. Fazio, L.A. Gleaves, K.J. Carter, C.F. Semenkovich, M.F. Linton. Macrophage Lipoprotein Lipase Promotes Foam Cell Formation and Atherosclerosis in Vivo. *J Clin Invest* **1999** *103* 1697-1705.
[7] Y.V. Bobryshev. Monocyte Recruitment and Foam Cell Formation in Atherosclerosis. *Micron* **2006** *37* 208-222.
[8] L. Hegyi, J.N. Skepper, N.R. Cary, M.J. Mitchinson. Foam Cell Apoptosis and the Development of the Lipid Core of Human Atherosclerosis. *J Pathol* **1996** *180* 423-429.
[9] D.J. Rader, E. Pure. Lipoproteins, Macrophage Function, and Atherosclerosis: Beyond the Foam Cell? *Cell Metab* **2005** *1* 223-230.
[10] P. Amarenco, J. Labreuche, P. Lavallee, P.J. Touboul. Statins in Stroke Prevention and Carotid Atherosclerosis: Systematic Review and up-to-Date Meta-Analysis. *Stroke* **2004** *35* 2902-2909.
[11] J.J. Kastelein, E.S. Stroes, E. de Groot. Subclinical Atherosclerosis as a Target of Therapy: Potential Role of Statins. *Am J Cardiol* **2004** *93* 737-740.
[12] B.R. Kwak, F. Mulhaupt, F. Mach. Atherosclerosis: Anti-Inflammatory and Immunomodulatory Activities of Statins. *Autoimmun Rev* **2003** *2* 332-338.
[13] S.J. Nicholls, M. Borgman, S.E. Nissen, J.S. Raichlen, C. Ballantyne, P. Barter, M.J. Chapman, R. Erbel, P. Libby. Impact of Statins on Progression of Atherosclerosis: Rationale and Design of Saturn (Study of Coronary Atheroma by Intravascular Ultrasound: Effect of Rosuvastatin Versus Atorvastatin). *Curr Med Res Opin* **2011** *27* 1119-1129.
[14] G. Novo, G. Fazio, C. Visconti, P. Carita, E. Maira, K. Fattouch, S. Novo. Atherosclerosis, Degenerative Aortic Stenosis and Statins. *Curr Drug Targets* **2011** *12* 115-121.
[15] A. Rubinstein, E. Izkhakov. Statins: An Effective Anti-Atherosclerosis Therapy. *Isr Med Assoc J* **2002** *4* 456-457.
[16] C.J. Vaughan, A.M. Gotto, Jr., C.T. Basson. The Evolving Role of Statins in the Management of Atherosclerosis. *J Am Coll Cardiol* **2000** *35* 1-10.
[17] M. Yoshida. Potential Role of Statins in Inflammation and Atherosclerosis. *J Atheroscler Thromb* **2003** *10* 140-144.
[18] G.A. Ramm, R.W. Shepherd, A.C. Hoskins, S.A. Greco, A.D. Ney, T.N. Pereira, K.R. Bridle, J.D. Doecke, P.J. Meikle, B. Turlin, P.J. Lewindon. Fibrogenesis in Pediatric Cholestatic Liver Disease: Role of Taurocholate and Hepatocyte-Derived Monocyte Chemotaxis Protein-1 in Hepatic Stellate Cell Recruitment. *Hepatology* **2009** *49* 533-544.
[19] Z. Shah, T. Kampfrath, J.A. Deiuliis, J. Zhong, C. Pineda, Z. Ying, X. Xu, B. Lu, S. Moffatt-Bruce, R. Durairaj, Q. Sun, G. Mihai, A. Maiseyeu, S. Rajagopalan. Long-Term Dipeptidyl-Peptidase 4 Inhibition Reduces Atherosclerosis and Inflammation Via Effects on Monocyte Recruitment and Chemotaxis. *Circulation* **2011** *124* 2338-2349.
[20] K. Yoshiizumi, F. Nakajima, R. Dobashi, N. Nishimura, S. Ikeda. Studies on Scavenger Receptor Inhibitors. Part 1: Synthesis and Structure-Activity Relationships of Novel Derivatives of Sulfatides. *Bioorg Med Chem* **2002** *10* 2445-2460.
[21] A.C. Li, C.J. Binder, A. Gutierrez, K.K. Brown, C.R. Plotkin, J.W. Pattison, A.F. Valledor, R.A. Davis, T.M. Willson, J.L. Witztum, W. Palinski, C.K. Glass. Differential Inhibition of Macrophage Foam-Cell Formation and Atherosclerosis in Mice by Pparalpha, Beta/Delta, and Gamma. *J Clin Invest* **2004** *114* 1564-1576.
[22] E. Chnari, H.B. Lari, L. Tian, K.E. Uhrich, P.V. Moghe. Nanoscale Anionic Macromolecules for Selective Retention of Low-Density Lipoproteins. *Biomaterials* **2005** *26* 3749-3758.

[23] E. Chnari, J.S. Nikitczuk, K.E. Uhrich, P.V. Moghe. Nanoscale Anionic Macromolecules Can Inhibit Cellular Uptake of Differentially Oxidized Ldl. *Biomacromolecules* **2006** *7* 597-603.
[24] N.M. Iverson, S.M. Sparks, B. Demirdirek, K.E. Uhrich, P.V. Moghe. Controllable Inhibition of Cellular Uptake of Oxidized Low-Density Lipoprotein: Structure-Function Relationships for Nanoscale Amphiphilic Polymers. *Acta Biomater* **2010** *6* 3081-3091.
[25] J. Wang, N.M. Plourde, N. Iverson, P.V. Moghe, K.E. Uhrich. Nanoscale Amphiphilic Macromolecules as Lipoprotein Inhibitors: The Role of Charge and Architecture. *Int J Nanomedicine* **2007** *2* 697-705.
[26] N.M. Plourde, S. Kortagere, W. Welsh, P.V. Moghe. Structure-Activity Relations of Nanolipoblockers with the Atherogenic Domain of Human Macrophage Scavenger Receptor A. *Biomacromolecules* **2009** *10* 1381-1391.
[27] L.Y. Tian, L.; Zhou, N.; Tat, H.; Uhrich, K. E. Amphiphilic Scorpion-Like Macromolecules: Design, Synthesis, and Characterization. *Macromolecules* **2004** *37* 538-545.
[28] G. Jones, P. Willett, R.C. Glen, A.R. Leach, R. Taylor. Development and Validation of a Genetic Algorithm for Flexible Docking. *Journal of Molecular Biology* **1997** *267* 727-748.
[29] N.M. Plourde, S. Kortagere, W. Welsh, P.V. Moghe. Structure-Activity Relations of Nanolipoblockers with the Atherogenic Domain of Human Macrophage Scavenger Receptor A. *Biomacromolecules* **2009** *10* 1381-1391.
[30] K.S. Focsaneanu, J.C. Scaiano. Potential Analytical Applications of Differential Fluorescence Quenching: Pyrene Monomer and Excimer Emissions as Sensors for Electron Deficient Molecules. *Photochem Photobiol Sci* **2005** *4* 817-821.
[31] L. Gai, H. Chen, B. Zou, H. Lu, G. Lai, Z. Li, Z. Shen. Ratiometric Fluorescence Chemodosimeters for Fluoride Anion Based on Pyrene Excimer/Monomer Transformation. *Chem Commun (Camb)* **2012** *48* 10721-10723.
[32] A.G. Macdonald, K.W. Wahle, A.R. Cossins, M.K. Behan. Temperature, Pressure and Cholesterol Effects on Bilayer Fluidity; a Comparison of Pyrene Excimer/Monomer Ratios with the Steady-State Fluorescence Polarization of Diphenylhexatriene in Liposomes and Microsomes. *Biochim Biophys Acta* **1988** *938* 231-242.
[33] J.M. Wang, P. Cieplak, P.A. Kollman. How Well Does a Restrained Electrostatic Potential (Resp) Model Perform in Calculating Conformational Energies of Organic and Biological Molecules? *Journal of Computational Chemistry* **2000** *21* 1049-1074.
[34] A. Sali, T.L. Blundell. Comparative Protein Modeling by Satisfaction of Spatial Restraints. *Journal of Molecular Biology* **1993** *234* 779-815.

7 Appendix 2: Synthesis of polyAmfenac

7.1 Introduction

Uveitis is an ocular inflammatory disease that is the leading cause of blindness in the world [1-5]. Typical uveitis occurs in the anterior, intermediate, posterior, and/or throughout the whole eye. Amfenac is a non-steriod anti-inflammatory drug used to treat eye inflammation. Typical treatment for anterior uveitis is topical administration (eyedrop) of nepafenac, a prodrug form of amfenac. (Figure 7.1).

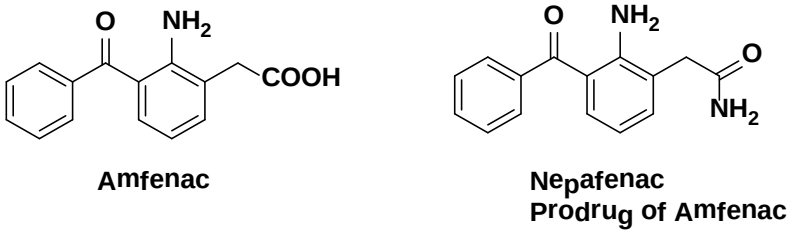

Figure 7.1 Structures of amfenac and nepafenac

However, topical administration of amfenac is not sufficient to reach the posterior area of eye. Amfenac is effective and safe to treat anterior uveitis, and likely demonstrates effectiveness in treating posterior uveitis. Due to the poor penetration to the posterior area, frequent intraocular injection of amfenac into the eye is required to achieve therapeutic concentration in the posterior region. However, daily intraocular injection increases the burden of the patient and is not feasible for commercialization. Therefore, sustained release of amfenac in posterior area will be desirable to obtain long term therapeutic effectiveness in the eye.

Sustained release of amfenac can be achieved by incorporating amfenac into a degradable polymeric backbone. Using the drug molecule as repeat unit can result in the formation of polymer with high drug content. This idea has been investigated by the Uhrich group. One initial example developed is PolyAspirin in which salicylic acid, the metabolite of aspirin, is chemical incorporated into a poly(anhydride-ester) via a linker molecule (Figure 7.2). Salicylic acid is then sustainably released upon hydrolytic degradation of the polymer anhydride and ester bonds (Figure 7.2) [6, 7]. Utilizing the idea of PolyAspirin, PolyAmfenac is synthesized with amfenac embedded in a hydrolytically degradable anhydride-imine backbone.

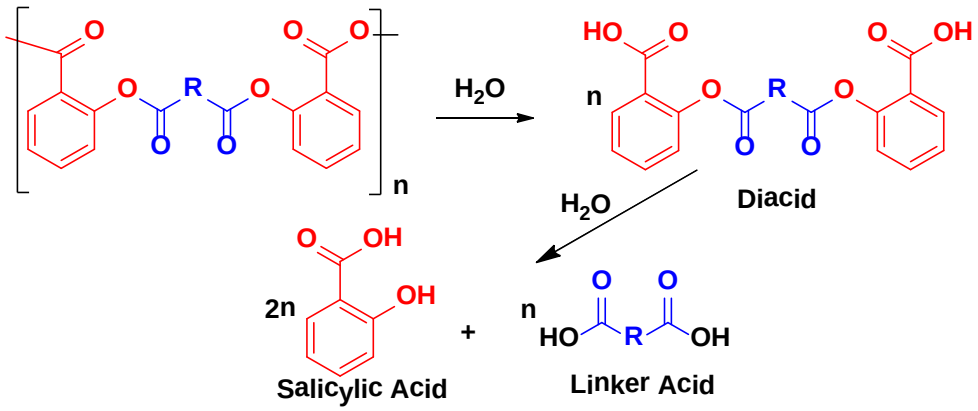

Figure 7.2 Chemical structure of PolyAspirin and its degradation pathway

7.2 Results and discussion

Prior to polymerization it is necessary to synthesize an amfenac-containing Schiff base intermediate (**1**, Figure 7.3) by reacting amfenac with 4-formylbenzoic acid in the presence of trifluoroacetic acid. The resulting product (**1**) was charcterized via ^{1}H NMR and ^{13}C NMR spectroscopes. The disappearance of aldehyde hydrogen (10.51 ppm) in 4-formylbenzoic acid

and appearance of imine hydrogen (7.96 ppm) indicate the formation of imine. Mass spectroscopy also confirmed the formation of **1** (Figure 7.3). The amfenac-containing schiff base intermediate (**1**, Figure 7.3) is then polymerized using solution polymerization to give PolyAmfenac (**2**, Figure 7.3). The polymer is characterized using gel permeation chromatography (GPC). The formation of polymer is confirmed by the Mw = 4400, indicating approximate 10 repeat units.

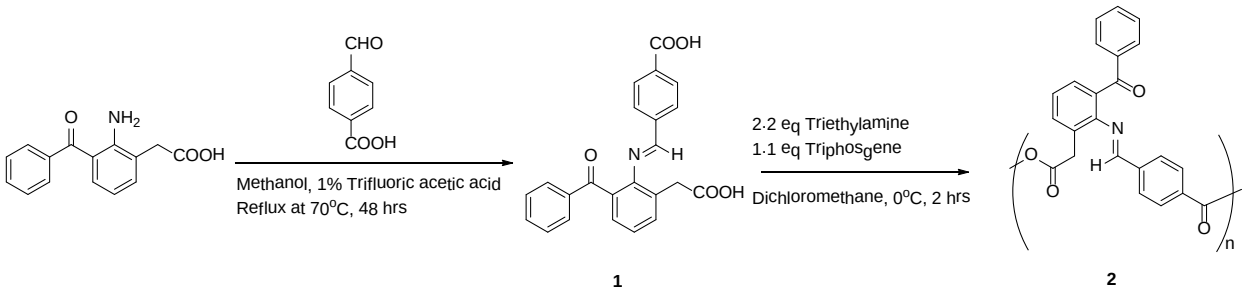

Figure 7.3 Synthetic route of PolyAmfenac

The proposed degradation pathway of PolyAmfenac is illustrated (Figure 7.4). PolyAmfenac will first be degraded into the amfenac-containing schiff base intermediate (Figure 7.4) through hydrolysis of anhydride bond in PolyAmfenac. Following the first degradation step, the amfenac-containing schiff base intermediate (Figure 7.4) will then be hydrolyzed to amfenac and 4-formylbenzoic acid via the cleavage of imine bond. In the presence of aldehyde dehydrogenase, 4-formylbenzoic acid will be readily oxidized to terephthalic acid, which will be rapidly excreted either unchanged or as a glycine conjugate *in vivo*. However, the proposed mechanism still needs further studies to confirm the actual pathway.

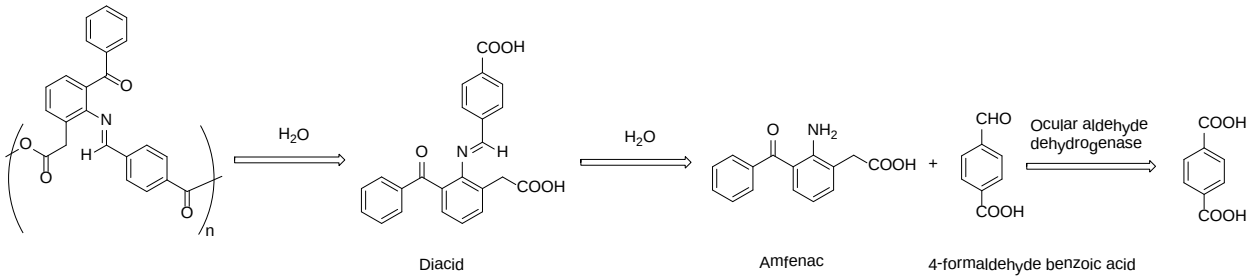

Figure 7.4 Proposed degradation pathway of PolyAmfenac

7.3 Experimental

7.3.1 Materials

All materials are received from Sigma Aldrich and used without further purification

7.3.2 Characterization methods

^{1}H NMR spectra measurements were taken at 25 ºC on a Varian 400 MHz spectrometer using deuterated chloroform ($CDCl_3$) as a solvent and tetramethylsilane as an internal standard. Mass spectra were obtained on a Finnigan LDQ-DUO equipped with an adjustable atmospheric pressure ionization-electrospray ionization (API-ESI) Ion source. FTIR spectra were recorded on a Thermo Nicolet/Avatar 360 spectrometer using sample discs compressed with potassium bromide (KBr). Molecular weights (Mw) were determined using gel permeation chromatography (GPC) with respect to polystyrene standards (Sigma-Aldrich) on a Waters Stryagel® HR 3 DMF column (7.8 x 300 mm). The Waters LC system (Milford, MA) was equipped with a 2414 refractive index detector, a 1515 isocratic HPLC pump, and 717plus autosampler. Samples (10

mg/mL) were dissolved in DMF and filtered using 0.45 μm pore size nylon or PTFE syringe filters (Fisher Scientific).

7.3.3 Synthesis of monomer (1, Figure 7.3)

Sodium amfenac (0.500 g, 0.180 mmol) is dissolved in anhydrous methanol (10 mL). Trifluoroacetic acid (0.140 mL, 0.180 mmol) is added to the sodium amfenac solution and the mixture stirred for 30 mins to complete acidification. Trifluoroacetic acid (1.4 μL, 1.8×10^{-3} mmol) and 4-formylbenzoic acid (0.027 g, 0.18 mmol) are then added to the acidified solution. The reaction mixture is allowed to reflux at 70^{o}C for 24 hrs. After the reaction is complete, yellow precipitates are formed and filtered. Cold methanol (20 mL) is then used to wash to precipitates 3 times. The residue yellow solid is dried under high vacuum overnight. Yield% = 67% (0.345 g). ^{1}H-NMR (400 MHz, CDCl3): (δ) 13.15 (s, 1H, Ar-COOH), 10.60 (s, 1H, COOH), 8.07 (d, 2H, Ar-H), 7.83 (d, 2H, Ar-H), 7.79 (s, 1H, N=C-H), 7.74 (d, 2H, Ar-H), 7.67 (d, 2H, Ar-H), 7.56 (t, 2H, Ar-H), 7.38(d, 2H, Ar-H), 6.98 (t, 1H, Ar-H), 3.31 (s, 2H, CH2). ^{13}C-NMR (100 MHz, CDCl3): (δ) 195.1, 169.5, 167.3, 144.2, 139.7, 137.5, 136.8, 133.7, 132.5, 131.6, 130.3, 129.5, 126.8, 122.9, 121.5, 120.3. IR (KBr, cm^{-1}): 1720 (vs C=O carbonyl), 1700 (vs C=O COOH), 1650 (vs, C=N, imine) ESI-MS: *m/z* 387.2 (M+H). Calculated Mw = 386.2

7.3.4 Synthesis of polyAmfenac (2, Figure 7.3)

Monomer (**1**, Figure 7.3) (50 mg, 0.129 mmol) and triethylamine (40 μL, 0.28 mmol) are dissolved in anhydrous dichloromethane (10 mL). Triphosgene (42.1 mg, 0.142 mmol) is

dissolved in anhydrous dichloromethane (2 mL) and resulting solution is added to the monomer/triethylamine solution drop wise over 15 minutes. The reaction mixture is allowed to stir for 6 hrs until CO2 evolution ceased. After the reaction, the mixture is dried using rotary evaporation. Crude product was characterized by GPC: Mw = 4400, PDI = 1.26

7.4 References

[1] S.D. Anesi, C.S. Foster. Importance of Recognizing and Preventing Blindness from Juvenile Idiopathic Arthritis-Associated Uveitis. *Arthritis Care Res (Hoboken)* **2012** *64* 653-657.
[2] H.N. Cole, J.R. Driver. Sarcoidosis with Uveitis and Blindness. *AMA Arch Derm Syphilol* **1952** *66* 409-410.
[3] C.G. Espiritu, R. Gelber, H.B. Ostler. Chronic Anterior Uveitis in Leprosy: An Insidious Cause of Blindness. *Br J Ophthalmol* **1991** *75* 273-275.
[4] R.S. Rosner. Uveitis and Blindness. *Med Trial Tech Q* **1967** *14* 39-42.
[5] M.S. Suttorp-Schulten, A. Rothova. The Possible Impact of Uveitis in Blindness: A Literature Survey. *Br J Ophthalmol* **1996** *80* 844-848.
[6] L. Erdmann, B. Macedo, K.E. Uhrich. Degradable Poly(Anhydride Ester) Implants: Effects of Localized Salicylic Acid Release on Bone. *Biomaterials* **2000** *21* 2507-2512.
[7] L. Erdmann, K.E. Uhrich. Synthesis and Degradation Characteristics of Salicylic Acid-Derived Poly(Anhydride-Esters). *Biomaterials* **2000** *21* 1941-1946.